Pergamon

Atmospheric Environment Vol. 31, No. 12, pp. 1851–1904, 1997

1352-2310/97 $17.00 + 0.00

PII: S1352-2310(96)00334-2

CLIMATOLOGIES OF NO_x AND NO_y: A COMPARISON OF DATA AND MODELS

L. K. EMMONS,* M. A. CARROLL,* D. A. HAUGLUSTAINE,†‡ G. P. BRASSEUR,† C. ATHERTON,§ J. PENNER,* S. SILLMAN,* H. LEVY II,¶ F. ROHRER,‖ W. M. F. WAUBEN,** P. F. J. VAN VELTHOVEN,** Y. WANG,†† D. JACOB,†† P. BAKWIN,‡‡ R. DICKERSON,§§ B. DODDRIDGE,§§ C. GERBIG,‖ R. HONRATH,¶¶ G. HÜBLER,‖ ‖ D. JAFFE,*** Y. KONDO,††† J. W. MUNGER,†† A. TORRES,‡‡‡ A. VOLZ-THOMAS‖

*Department of Atmospheric, Oceanic and Space Sciences, University of Michigan, Ann Arbor MI 48109-2143, U.S.A.; †National Center for Atmospheric Research, Boulder CO, U.S.A.; §Lawrence Livermore National Laboratory, Livermore CA, U.S.A.; ¶NOAA Geophysical Fluid Dynamics Laboratory, Princeton NJ, U.S.A.; ‖ICG, Forschungszentrum Jülich, Jülich, Germany; **Royal Netherlands Meteorological Institute, De Bilt, The Netherlands; ††Harvard University, Cambridge MA, U.S.A.; ‡‡NOAA/Climate Monitoring and Diagnostics Laboratory, Boulder CO, U.S.A.; §§University of Maryland, College Park MD, U.S.A.; ¶¶Michigan Technological University, Houghton MI, U.S.A.; ‖ ‖NOAA/Aeronomy Lab, Boulder CO, U.S.A.; ***University of Alaska, Fairbanks AK, U.S.A.; †††Nagoya University, Japan; and ‡‡‡NASA Wallops Flight Facility, Wallops Island VA, U.S.A.

(*First received* 5 *March* 1996 *and in final form* 5 *August* 1996. *Published March* 1997)

Abstract—Climatologies of tropospheric NO_x ($NO + NO_2$) and NO_y (total reactive nitrogen: $NO_x + NO_3 + 2 \times N_2O_5 + HNO_2 + HNO_3 + HNO_4 + ClONO_2$ + PAN (peroxyacetylnitrate) + other organic nitrates) have been compiled from data previously published and, in most cases, publicly archived. Emphasis has been on non-urban measurements, including rural and remote ground sites, as well as aircraft data. Although the distribution of data is sparse, a compilation in this manner can begin to provide an understanding of the spatial and temporal distributions of these reactive nitrogen species. The cleanest measurements in the boundary layer are in Alaska, northern Canada and the eastern Pacific, with median NO mixing ratios below 10 pptv, NO_x below 50 pptv, and NO_y below 300 pptv. The highest NO values (greater than 1 ppbv) were found in eastern North America and Europe, with correspondingly high NO_y ($\sim$5 ppbv). A significantly narrower range of concentrations is seen in the free troposphere, particularly at 3–6 km, with NO typically about 10 pptv in the boreal summer. NO increases with altitude to $\sim$100 pptv at 9–12 km, whereas NO_y does not show a trend with altitude, but varies between 100 and 1000 pptv. Decreasing mixing ratios eastward of the Asian and North American continents are seen in all three species at all altitudes.

Model-generated climatologies of NO_x and NO_y from six chemical transport models are also presented and are compared with observations in the boundary layer and the middle troposphere for summer and winter. These comparisons test our understanding of the chemical and transport processes responsible for these species distributions. Although the model results show differences between them, and disagreement with observations, none are systematically different for all seasons and altitudes. Some of the differences between the observations and model results may likely be attributed to the specific meteorological conditions at the time that measurements were made differing from the model meteorology, which is either climatological flow from GCMs or actual meteorology for an arbitrary year. Differences in emission inventories, and convection and washout schemes in the models will also affect the calculated NO_x and NO_y distributions.

1. INTRODUCTION

Reactive nitrogen species play an important role in determining levels of tropospheric ozone, as well as other aspects of photochemistry. Measurements of NO_x ($NO + NO_2$) and total reactive nitrogen NO_y ($NO_x + NO_3 + 2 \times N_2O_5 + HNO_2 + HNO_3 + HNO_4 + ClONO_2$ + PAN (peroxyacetylnitrate) + other organic nitrates) have been made for a number of years in various non-urban environments. Previous discussions of such NO_x and NO_y measurements have been made by Fehsenfeld *et al.* (1988) and Carroll and Thompson (1995).

Published results from NO, NO_2 and NO_y measurements not previously available have been

‡Permanent affiliation: Service d'Aéronomie du Centre National del la Recherche Scientifique, Paris, France.

archived in the SASS (Subsonic Assessment) archive (Emmons and Carroll, 1996). Other data sets that are publicly available and are used here include the GTE (Global Tropospheric Experiment) archives at NASA Langley's Distributed Active Archive Center (DAAC), and AASE (Airborne Arctic Stratospheric Expedition) 1 and 2, which have been released on CD-ROM. Most of the data sets in the SASS archive contain in one data file all the measurements made simultaneously during a single campaign. The GTE and AASE data have been archived with only one or two species in a file and with location and other parameters in separate files. Merged data sets of these campaigns, however, have been produced by S. Sandholm at the Georgia Institute of Technology.

The generation of climatologies may be somewhat premature, as there are substantial regions where no measurements have been made in a given season. Also, in the case of aircraft campaigns, measurements have usually only been made during one season. However, we are able to begin to examine the data and make comparisons with model-generated climatologies to test our understanding of tropospheric photochemistry, and it is useful to do so at this point, despite the limited data.

In the next section, each of the data sets used in the climatologies will be briefly discussed. The third section briefly describes five chemical transport models and compares their outputs with the data. The final section outlines some outstanding questions that might be answered by further examination of these data sets, or in future campaigns. All of the tropospheric data (up to 12 km) that has been archived is presented, however we have chosen to concentrate on the lower to middle troposphere for the comparisons to models made here. A subsequent paper will continue these comparisons into the upper troposphere and address further questions of that region, such as aircraft and lightning emissions.

2. DATA

This section presents the summaries of data that have been compiled and discusses each set of measurements briefly. After an introduction to the figures showing the data, the general measurement techniques used for all the data discussed here are described. Next, the surface measurements are discussed followed by the aircraft measurements (all acronyms are given in the appendix).

The median mixing ratios of NO at midday, NO_x and NO_y are plotted in the maps shown in Figs 1–3. Midday data include only measurements between 10 a.m. and 3 p.m. local time. NO_x data are the sum of measured NO and NO_2, and calculated NO_2 values have not been used. However, there have been discrepancies between calculated and observed NO_2 values in several campaigns (e.g. CITE-3 and PEM West-A), with the observations significantly higher than the calculated concentrations (e.g., Davis *et al.*, 1993; Crawford *et al.*, 1996). The measurements of each campaign have been binned by 3 km altitude ranges and small geographical regions, and the season of each measurement is indicated by the type of shading. The regions plotted in many cases are larger than the actual location of data. Where appropriate, data from more than one flight track have been combined, as in the TRACE-A data where several flights were made over the South Atlantic and over Africa. Other regions that do contain only one or two flights are made with large enough dimensions to show up in the figures.

The data from the surface layer are omitted from these plots for clarity. Data from surface observations and aircraft measurements below 0.5 km are included in the "boundary layer" plots in Figs 4–7. Figure 4 shows the location of measurements in each season, with asterisks representing surface measurements and shaded regions indicating where aircraft measurements have been made below 0.5 km. The mean, median, central 67 and 90% of each data set for NO, NO_x and NO_y are shown in Figs 5–7, and the three-letter codes are identified in Table 1, giving the name and dates of each campaign. The data from the four other altitude ranges are shown similarly in Figs 9–23, accompanied by Tables 2–5.

Measurements from the MLOPEX campaigns at Mauna Loa Observatory (elevation 3.4 km) are shown on the 3–6 km maps in Figs 1–3 and 12. The data in the 9–12 km region (Figs 1–3 and 21–23) have been filtered to represent only the troposphere (except for STRATOZ and TROPOZ). For AASE 1, tropospheric air was defined for H_2O mixing ratios greater than 10 ppmv and O_3 less than 100 ppbv (following Carroll *et al.*, 1990). For other campaigns for which reliable low-temperature water vapor measurements were not available (e.g. AASE 2, TRACE-A) a filter of $O_3 < 100$ ppbv and $N_2O > 309$ ppbv was used. Unless otherwise stated, the data have been sorted into four seasons, defined as 1 December–28 February, 1 March–31 May, 1 June–31 August, 1 September–30 November.

The maps in Figs 1–3 show only the area of the globe where measurements are available (60°S–90°N, 260°W–40°E), and do not include most of Asia or Antarctica. These plots strikingly show how limited our knowledge of tropospheric NO_x and NO_y is, even over all seasons. Results from several of the campaigns show C-shaped profiles of NO and NO_x. For example, the PEM West-A campaign in the western Pacific during September shows lower mixing ratios of NO and NO_x at 3–6 km than at 0.5–3 and 6–9 km. The TRACE-A measurements, also during September, of NO_x over southern Africa and NO over eastern South America show a similar pattern. In the 0.5–3 km range, all three species have lower values over Alaska and Canada than the United States or the western North Atlantic Ocean, which are affected much more by pollution sources. The very high mixing ratios of NO over the South Atlantic at 9–12 km measured by TRACE-A and TROPOZ-2 during the

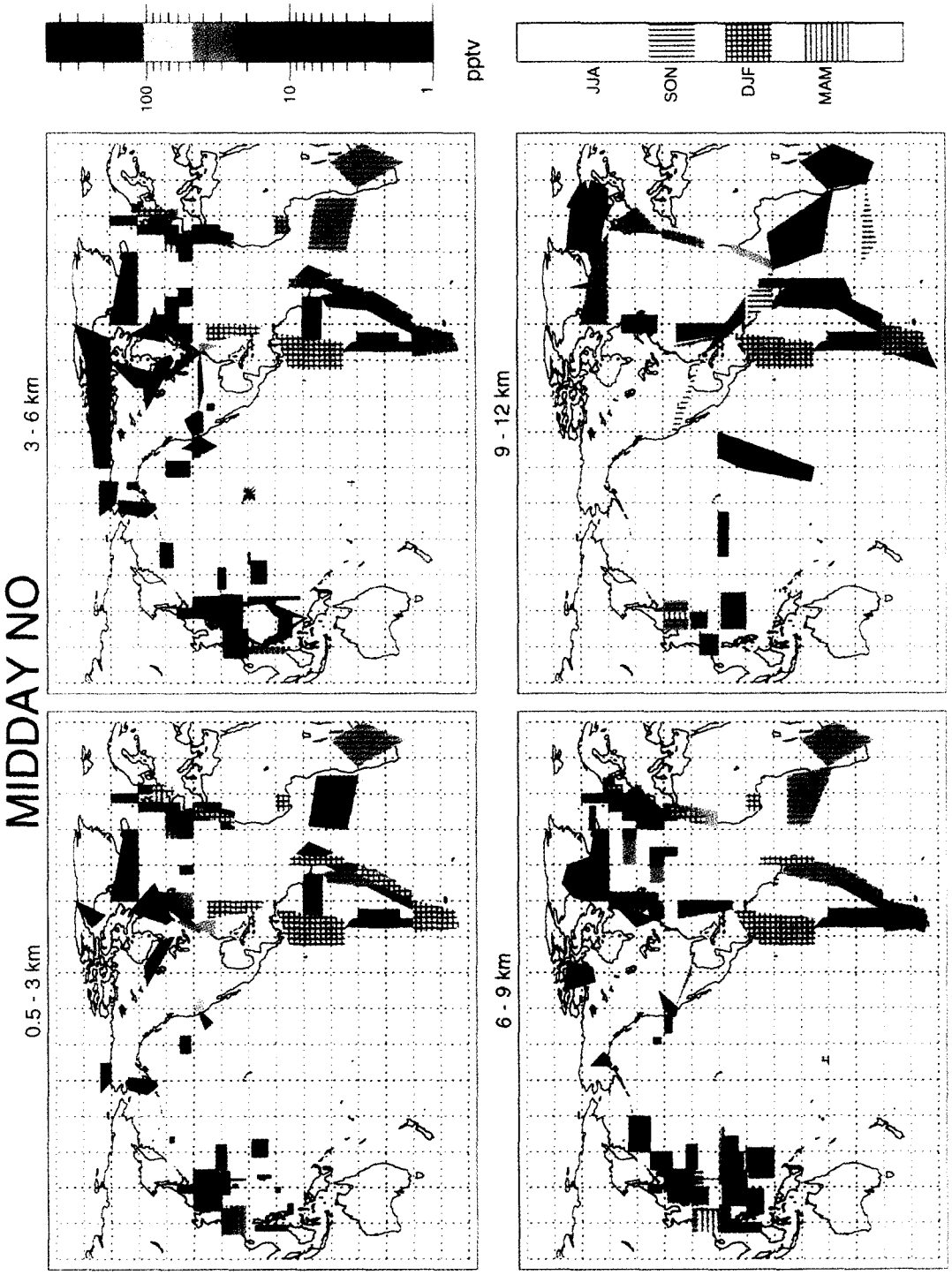

Fig. 1. Median midday NO mixing ratios indicated by color for 3 km altitude bins. The type of shading indicates the season the measurements were made.

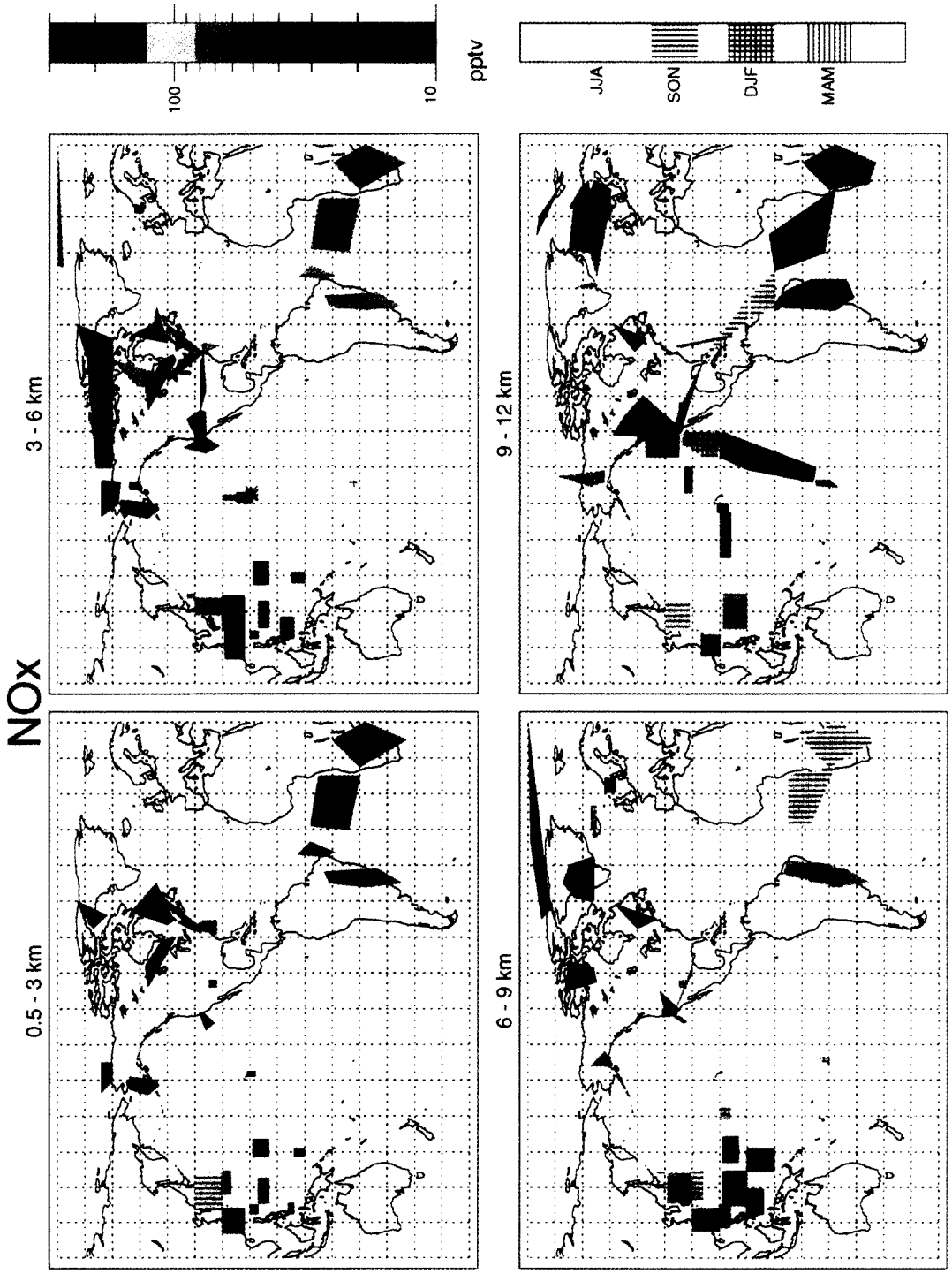

Fig. 2. Median NO_x mixing ratios.

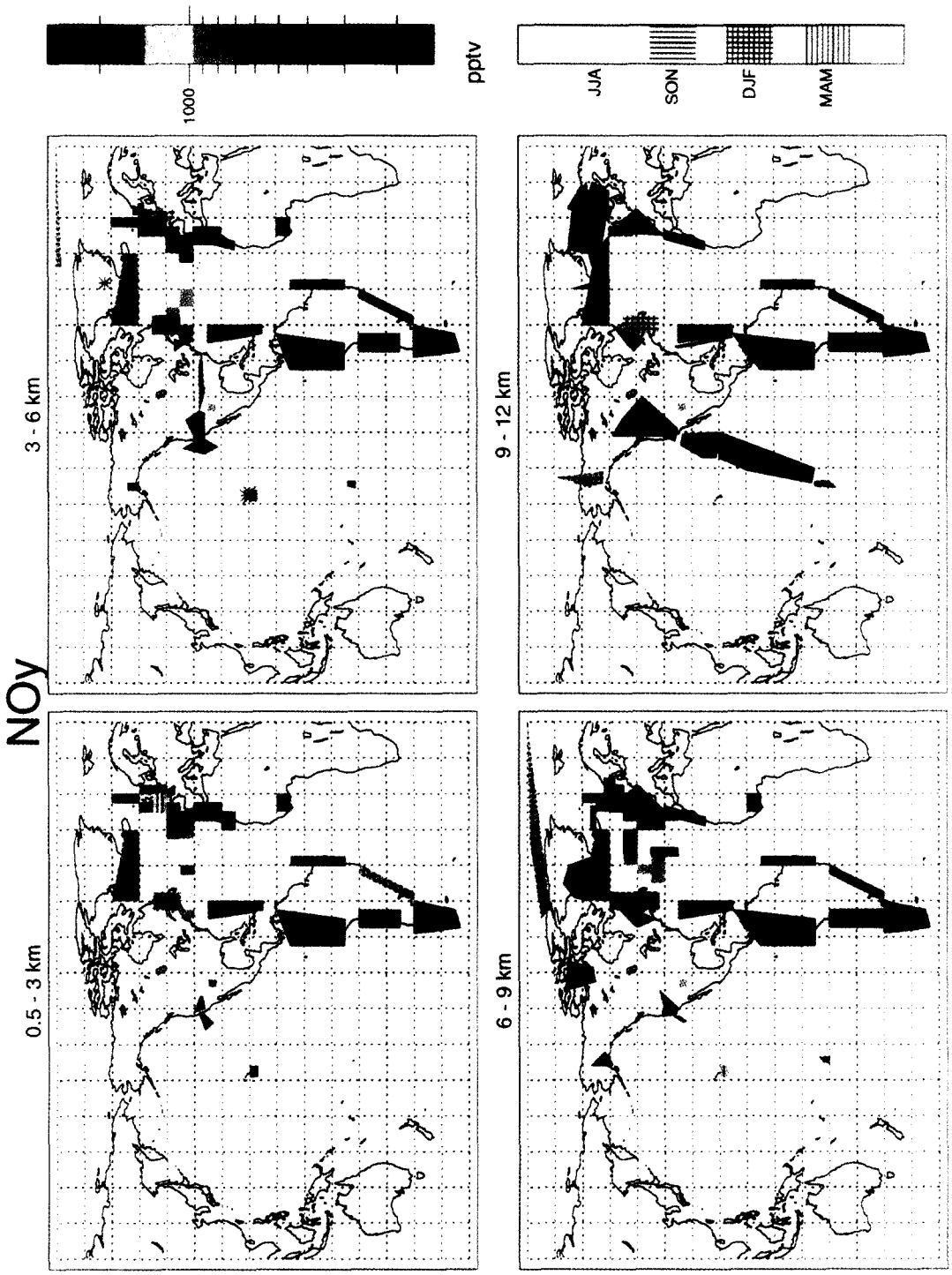

Fig. 3. Median NO_y mixing ratios.

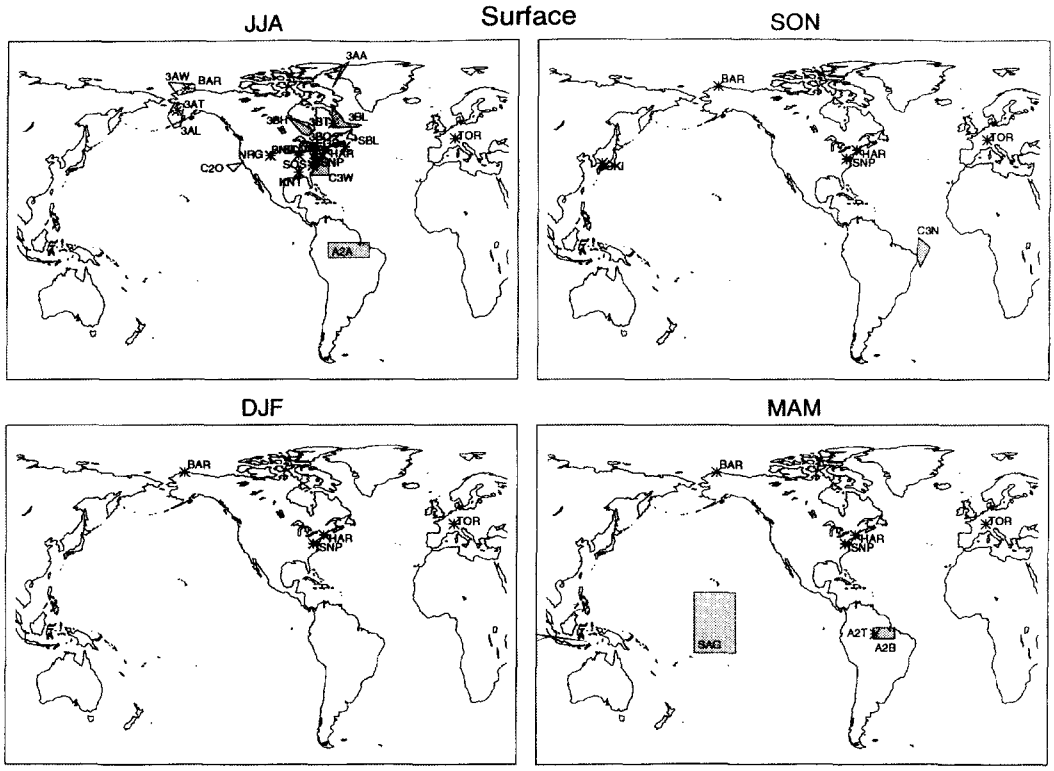

Fig. 4. Location of surface layer data, separated by season. Three-character codes are identified in Table 1. Extended regions indicate aircraft measurements below 0.5 km.

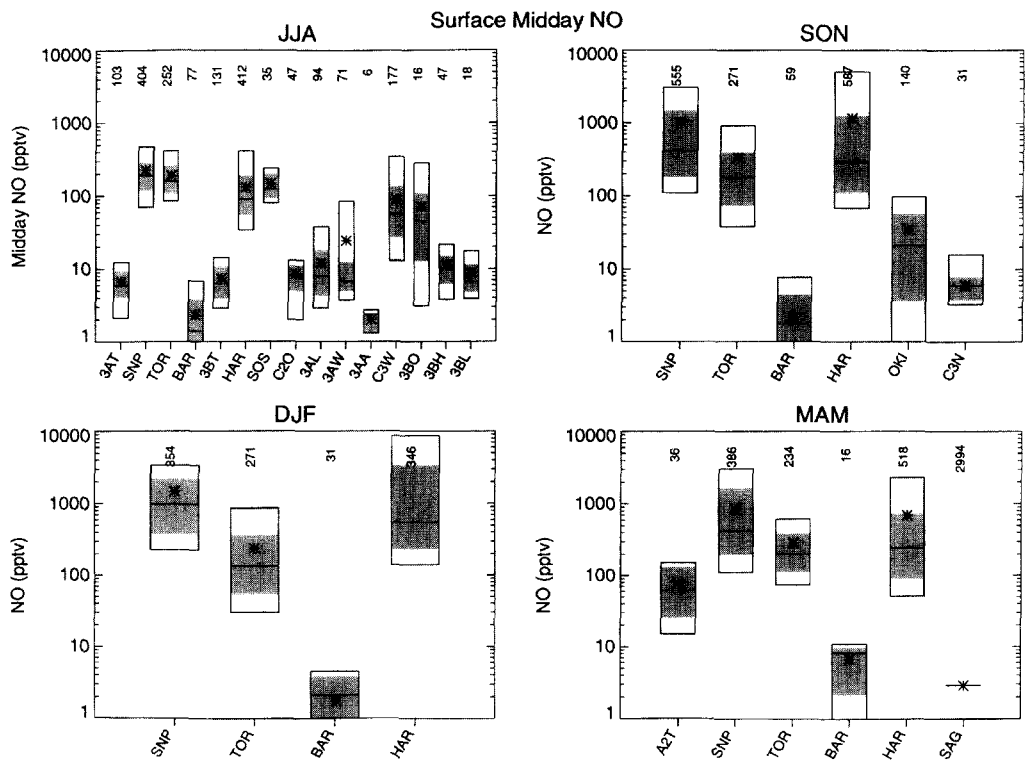

Fig. 5. Midday NO distributions for four seasons for the surface layer. Three-character codes match those on Fig. 4, and are identified in Table 1. The star indicates mean, line median, gray shading central 67%, outer box central 90%. The number of points in each summary is given along the top of each plot.

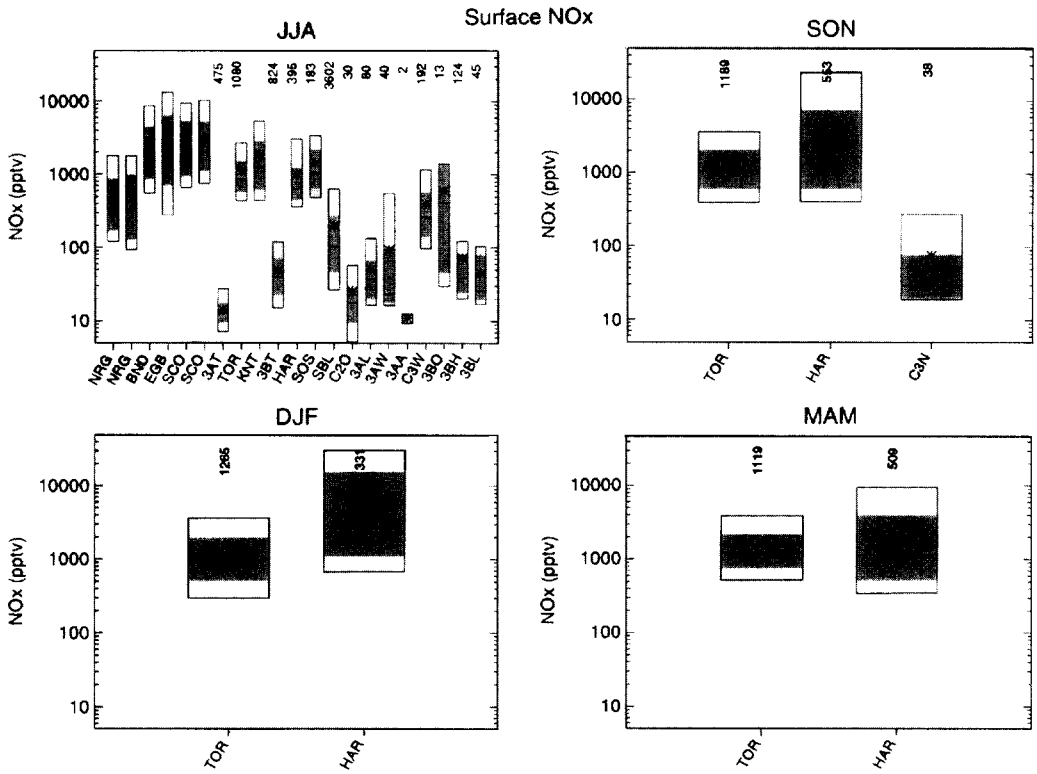

Fig. 6. NO_x distributions for the surface layer (as Fig. 5).

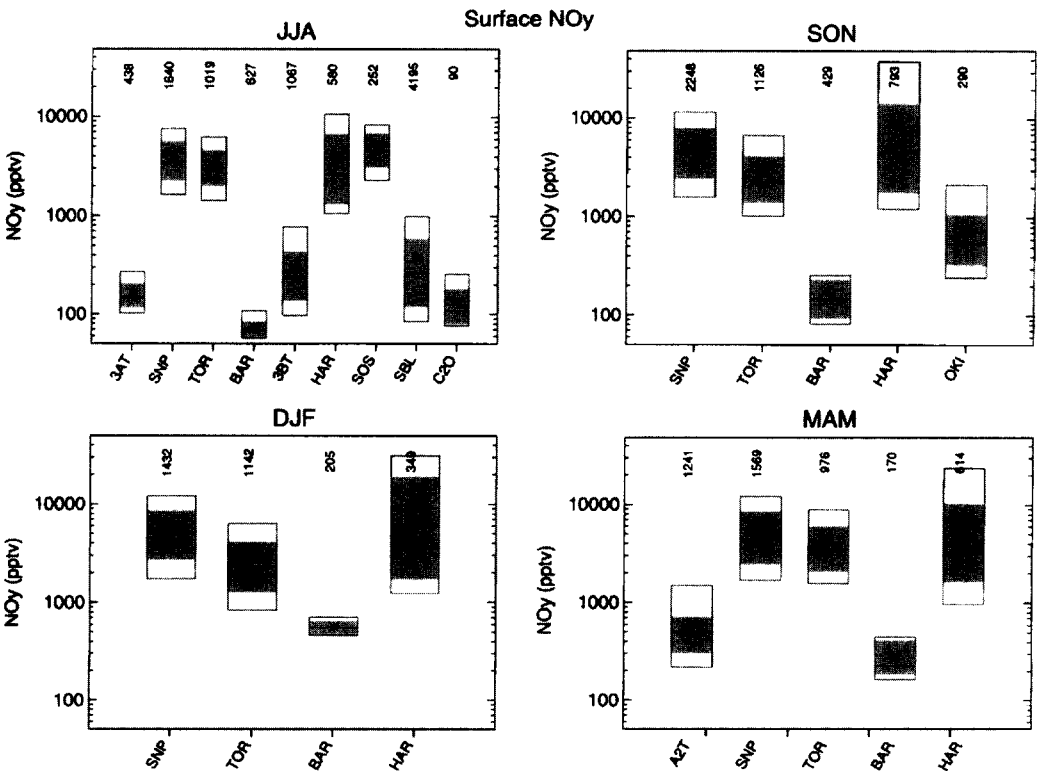

Fig. 7. NO_y distributions for the surface layer (as Fig. 5).

Table 1. Legend for boundary layer data

Code	Campaign/Site	Date
JJA		
3AA	ABLE 3A, Arctic flights	10 Jul–17 Aug 1988
3AL	ABLE 3A, Bethel flights	24 Jul–11 Aug 1988
3AT	ABLE 3A Tower, Bethel, AK	10 Jul–12 Aug 1988
3AW	ABLE 3A, Barrow flights	10–24 Jul 1988
3BH	ABLE 3B, Hudson Bay flights	6–30 Jul 1990
3BL	ABLE 3B, Labrador flights	30 Jul–14 Aug 1990
3BO	ABLE 3B, Wallops–Ontario flights	6 Jul–15 Aug 1990
3BT	ABLE 3B Tower, Schefferville, Quebec	27 Jun–16 Aug 1990
A2A	ABLE 2A	11 Jul–13 Aug 1985
BAR	Barrow, AK	19 Jun–28 Aug 1990
BND	Bondville, IL	1988
C2O	CITE 2, Ocean flights	11 Aug–5 Sep 1986
C3W	CITE 3, Wallops, VA flights	22 Aug–1 Sep 1989
EGB	Egbert, Ontario	1988
HAR	Harvard Forest, MA	1 Jun–31 Aug 1990–1993
KNT	Kinterbush, AL	1990
NRG	Niwot Ridge, CO	1984
SBL	NARE, Sable Island, Nova Scotia	Aug–Sep 1993
SCO	Scotia, PA	1986
SNP	Shenandoah NP, VA	1 Jun–31 Aug 1989
SOS	SOS/SONIA	7–17 Aug 1991
TOR	TOR/Schauinsland, Germany	Jun–Aug, 1989–1993
SON		
BAR	Barrow, AK	28 Aug–16 Nov 1990
C3N	CITE 3, Natal, Brazil	12–28 Sep 1989
HAR	Harvard Forest, MA	1 Sep –31 Nov 1990–1993
OKI	PEM WEST-A, Oki Island	10 Sep–24 Oct 1991
SNP	Shenandoah NP, VA	1 Sep–31 Nov 1989
TOR	TOR/Schauinsland, Germany	1 Sep–31 Nov 1989–1993
DJF		
BAR	Barrow, AK	1–31 Mar 1990
HAR	Harvard Forest, MA	1 Dec–28 Feb 1990–1993
SNP	Shenandoah NP, VA	1 Dec–28 Feb 1989
TOR	TOR/Schauinsland, Germany	1 Dec–28 Feb 1989–1993
MAM		
A2B	ABLE-2B flights	1 Apr–13 May 1987
A2T	ABLE 2B Tower	22 Apr–7 May 1987
BAR	Barrow, AK	10 Apr–30 May 1990
HAR	Harvard Forest, MA	1 Mar–31 May 1990–1993
SAG	SAGA 3 (ship)	14 Feb–10 Mar 1990
SNP	Shenandoah NP, VA	1 Mar–31 May 1989
TOR	TOR/Schauinsland, Germany	1 Mar–31 May 1989–1993

austral spring and summer are due to lightning production and convection of surface emissions (discussed further below). The high median values of NO (above 200 pptv) over the western North Atlantic (during TROPOZ-2), however, are very likely skewed by stratospheric air, as these data were not filtered for the troposphere, because coincident data for other species were not available. The AASE-2 data (30–70 pptv), which were filtered, were also sampled in winter and are much lower.

The decreasing concentrations eastward over the Atlantic and Pacific Oceans from the continents is evident in these maps. In the NO and NO_x maps, the mixing ratios are generally lower to the south and east of China (measured during PEM West-A). Very clean air was sampled in some regions of the eastern Atlantic, where NO mixing ratios were below 5 pptv, but significantly higher values were also observed, when airflow was from the European and African continents (see discussion of OCTA data below). The lowest values of all species were measured in the remotest regions of the world, such as northern Canada and Alaska, the central Pacific (Hawaii), and the southern tip of South America. Individual data sets are discussed in Sections 2.2 and 2.3 and additional comparisons of the data are in Section 2.4.

Table 2. Legend for 0.5–3 km data

Code	Campaign/site	Date
JJA		
3AA	ABLE 3A, Canadian Arctic	7 Jul–17 Aug 1988
3AL	ABLE 3A, Bethel	24 Jul–11 Aug 1988
3AN	ABLE 3A, Northeast U.S.	7 Jul–17 Aug 1988
3AW	ABLE 3A, Barrow	10–24 Jul 1988
3BH	ABLE 3B, Hudson Bay	6–30 Jul 1990
3BL	ABLE 3B, Labrador	30 Jul–14 Aug 1990
3BN	ABLE 3B, New England	6 Jul–15 Aug 1990
A2A	ABLE-2A	11 Jul–13 Aug 1985
C2C	CITE-2, CA	11 Aug–5 Sep 1986
C2O	CITE-2, Ocean	11 Aug–5 Sep 1986
C3W	CITE-3, Wallops	22 Aug–1 Sep 1989
ELC	ELCHEM	27 Jul–22 Aug 1989
OCA	OCTA (45,-15)	Summer 1993
OCB	OCTA (40,-15)	Summer 1993
OCC	OCTA (35,-15)	Summer 1993
OCD	OCTA (35,-10)	Summer 1993
OCE	OCTA (30,-15)	Summer 1993
OCF	OCTA (30,-10)	Summer 1993
OCG	OCTA (25,-20)	Summer 1993
OCH	OCTA (25,-15)	Summer 1993
OCI	OCTA (40,-70)	Summer 1993
OCJ	OCTA (40,-65)	Summer 1993
OCK	OCTA (40,-60)	Summer 1993
OCL	OCTA (40,-45)	Summer 1993
ST1	STRATOZ 3, S. America 15°N–15°S	4–26 June 1984
ST2	STRATOZ 3, W. S. America 15°–40°S	4–26 June 1984
ST3	STRATOZ 3, S. America < 40°S	4–26 June 1984
ST4	STRATOZ 3, E. S. America 40°S–Eq	4–26 June 1984
ST5	STRATOZ 3, E. Atlantic 20°–40°N	4–26 June 1984
SON		
C3N	CITE-3, Natal, Brazil	12–28 Sep 1989
PAD	PEMWEST-A	16 Sep–21 Oct 1991
PAE	PEMWEST-A	16 Sep–21 Oct 1991
PAF	PEMWEST-A	16 Sep–21 Oct 1991
PAG	PEMWEST-A	16 Sep–21 Oct 1991
PAH	PEMWEST-A	16 Sep–21 Oct 1991
PAI	PEMWEST-A	16 Sep–21 Oct 1991
PAJ	PEMWEST-A	16 Sep–21 Oct 1991
PAK	PEMWEST-A	16 Sep–21 Oct 1991
PAM	PEMWEST-A	16 Sep–21 Oct 1991
TAF	TRACE-A, S.Africa	3–11 Oct 1992
TAM	TRACE-A, E. South America	24 Sep–3 Oct 1992
TAT	TRACE-A, Trop. S.Atlantic	11–24 Oct 1992
DJF		
OCA	OCTA (55, 0)	Winter 1994
OCB	OCTA (50, -5)	Winter 1994
OCC	OCTA (50, 0)	Winter 1994
OCD	OCTA (40,-15)	Winter 1994
T10	TROPOZ 2, W. Africa 0°–20°N	9 Jan–1 Feb 1991
T11	TROPOZ 2, E. Atlantic 20°–40°N	9 Jan–1 Feb 1991
TR1	TROPOZ 2, Europe 40°–60°N	9 Jan–1 Feb 1991
TR2	TROPOZ 2, Greenland 60°–70°N	9 Jan–1 Feb 1991
TR3	TROPOZ 2, E. Canada 40°–60°N	9 Jan–1 Feb 1991
TR4	TROPOZ 2, W. Atlantic 15°–40°N	9 Jan–1 Feb 1991
TR5	TROPOZ 2, S. America 15°N–15°S	9 Jan–1 Feb 1991
TR6	TROPOZ 2, W. S. America 15°–40°S	9 Jan–1 Feb 1991
TR7	TROPOZ 2, S. America < 40°S	9 Jan–1 Feb 1991
TR8	TROPOZ 2, E. S. America 40°–15°S	9 Jan–1 Feb 1991
TR9	TROPOZ 2, NE S. America 15°S–5°N	9 Jan–1 Feb 1991
MAM		
A2B	ABLE-2B	1 Apr-13 May 1987
INB	INSTAC-1, Biak	5–10 May 1989
IND	INSTAC-1, Davao	5–10 May 1989
INH	INSTAC-1, Naha	5–10 May 1989

Table 2. (Continued)

Code	Campaign/site	Date
INI	INSTAC-1, Iwo	5–10 May 1989
INM	INSTAC-1, Manila	5–10 May 1989
INN	INSTAC-1, Narita	5–10 May 1989
INS	INSTAC-1, Saipan	5–10 May 1989
INY	INSTAC-1, Yao	5–10 May 1989
INY	INSTAC-1, Yap	5–10 May 1989
MLA	MLOPEX-2	22 Apr–11 May 1992
OCA	OCTA (60, -5)	Spring 1993
OCB	OCTA (55,-10)	Spring 1993
OCC	OCTA (50, -5)	Spring 1993
OCD	OCTA (45,-25)	Spring 1993
OCE	OCTA (45,-20)	Spring 1993
OCF	OCTA (65, -5)	Spring 1994
OCG	OCTA (55,-10)	Spring 1994
OCH	OCTA (50,-10)	Spring 1994
OCI	OCTA (50, -5)	Spring 1994
OCJ	OCTA (45,-20)	Spring 1994
OCK	OCTA (45,-15)	Spring 1994
OCL	OCTA (45,-10)	Spring 1994
OCM	OCTA (40,-25)	Spring 1994
OCN	OCTA (40,-20)	Spring 1994
PBC	PEMWEST-B	7 Feb–14 Mar 1994
PBD	PEMWEST-B	7 Feb–14 Mar 1994
PBE	PEMWEST-B	7 Feb–14 Mar 1994
PBG	PEMWEST-B	7 Feb–14 Mar 1994
PBH	PEMWEST-B	7 Feb–14 Mar 1994
PBI	PEMWEST-B	7 Feb–14 Mar 1994
PBJ	PEMWEST-B	7 Feb–14 Mar 1994
PBK	PEMWEST-B	7 Feb–14 Mar 1994
PBL	PEMWEST-B	7 Feb–14 Mar 1994
PBM	PEMWEST-B	7 Feb–14 Mar 1994
PBO	PEMWEST-B	7 Feb–14 Mar 1994
PBP	PEMWEST-B	7 Feb–14 Mar 1994
PBQ	PEMWEST-B	7 Feb–14 Mar 1994
PBR	PEMWEST-B	7 Feb–14 Mar 1994
PBS	PEMWEST-B	7 Feb–14 Mar 1994

For the OCTA data, the coordinates of the southwest corner of each region are given.

2.1. *Measurement techniques*

The NO measurements presented here were made using one of two methods: ozone chemiluminescence (O_3–CL) or photofragmentation two-photon laser-induced fluorescence (TP/LIF). In O_3–CL ozone is added to the sample stream, reacting with NO to form an excited state NO_2 (NO_2^*) and the photons emitted from its decay are detected (Ridley and Howlett, 1974). Detection of NO by TP/LIF requires the laser excitation of rotational–vibrational transitions of NO (at 226 nm and 1.1 μm) and the resulting fluorescence is detected at 187 nm (Sandholm *et al.*, 1990).

NO_2 is generally measured by photolyzing NO_2 (at 300–400 nm) to NO, followed by NO detection, as described above (Kley and McFarland, 1980). In most cases a Xe arc lamp (of 300, 500 or 1000 W) is used for photolysis, but a XeF laser has also been used (Sandholm *et al.*, 1990).

Two methods have been used for the conversion of NO_y species to NO in the data shown here. In most cases, a heated gold tube catalyst with a reducing agent of CO (Bollinger *et al.*, 1983; Fahey *et al.*, 1985) or H_2 (e.g. Munger *et al.*, 1996) has been used. A molybdenum (MoO) catalyst has also been used in several cases (Luke and Dickerson, 1987). Extensive work has been done over the years to fully characterize various NO_y catalysts and to determine the conversion efficiencies of many gases (cf. Fehsenfeld *et al.*, 1987; Crosley, 1994) and particulate nitrates (Nunnermacker, 1990). Recent studies indicate that C–N bonded species (e.g. HCN) are converted with varying efficiencies depending on humidity and condition of the converter (Kliner *et al.*, 1997; Kondo *et al.*, 1997b; J. Bradshaw, personal communication). Therefore, questions have arisen regarding the lack of specificity for measurements of the NO_{yi} species of interest, and the significance of previously obtained free tropospheric NO_y measurements is not fully understood. In light of this concern, previously published (or in press) NO_y data from the ABLE-3A, -3B, CITE-3, PEM West-A, -B and TRACE-A campaigns are not used here.

In the descriptions of the data sets below, the specifics of the measurement techniques will not be discussed if they have been previously published. The

Table 3. Legend for 3–6 km data

Code	Campaign/site	Date
JJA		
3AA	ABLE 3A, Canadian Arctic	7 Jul–17 Aug 1988
3AL	ABLE 3A, Bethel	24 Jul–11 Aug 1988
3AN	ABLE 3A, Northeast U.S	Jul 7–Aug 17, 1988
3AO	ABLE 3A, Ontario	7 Jul–17 Aug 1988
3AW	ABLE 3A, Barrow	10 Jul–24 Jul 1988
3BH	ABLE 3B, Hudson Bay	6 Jul–30 Jul 1990
3BL	ABLE 3B, Labrador	30 Jul–14 Aug 1990
3BN	ABLE 3B, New England	6 Jul–15 Aug 1990
A2A	ABLE-2A	11 Jul–13 Aug 1985
C2C	CITE-2, CA flights	11 Aug–5 Sep 1986
C2F	CITE-2, Ferry flights: VA–CO	11 Aug–5 Sep 1986
C2O	CITE-2, Ocean flights	11 Aug–5 Sep 1986
C3W	CITE-3, Wallops flights	22 Aug–1 Sep 1989
ELC	ELCHEM	27 Jul–22 Aug 1989
ML2	MLOPEX 2 (ground)	15 Jul–15 Aug 1992
OCA	OCTA (45,-10)	Summer 1993
OCB	OCTA (40,-10)	Summer 1993
OCC	OCTA (35,-10)	Summer 1993
OCD	OCTA (35,-5)	Summer 1993
OCE	OCTA (30,-10)	Summer 1993
OCF	OCTA (30,-5)	Summer 1993
OCG	OCTA (45,-60)	Summer 1993
OCH	OCTA (40,-65)	Summer 1993
OCI	OCTA (40,-60)	Summer 1993
OCJ	OCTA (45,-55)	Summer 1993
OCK	OCTA (45,-50)	Summer 1993
OCL	OCTA (45,-45)	Summer 1993
OCM	OCTA (40,-45)	Summer 1993
OCN	OCTA (40,-40)	Summer 1993
ST1	STRATOZ 3, Europe 40–60°N	4–26 June 1984
ST2	STRATOZ 3, S. America 15°N–15°S	4–26 June 1984
ST3	STRATOZ 3, W. S. America 15°S–40°S	4–26 June 1984
ST4	STRATOZ 3, S. America $< 40°S$	4–26 June 1984
ST5	STRATOZ 3, E. S. America 40°S–Eq	4–26 June 1984
ST6	STRATOZ 3, E. Atlantic 20–40°N	4–26 June 1984
SUM	Summit, Greenland (ground)	4 May–19 July 1995
SON		
C3N	CITE-3, Natal, Brazil	12–28 Sep 1989
ML2	MLOPEX 2 (ground)	15 Sep–23 Oct 1991
PAC	PEMWEST-A	16 Sep–21 Oct 1991
PAD	PEMWEST-A	16 Sep–21 Oct 1991
PAE	PEMWEST-A	16 Sep–21 Oct 1991
PAF	PEMWEST-A	16 Sep–21 Oct 1991
PAG	PEMWEST-A	16 Sep–21 Oct 1991
PAH	PEMWEST-A	16 Sep–21 Oct 1991
PAI	PEMWEST-A	16 Sep–21 Oct 1991
PAJ	PEMWEST-A	16 Sep–21 Oct 1991
PAK	PEMWEST-A	16 Sep–21 Oct 1991
PAM	PEMWEST-A	16 Sep–21 Oct 1991
PAN	PEMWEST-A	16 Sep–21 Oct 1991
TAF	TRACE-A, S. Africa	3–11 Oct 1992
TAM	TRACE-A, E. South America	24 Sep–3 Oct 1992
TAT	TRACE-A, Trop. S. Atlantic	11–24 Oct 1992
DJF		
A1C	AASE 1, W. U.S.	2 Jan–15 Feb 1989
A1N	AASE 1, Norway	2 Jan–15 Feb 1989
A2A	AASE 2, Alaska	11 Jan–20 Mar 1992
A2C	AASE 2, West. U.S.	11 Jan–20 Mar 1992
A2M	AASE 2, Maine	11 Jan–20 Mar 1992
A2N	AASE 2, Norway	11 Jan–20 Mar 1992
A2P	AASE 2, Arctic	11 Jan–20 Mar 1992
A2T	AASE 2, Tahiti	11 Jan–20 Mar 1992
ML2	MLOPEX 2 (ground)	15 Jan–15 Feb 1992
OCA	OCTA (55,5)	Winter 1994
OCB	OCTA (50,0)	Winter 1994

Table 3. (Continued)

Code	Campaign/site	Date
OCC	OCTA (50,5)	Winter 1994
OCD	OCTA (40,-10)	Winter 1994
OCE	OCTA (45,-5)	Winter 1994
T10	TROPOZ 2, W. Africa 0–20°N	9 Jan–1 Feb 1991
T11	TROPOZ 2, E. Atlantic 20–40°N	9 Jan–1 Feb 1991
TR1	TROPOZ 2, Europe 40–60°N	9 Jan–1 Feb 1991
TR2	TROPOZ 2, Greenland 60–70°N	9 Jan–1 Feb 1991
TR3	TROPOZ 2, E. Canada 40–60°N	9 Jan–1 Feb 1991
TR4	TROPOZ 2, W. Atlantic 15–40°N	9 Jan–1 Feb 1991
TR5	TROPOZ 2, S. America 15°N–15°S	9 Jan–1 Feb 1991
TR6	TROPOZ 2, W. S. America 15°S–40°S	9 Jan–1 Feb 1991
TR7	TROPOZ 2, S. America < 40°S	9 Jan–1 Feb 1991
TR8	TROPOZ 2, E. S. America 40°S–15°S	9 Jan–1 Feb 1991
TR9	TROPOZ 2, NE S. America 15°S–5°N	9 Jan–1 Feb 1991
MAM		
A2B	ABLE-2B	1 Apr–13 May 1987
INB	INSTAC-1, Biak–Manila	5–10 Mar 1989
INM	INSTAC-1, Manila–Narita	5–10 Mar 1989
INN	INSTAC-1, Narita–Saipan	5–10 Mar 1989
INS	INSTAC-1, Saipan–Biak	5–10 Mar 1989
ML1	MLOPEX 1 (ground)	1 May–4 June 1988
ML2	MLOPEX 2 (ground)	15 Apr–15 May 1992
MLA	MLOPEX 2 flights	22 Apr–11 May 1992
OCA	OCTA (60,0)	Spring 1993
OCB	OCTA (55,-5)	Spring 1993
OCC	OCTA (55,0)	Spring 1993
OCD	OCTA (50,0)	Spring 1993
OCE	OCTA (45,-15)	Spring 1993
OCF	OCTA (45,-10)	Spring 1993
OCG	OCTA (45,-5)	Spring 1993
OCH	OCTA (65,0)	Spring 1994
OCI	OCTA (55,-5)	Spring 1994
OCJ	OCTA (50,-5)	Spring 1994
OCK	OCTA (50,0)	Spring 1994
OCL	OCTA (45,-10)	Spring 1994
OCM	OCTA (45,-5)	Spring 1994
OCN	OCTA (40,-20)	Spring 1994
OCO	OCTA (40,-15)	Spring 1994
OCP	OCTA (40,-10)	Spring 1994
PBB	PEMWEST-B	7 Feb–14 Mar 1994
PBC	PEMWEST-B	7 Feb–14 Mar 1994
PBD	PEMWEST-B	7 Feb–14 Mar 1994
PBE	PEMWEST-B	7 Feb–14 Mar 1994
PBG	PEMWEST-B	7 Feb–14 Mar 1994
PBH	PEMWEST-B	7 Feb–14 Mar 1994
PBI	PEMWEST-B	7 Feb–14 Mar 1994
PBJ	PEMWEST-B	7 Feb–14 Mar 1994
PBK	PEMWEST-B	7 Feb–14 Mar 1994
PBL	PEMWEST-B	7 Feb–14 Mar 1994
PBM	PEMWEST-B	7 Feb–14 Mar 1994
PBO	PEMWEST-B	7 Feb–14 Mar 1994
PBP	PEMWEST-B	7 Feb–14 Mar 1994
PBQ	PEMWEST-B	7 Feb–14 Mar 1994
PBR	PEMWEST-B	7 Feb–14 Mar 1994
PBS	PEMWEST-B	7 Feb–14 Mar 1994

For the OCTA data, the coordinates of the southwest corner of each region are given.

measurement method, detection limits and uncertainties for each data set are listed in Table 6.

2.2. *Surface sites*

Data from all of the surface sites, except for the MLOPEX and Summit data sets, are shown in the "boundary layer" plots, along with aircraft measurements below 0.5 km. Figure 4 shows the location of the measurements and Figs 5–7 give the statistics (mean, median, central 67 and 90%) of the data for NO, NO_x and NO_y. The ground-based measurements are discussed here (in chronological order), and all of the aircraft measurements are discussed in Section 2.3.

Table 4. Legend for 6–9 km data

Code	Campaign/site	Date
JJA		
ELC	ELCHEM	27 Jul–22 Aug 1989
OCA	OCTA (50,-40)	Summer 1993
OCB	OCTA (50,-35)	Summer 1993
OCC	OCTA (50,-30)	Summer 1993
OCD	OCTA (50,-25)	Summer 1993
OCE	OCTA (50,-15)	Summer 1993
OCF	OCTA (45,-65)	Summer 1993
OCG	OCTA (45,-60)	Summer 1993
OCH	OCTA (45,-45)	Summer 1993
OCI	OCTA (40,-70)	Summer 1993
OCJ	OCTA (40,-65)	Summer 1993
OCK	OCTA (40,-50)	Summer 1993
OCL	OCTA (40,-45)	Summer 1993
OCM	OCTA (40,-40)	Summer 1993
OCN	OCTA (40,-35)	Summer 1993
OCO	OCTA (40,-15)	Summer 1993
OCP	OCTA (35,-35)	Summer 1993
OCQ	OCTA (35,-15)	Summer 1993
ST1	STRATOZ 3, Europe 40°–60°N	4–26 June 1984
ST2	STRATOZ 3, N. S. America 15°N–15°S	4–26 June 1984
ST3	STRATOZ 3, W. S. America 15°–40°S	4–26 June 1984
ST4	STRATOZ 3, S. S. America < 40°S	4–26 June 1984
ST5	STRATOZ 3, E. S. America 40°S–Eq	4–26 June 1984
ST6	STRATOZ 3, E. Atlantic 20°–40°N	4–26 June 1984
SON		
PAC	PEMWEST-A	17 Sep–21 Oct 1991
PAD	PEMWEST-A	17 Sep–21 Oct 1991
PAE	PEMWEST-A	17 Sep–21 Oct 1991
PAF	PEMWEST-A	17 Sep–21 Oct 1991
PAG	PEMWEST-A	17 Sep–21 Oct 1991
PAH	PEMWEST-A	17 Sep–21 Oct 1991
PAI	PEMWEST-A	17 Sep–21 Oct 1991
PAJ	PEMWEST-A	17 Sep–21 Oct 1991
PAK	PEMWEST-A	17 Sep–21 Oct 1991
PAL	PEMWEST-A	17 Sep–21 Oct 1991
TAF	TRACE-A, S. Africa	3–11 Oct 1992
TAM	TRACE-A, E. South America	24 Sep–3 Oct 1992
TAT	TRACE-A, Trop. S Atlantic	11–24 Oct 1992
TUS	TRACE-A, Southern U.S.	21 Sep–26 Oct 1992
DJF		
A1C	AASE 1, Western U.S.	2 Jan–15 Feb 1989
A1G	AASE 1, Greenland	2 Jan–15 Feb 1989
A1I	AASE 1, Iceland	2 Jan–15 Feb 1989
A1N	AASE 1, Norway	2 Jan–15 Feb 1989
A2A	AASE 2, Alaska	11 Jan–20 Mar 1992
A2C	AASE 2, Western U.S.	11 Jan–20 Mar 1992
A2M	AASE 2, Northeast U.S.	11 Jan–20 Mar 1992
A2N	AASE 2, Norway	11 Jan–20 Mar 1992
A2O	AASE 2, Pacific (20°–35°N)	11 Jan–20 Mar 1992
A2P	AASE 2, Arctic > 80° N	11 Jan–20 Mar 1992
A2R	AASE 2, Canadian Arctic	11 Jan–20 Mar 1992
A2T	AASE 2, Tahiti	11 Jan–20 Mar 1992
OCA	OCTA (55, 0)	Winter 1994
OCB	OCTA (45,-15)	Winter 1994
OCC	OCTA (40,-15)	Winter 1994
T10	TROPOZ 2, W. Africa 0°–20°N	9 Jan–1 Feb 1991
T11	TROPOZ 2, E. Atlantic 20°–40°N	9 Jan–1 Feb 1991
TR1	TROPOZ 2, Europe 40°–60°N	9 Jan–1 Feb 1991
TR2	TROPOZ 2, Greenland 60°–70°N	9 Jan–1 Feb 1991
TR3	TROPOZ 2, E. Canada 40°–60°N	9 Jan–1 Feb 1991
TR4	TROPOZ 2, W. Atlantic 15°–40°N	9 Jan–1 Feb 1991
TR5	TROPOZ 2, N. S. America 15°N–15°S	9 Jan–1 Feb 1991
TR6	TROPOZ 2, W. S. America 15°–40°S	9 Jan–1 Feb 1991
TR7	TROPOZ 2, S. S. America < 40°S	9 Jan–1 Feb 1991
TR8	TROPOZ 2, E. S. America 40°–15°S	9 Jan–1 Feb 1991

Table 4. (Continued)

Code	Campaign/site	Date
TR9	TROPOZ 2, NE S.America 15°S–5°N	9 Jan–1 Feb 1991
MAM		
OCA	OCTA (60,-10)	Spring 1993
OCB	OCTA (55,-10)	Spring 1993
OCC	OCTA (55, -5)	Spring 1993
OCD	OCTA (50,-10)	Spring 1993
OCE	OCTA (50, -5)	Spring 1993
OCF	OCTA (45,-20)	Spring 1993
OCG	OCTA (45,-10)	Spring 1993
OCH	OCTA (65, -5)	Spring 1994
OCI	OCTA (60, -5)	Spring 1994
OCJ	OCTA (55,-10)	Spring 1994
OCK	OCTA (55, -5)	Spring 1994
OCL	OCTA (50,-10)	Spring 1994
OCM	OCTA (50, -5)	Spring 1994
OCN	OCTA (45,-15)	Spring 1994
OCO	OCTA (45,-10)	Spring 1994
OCP	OCTA (40,-20)	Spring 1994
OCQ	OCTA (40,-15)	Spring 1994
PBB	PEMWEST-B	7 Feb–14 Mar 1994
PBC	PEMWEST-B	7 Feb–14 Mar 1994
PBD	PEMWEST-B	7 Feb–14 Mar 1994
PBE	PEMWEST-B	7 Feb–14 Mar 1994
PBG	PEMWEST-B	7 Feb–14 Mar 1994
PBH	PEMWEST-B	7 Feb–14 Mar 1994
PBI	PEMWEST-B	7 Feb–14 Mar 1994
PBJ	PEMWEST-B	7 Feb–14 Mar 1994
PBK	PEMWEST-B	7 Feb–14 Mar 1994
PBL	PEMWEST-B	7 Feb–14 Mar 1994
PBM	PEMWEST-B	7 Feb–14 Mar 1994
PBN	PEMWEST-B	7 Feb–14 Mar 1994
PBO	PEMWEST-B	7 Feb–14 Mar 1994
PBP	PEMWEST-B	7 Feb–14 Mar 1994
PBQ	PEMWEST-B	7 Feb–14 Mar 1994
PBR	PEMWEST-B	7 Feb–14 Mar 1994
PBS	PEMWEST-B	7 Feb–14 Mar 1994

For the OCTA data, the coordinates of the southwest corner of each region are given.

ABLE-2B: Tower. The Amazon Boundary Layer Expedition (ABLE-2) consisted of two phases (wet and dry seasons) of ground and airborne measurements made in the same region near Manaus, Brazil (described further in Section 2.3). Ground measurements during the wet season, ABLE-2B, were made from 1 April to 13 May, 1987 (see Harriss *et al.*, 1990 for an overview, in the special issue of *J. geophys. Res.*, 20 September 1990).

NO, NO_y and O_3 measurements were made from a tower in the Ducke Forest Reserve (2°56′S, 59°57.7′W), 40 km north of Manaus, Brazil (Bakwin *et al.*, 1990a, b). Other measurements made on the ground, but not on the tower, included CH_4, N_2O, CO_2, CO, aerosols, isoprene and sulfur compounds. NO and O_3 were measured from eight levels, and NO_y at two levels, on a 43 m tower. Measurements from the highest inlets, 41 m for NO and 39 m for NO_y, were used for the summaries shown here. The NO detector was a modified TECO-14A. NO_y was converted to NO and then NO_2, which was measured by a Scintrex LMA-3 luminol-based detector.

The values of NO_y measured were very low during the wet season (450 pptv), and soil emissions of NO were weak. It was found that the tropical forest acts as a net sink for NO_y, thus reducing atmospheric levels of NO and, consequently, O_3 (Bakwin *et al.*, 1990b).

ABLE-3A: Bethel Tower. As part of the Arctic Boundary Layer Experiment 3A campaign measurements of NO, NO_2 and NO_y were made from a tower site at Bethel, Alaska (61°5′N, 162°1′W), from 10 July to 12 August, 1988 (Bakwin *et al.*, 1992). NO and NO_2 were sampled at eight levels on a 12 m tower, but only data from the inlet at 10.8 m are shown here. NO and NO_2 were measured alternately with a single O_3-chemiluminescent detector, with an averaging time of 2 min for each, every half hour. NO_y was catalyzed to NO and detected by a luminol-based NO_2 detector. Also measured from the tower were profiles of O_3, CO_2, and CH_4, eddy correlation flux measurements of O_3, CO_2, CH_4, and NO_y, as well as water vapor, winds and temperature. It was found that the tundra ecosystem is a net sink for nitrogen species, and that high values of NO_x and NO_y had

Table 5. Legend for 9–12 km data

Code	Campaign/site	Date
JJA		
ELC	ELCHEM	27 Jul–22 Aug 1989
ST1	STRATOZ 3, Europe 40°–60°N	4–26 June 1984
ST2	STRATOZ 3, Greenland 60°–70°N	4–26 June 1984
ST3	STRATOZ 3, N. S. America 15°N–15°S	4–26 June 1984
ST4	STRATOZ 3, W. S. America 15°S–40°S	4–26 June 1984
ST5	STRATOZ 3, S. S. America < 40°S	4–26 June 1984
ST6	STRATOZ 3, E. S. America 40°S–Eq	4–26 June 1984
ST7	STRATOZ 3, Atlantic 0°–20°N	4–26 June 1984
ST8	STRATOZ 3, E. Atlantic 20°–40°N	4–26 June 1984
SON		
PAD	PEMWEST-A	17 Sep–21 Oct 1991
PAF	PEMWEST-A	17 Sep–21 Oct 1991
PAH	PEMWEST-A	17 Sep–21 Oct 1991
PAL	PEMWEST-A	17 Sep–21 Oct 1991
PAM	PEMWEST-A	17 Sep–21 Oct 1991
PAN	PEMWEST-A	17 Sep–21 Oct 1991
PAP	PEMWEST-A	17 Sep–21 Oct 1991
TAF	TRACE-A, S. Africa	21 Sep–26 Oct 1992
TAM	TRACE-A, E. S. America	21 Sep–26 Oct 1992
TAT	TRACE-A, Tropical S Atlantic	21 Sep–26 Oct 1992
TCB	TRACE-A, Carribean	21 Sep–26 Oct 1992
TNA	TRACE-A, Tropical N Atlantic	21 Sep–26 Oct 1992
TSA	TRACE-A, S. Atlantic (30°–40°S)	21 Sep–26 Oct 1992
TUS	TRACE-A, Southern U.S.	21 Sep–26 Oct 1992
DJF		
A1C	AASE 1, Western U.S.	2 Jan–15 Feb 1989
A1G	AASE 1, Greenland	2 Jan–15 Feb 1989
A1I	AASE 1, Iceland	2 Jan–15 Feb 1989
A1N	AASE 1, Norway	2 Jan–15 Feb 1989
A1P	AASE 1, Above 78°N	2 Jan–15 Feb 1989
A2A	AASE 2, Alaska	11 Jan–20 Mar 1992
A2C	AASE 2, Western U.S.	11 Jan–20 Mar 1992
A2E	AASE 2, Pacific 15°S–20°N	11 Jan–20 Mar 1992
A2I	AASE 2, Iceland	11 Jan–20 Mar 1992
A2L	AASE 2, Atlantic	11 Jan–20 Mar 1992
A2M	AASE 2, Northeast U.S.	11 Jan–20 Mar 1992
A2N	AASE 2, Norway	11 Jan–20 Mar 1992
A2O	AASE 2, Pacific 20°–35°N	11 Jan–20 Mar 1992
A2R	AASE 2, Canadian Arctic	11 Jan–20 Mar 1992
A2T	AASE 2, Tahiti	11 Jan–20 Mar 1992
T11	TROPOZ 2, E. Atlantic 20°–40°N	9 Jan–1 Feb 1991
TR1	TROPOZ 2, Europe 40°–60°N	9 Jan–1 Feb 1991
TR2	TROPOZ 2, Greenland 60°–70°N	9 Jan–1 Feb 1991
TR3	TROPOZ 2, E. Canada 40°–60°N	9 Jan–1 Feb 1991
TR4	TROPOZ 2, W. Atlantic 15°–40°N	9 Jan–1 Feb 1991
TR5	TROPOZ 2, N. S. America 15°N–15°S	9 Jan–1 Feb 1991
TR6	TROPOZ 2, W. S. America 15°–40°S	9 Jan–1 Feb 1991
TR7	TROPOZ 2, S. S. America < 40°S	9 Jan–1 Feb 1991
TR8	TROPOZ 2, E. S. America 40°–15°S	9 Jan–1 Feb 1991
TR9	TROPOZ 2, NE S. America 15°S–5°N	9 Jan–1 Feb 1991
MAM		
OCA	OCTA (55,-10)	Spring 1993
OCB	OCTA (50, -5)	Spring 1994
PBA	PEMWEST-B	7 Feb–14 Mar 1994
PBD	PEMWEST-B	7 Feb–14 Mar 1994
PBE	PEMWEST-B	7 Feb–14 Mar 1994
PBI	PEMWEST-B	7 Feb–14 Mar 1994
PBL	PEMWEST-B	7 Feb–14 Mar 1994
PBM	PEMWEST-B	7 Feb–14 Mar 1994

For the OCTA data, the coordinates of the southwest corner of each region are given.

Table 6. Summary of measurement techniques used for each campaign, with detection limits, overall uncertainty and the integration time used for determining those. Other details of each campaign are discussed in the text

Site	Species	Measurement technique[a]	DL (pptv)	Uncertainty[b]	Integ. Time
STRATOZ 3	NO	O_3–CL	6	15%	3 min
ABLE-2A Flights	NO	O_3–CL		5 pptv + 15%	40 s
ABLE-2B Tower	NO	O_3–CL	40		2 min
	NO_y	Au@300°w/H_2	15		1 min
ABLE-2B Flights	NO	O_3–CL			
CITE-2	NO	O_3–CL	2	p: 3 pptv	1 min
(NOCAR)	NO_2	UV Phot.	9	p: 10 pptv	1 min
	NO_y	Au@300°C w/CO	10	15%	1 min
ABLE-3A Tower	NO	O_3–CL	2–3	p: 10%	1 min
(Bethel)	NO_2	UV Phot.	5	p: 25%	1 min
	NO_y	Au@300°C w/ H_2	3	p: 20%	1 min
ABLE-3A Flights	NO	TP/LIF	3	16%	3 min
	NO_2	XeF laser	8	18%	3 min
MLOPEX 1	NO	O_3–CL	2	31%	1 min
	NO_2	UV Phot.(500W)	4	25%	1 min
	NO_y	Au@300°C w/CO	10	15%	1 min
Shenandoah	NO	O_3–CL	10–20		20 s
	NO_y	MoO@375°C		30%	
TOR/Schauinsland	NO	O_3–CL	20–40		1 min
	NO_x	UV Phot.	30–70		1 min
	NO_y	Au@300°C w/CO	30–70		1 min
CITE-3	NO	TP/LIF	2.5	16%	3 min
	NO_2	UV Phot.(1 kW)	12	18%	3 min
AASE 1	NO	O_3–CL	2–4	12%	1 min
	NO_2	UV Phot.	4–8	12%	1 min
	NO_y	Au@300°C w/CO	10	15%	10 s
	(lower values for < 10 km, higher for > 10 km)				
INSTAC-1	NO	O_3–CL	5	5 pptv	2 min
ELCHEM	NO	O_3–CL	5–11	15–27%	2 s
	NO_2	UV Phot.	9–20	16–27%	14 s
	NO_y	Au@300°C w/CO	7–15	6–11%	2 s
	(lower values for 0–4 km, higher for 12 km)				
Barrow	NO	O_3–CL	9	6% or 10 pptv	40 s
	NO_y	Au@300°C w/CO	14	$^{+26}_{-6}$% or 15 pptv	20 s
ABLE-3B Tower	NO	O_3–CL	2–3	p: 10%	1 min
(Schefferville)	NO_2	UV Phot.	5	p: 25%	1 min
	NO_y	Au@300°C w/ H_2	3	p: 20%	1 min
ABLE-3B Flights	NO	TP/LIF	2	p: 25%	3 min
	NO_2	UV Phot.(1 kW)	6	p: 35%	3 min
Harvard Forest	NO	O_3–CL	50	4%	1 min
	NO_2	UV Phot.	50	4%	
	NO_y	Au@300°w/H_2	50	4%	
TROPOZ 2	NO	O_3–CL	25	15%	25 s
	NO_y		30	50 pptv + 15%	25 s
SOS/SONIA	NO	O_3–CL	20	15%	20 s
	NO_2	UV Phot.	50	25%	20 s
	NO_y	MoO@375°C		25%	20 s
Oki Island	NO	O_3–CL	5 pptv	12%	1 hr
(PEMWEST-A)	NO_y	Au@300°C w/CO		28%	
PEMWEST-A,B	NO	TP/LIF	2	p: 25%	3 min
(GIT)	NO_2	UV Phot.	6	p: 35%	3 min
AASE 2	NO	O_3–CL	2	31%	1 min
	NO_2	UV Phot.	4	25%	1 min
	NO_y	Au@300°C w/CO	10	15%	1 min
MLOPEX 2	NO	O_3–CL	0.5	0.9 pptv + 4%	1 min
(gnd)	NO_2	UV Phot.	0.5	nt: 2.5 + 4% day: 4 + 4%	1 min
	NO_y	Au@300°C w/CO			1 min
MLOPEX 2 Flights	NO_y	Au@300°C w/CO			1 min
TRACE-A	NO	TP/LIF			
	NO_2	UV Phot.			
NARE/Sable I.	NO	O_3–CL	2	19%	2 min
	NO_2	UV Phot.	9	31%	2 min
	NO_y	Au@300°C w/CO	3	26%	2 min
OCTA	NO	O_3–CL	10	10 pptv + 10%	1 min
	NO_2	Calculated	15–50	p: 17%	
	NO_y	Au@300°C w/CO	50	$^{+30}_{-13}$% or 50 pptv	1 min
Summit	NO_y	Au@300°C w/ H_2	100	20%	10 min

[a]O_3–CL: Ozone chemiluminescence; TP/LIF: Two-photon/laser-induced fluorescence; UV Phot: Photolysis by Xe arc lamp; XeF laser: Photolysis by XeF laser; Au@temp w/CO: Catalytic conversion by CO in a heated gold tube; MoO: Molybdenum catalyst.

[b]... unless preceded by 'p', indicating precision from counting ...

their origin from forest fire emissions (Harris *et al.*, 1992).

Shenandoah National Park. Measurements were made for one full year, October 1988–October 1989, in Shenandoah National Park at the Big Meadows site (38.5°N, 78.5°W, elevation 1100 m) (Doddridge *et al.*, 1991, 1992; Poulida *et al.*, 1991). O_3 and CO were also measured during this campaign and meteorological parameters were monitored by a NCAR PAM II station. This data set has not been filtered for local emissions, however, it is expected to reflect the regional distributions (Doddridge *et al.*, 1992).

A seasonal cycle in both NO and NO_y was observed, each having a maximum in winter and minimum in summer. The median mixing ratio of midday NO (9–15 LT) varied from 970 pptv in winter to 190 pptv in summer. The central 67% of the data was between 390 and 2210 pptv in winter and 120–280 in summer, showing there was much less variability in summer, as well. Less variation was observed in NO_y, with medians (central 67%) of 5.0 (2.7–8.6) and 3.5 (2.3–5.7) ppbv for winter and summer, respectively. The summer minima can be attributed to dilution by vigorous boundary layer mixing, as well as chemistry by an increase in conversion of NO to HNO_3, which is then removed by wet and dry deposition, and photochemical processing of NO to NO_2 (Doddridge *et al.*, 1992).

TOR/Schauinsland. The field-station Schauinsland (47°54′N, 7°48′E; elevation 1220 m) is operated as part of the EUROTRAC sub-project, Tropospheric Ozone Research (TOR). It is located in southwestern Germany on a saddle in the southern part of the Black Forest, surrounded by a variety of vegetation, including forests and grasslands. A ridge shields the site from direct influence of local traffic, and the 1.5 km road to the observatory is closed to public traffic. The largest precursor concentrations at Schauinsland occur with northwesterly winds, containing fresh emissions from the Rhine Valley and the city of Freiburg (about 11 km away), whereas the cleanest air reaches Schauinsland from southwest, which is from the Atlantic through southern France. Northwesterly winds are often observed during daytime in summer because of katabatic upslope flow, which brings polluted air from the Rhine valley and the city of Freiburg to the site. Southeasterly wind directions are more frequent at night and in winter.

Since the data with wind directions from northwest cannot be regarded as representative of a larger area, presented here are only measurements made under conditions of southwesterly flow, which has a frequency of occurrence of approximately 30%. These data are representative of continental background conditions over central Europe. Data collected between January 1989 and August 1994 are presented here, sorted by season.

The gas inlets and meteorological sensors are mounted 12 m above ground, about 2 m above the building. Continuous measurements at Schauinsland include O_3, NO_x, NO_y, CO, PAN, H_2O_2, particles, C_2–C_5 hydrocarbons, photolysis rates and meteorological data. For details see Volz-Thomas *et al.* (1990, 1991, 1992, 1994).

Barrow, Alaska. NO and NO_y were measured by ozone chemiluminescence from March through November of 1990 in Barrow, Alaska (Honrath and Jaffe, 1992). The monitoring site was at the NOAA/CMDL facility (71°19′N, 156°37′W, elevation 9 m) near the town of Barrow. Very conservative filtering of the data was used to remove any possible effects from local or regional pollution sources.

The long inlet line (100 cm) to the NO_y converter may have caused an under-estimation of NO_y due to deposition of HNO_3 in the line (Honrath and Jaffe, 1992). The original measurements were given as 40 s average NO values obtained approximately once per 8 min. NO_y measurements were made as 20 s averages obtained approximately once per 8 min. For this analysis 1 h averages were used, actually representing, on average, 5 min of measurement integration for NO and 2.5 min for NO_y.

Honrath and Jaffe (1992) grouped the data into four 'seasons', which are used here. The data taken during March, which are shown on the "DJF" plots here (Figs 5 and 7), had high NO_y (500–700 pptv) but low NO (5 pptv) levels. The spring transition period (April and May) showed NO_y levels dropping rapidly to roughly 200 pptv, and a pulse in NO, from the decomposition of PAN with the rise in temperature (Honrath and Jaffe, 1992). Summer (June, July, and August) had very low levels of NO_y (almost always < 100 pptv), as well as NO (generally less than 5 pptv). During the fall (September, October, and November) NO_y levels rose to 100–200 pptv, but NO remained low.

ABLE-3B: Schefferville Tower. The Arctic Boundary Layer Expedition 3B continued the study of the arctic and sub-arctic regions of North America begun in ABLE-3A, by focusing on the biosphere and atmosphere of central and eastern Canada (Harriss *et al.*, 1994 in a special issue of *J. geophys. Res.*, 20 January 1994). During ABLE-3B measurements were made from a 31 m tower at Schefferville, Quebec (55°50′N, 66°40′W), from 27 June to 16 August 1990. NO_y was sampled at 29 m, and NO and NO_2 at seven levels with only the 30.8 m data presented here (Bakwin *et al.*, 1994). Also measured on the tower were O_3, CO_2, CH_4 and hydrocarbons at several levels, with eddy correlation flux measurements of O_3, CO_2, CH_4 and NO_y at the top of the tower.

Eddy correlation flux measurements of NO_y, diel variation and flux and deposition rates of NO_x and NO_y are further discussed in Munger *et al.* (1996).

Harvard Forest. The Harvard Forest site is in Petersham, Massachusetts (42°32′N, 72°11′W), 100 km west of Boston, at an elevation of 340 m. The surroundings are rural and the immediate area is mixed deciduous forest dominated by oak.

Measurements from 1990 to 1993 are summarized here and the results of 5 years of deposition flux studies on NO_x, NO_y and O_3 are discussed in Munger *et al.* (1996).

NO and NO_2 measurements were made at 8 heights on a 30 m tower (5 m above the canopy) with a cycle time of $\approx$ 36 min and 4-minute equilibration and sampling time at each level. Data presented here are hourly averages based on approximately two observations per hour at the topmost level. The NO_y measurements were roughly continuous. Ozone was measured simultaneously with these species, and measurements of CO, CO_2 and hydrocarbons were also made during this period.

The data can be sorted according to three different flow regimes, from the northwest (270–45°), southwest (180–270°) and east (45–180°). Northwesterly flow is mainly associated with the passage of cold fronts and periods of subsiding air originating in northern Canada, and passes over a rural region. Flow from the southwest carries regional pollution generally aged at least half a day. Flow from the easterly sector is less frequent and is a mixture of air that may have passed over nearby towns and cities. For this work, data during NW and SW flows between 10 a.m. and 3 p.m. are used here, as the boundary layer is well-mixed only during midday and the influence of small local sources is minimal.

A distinct seasonal cycle can be seen in the combined NW and SW flow data for NO, NO_x and NO_y (shown in Figs 5–7). In each, a maximum is seen in winter and minimum in summer, with the spring and fall mixing ratios roughly the same. The central two-thirds of the NO_x data fall between 400 and 1200 pptv in summer, but are between 1 and 15 ppbv in winter. Midday NO medians are 90 pptv in summer, 550 in winter and about 250 in spring and fall. The variation in NO_y is not quite as large, with a median of 4.4 ppbv in winter and 2.7 ppbv in summer. The lower values in summer are due to the increased conversion of NO_x to higher oxides with increased OH levels and the presence of isoprene which may enhance the formation of PAN. The lifetime of NO is also reduced in the summer, as mentioned above in the discussion of the Shenandoah data. In addition, the boundary layer in winter is approximately half the height it is in summer, therefore reducing the volume for dilution of emissions (Munger *et al.*, 1996).

SOS/SONIA. As part of the Southern Oxidants Study, measurements were made at the SONIA (Southeastern Oxidant and Nitrogen Intensive Analysis) site in Candor, NC (35.26°N, 79.84°W, elev. 198 m), 7–18 August 1991 (Poulida *et al.*, 1994).

NO, NO_2 and NO_y, along with CO and UV flux, were measured by the University of Maryland's Air Chemistry Group. O_3 and all meteorological parameters were measured at the same site by the Environmental Protection Agency. The measurement site was in an open field (previously used for soybean crops) surrounded by deciduous and pine forest, with only small towns nearby.

The median midday NO mixing ratio was $\approx$ 100 pptv. Non-zero nighttime values were observed (30–60 pptv), indicating a local source was present, presumably the field (Poulida *et al.*, 1994). The median NO_x value was 980 pptv (central 67%: 610–2100), and NO_y ranged from 3.1 to 7.0 ppbv, with a median of 4.7 ppbv. These values are comparable to those observed at Shenandoah and other rural sites in the U.S.

MLOPEX. A large suite of measurements were made as part of the first Mauna Loa Photochemistry Experiment from 1 May to 4 June 1988. The species measured include NO, NO_2, NO_y, O_3, CO, HNO_3, NO_3^-, CO_2, CH_4, SO_2, hydrocarbons, halocarbons, peroxides, formaldehyde, alkyl and peroxyacetyl nitrates, methyl nitrate, sodium, ammonium, sulfate and organic acids. Condensation nuclei and NO_2 photolysis rates were also measured, along with meteorological parameters. An overview of the campaign is given by Ridley and Robinson (1992) in the *J. geophys. Res.* special issue, 30 June 1992.

A similar set of measurements were made during MLOPEX 2, which consisted of four 4–6 week campaigns in four seasons during 1991 and 1992 (15 September–23 October, 15 January–15 February, 15 April–15 May, 15 July–15 August), plus aircraft measurements (discussed in Section 2.3) in the spring (Atlas and Ridley, 1996 in a *J. geophys. Res.* special issue, 20 June 1996). During the day upslope local contamination can occur, so only data from downslope flow (always occurring between 10 p.m. and 10 a.m.), representative of free tropospheric air, were used here.

Measurements of NO, NO_2 and NO_y during MLOPEX 1 were consistent with previous measurements in the northern Pacific and were characteristic of well-aged maritime air, roughly 10 days from sources (Carroll *et al.*, 1992; Hübler *et al.*, 1992; Atlas *et al.*, 1992).

Measurements of NO, NO_2 and NO_y were made during all four intensives of MLOPEX 2 (e.g. Haglustaine *et al.*, 1996). Sharp spikes in the data from local automobiles, etc. were removed from the 5 s data before averaging for use here.

PEM West-A: Oki Island. Measurements of NO, NO_y, O_3, and CO were made at Oki Island, Japan (36.3°N, 133.2°E) during PEM West-A (discussed further below). Observations were made between 10 September and 21 October 1991 (Jaffe *et al.*, 1996). During the period of measurements, the wind was mainly from the north and northeast over low populations and observations were mostly of relatively clean air. On occasion, high NO_y and CO levels were observed, with high correlation indicating anthropogenic sources and were associated with flow from Japan and Korea (Jaffe *et al.*, 1996).

NARE: Sable Island. Measurements of NO, NO_2 and NO_y were made at Sable Island (59.5°W, 43.8°N) from 14 August to 6 September 1993 as part of the

North Atlantic Regional Experiment (NARE) 1993 Summer Intensive *J. geophys. Res.* special issue, 20 December 1996). Two ozone chemiluminescent detectors were used to measure NO: one with a photolytic converter upstream for detection of NO_2 alternately with NO, and a second for measurement of NO_y by gold-catalytic conversion with CO to NO (Wang *et al.*, 1996). Also measured were O_3, CO, UV radiation (Eppley radiometer), condensation nuclei, aerosols, scattering coefficients and meteorological parameters at the surface and from radiosondes.

The summaries of all the data are shown in Figs 6 and 7, however, the data were also sorted into clearly clean and clearly polluted categories. The clean data had a median of 98 pptv for NO_x and 189 pptv for NO_y, whereas the polluted category showed the NO_x median at 152 pptv, and for NO_y, 527 pptv (Wang *et al.*, 1996).

Summit, Greenland. During the 1995 field season NO_y was measured from an 18 m tower several hundred meters south of the main camp at Summit, Greenland (72.42°N, 36.67°W, elevation 3200 m). A 3-axis sonic anemometer (Gill, Solent Research Anemometer) and sampling inlets for NO_y, H_2O and O_3 measurements were mounted at 17.5 m facing the clean-air sector to the south and east. Instruments and data acquisition and control systems were housed in a covered trench at the tower base. NO_y was measured by catalysis on a heated (300°C) gold surface with H_2 and O_3-chemiluminescent detection following methods described by Bakwin *et al.* (1994) and Munger *et al.* (1996). The catalyst was mounted on the tower with no additional inlet. NO was added to the catalyst and directly upstream of the reaction cell to determine the instrument response several times per day. In addition, isopropylnitrate was added to the catalyst to monitor the conversion efficiency.

Measurements for the period 4 May–19 July 1995 are summarized here. The data are recorded at 4 Hz and initially extracted as 10 min average. Filters based on excessive variance in the 10 min mean (standard deviation greater than the mean) have been applied to exclude periods affected by camp pollution and anomalous values were rejected. The valid 10 min values are averaged to hours and used to generate the statistics.

Other continental U.S. sites. Measurements from several sites in the United States have not yet been publicly archived, but summaries of the data are available. The statistics of NO_x measurements at Niwot Ridge, CO (Parrish *et al.*, 1990), Point Arena, CA, Scotia, PA, Bondville, IL, Egbert, Ontario (Parrish *et al.*, 1993), and Kinterbush, AL have been presented by Carroll and Thompson (1995) and are included in the climatologies here. The data from these sites shown here are all from the summer: at Niwot Ridge for 1984 and 1987, at Scotia, 1986 and 1988, Bondville and Egbert, 1988, and Kinterbush, 1990.

Shipboard measurements—SAGA 3. The third Soviet–American Gases and Aerosols experiment consisted of shipboard measurements in the equatorial Pacific (overview by Johnson *et al.*, 1993 in a *J. geophys. Res.* special issue, 20 September 1993). The species and parameters measured include NO, NO_2, O_3, CO, CH_4, CO_2, N_2O, H_2O_2, hydrocarbons, alkyl nitrates, halocarbons, organic acids, photolysis rates, DMS, H_2S, HNO_3, SO_2, SO_4^{2-}, MSA, aerosols, condensation nuclei, ^{85}Kr, ^{222}Rn, ^{7}Be, ^{212}Pb.

Five transects of the equator were made between Hawaii and American Samoa between 14 February and 10 March 1990. A slight maximum in NO was seen at the equator of 4–6 pptv, with mixing ratios closer to 2–3 pptv at 8–12°S and 8–16°N (Torres and Thompson, 1993).

2.3. *Aircraft campaigns*

A number of aircraft campaigns have been made over the past 10 years, and several of them are discussed below. Results from the GTE campaigns are used in these summaries, including ABLE-2A, -2B, -3A, -3B, CITE-2, -3, PEM West-A and TRACE-A. Measurements from the DC-8 flown during the Airborne Arctic Stratospheric Expeditions (1 and 2), made during the winters of 1989 and 1992, are also included here. OCTA, sponsored by the European Commission and conducted by the U.K. Meteorological Office, consisted of flights over the North Atlantic during winter, summer and two spring seasons. The STRATOZ and TROPOZ campaigns were made during summer and winter, respectively. The flights during MLOPEX 2 are also discussed here. All of the data from the GTE campaigns are archived at NASA Langley, the AASE campaigns are available on CD, and the MLOPEX measurements have been archived by NCAR and are available from the SASS Archive. The OCTA, STRATOZ and TROPOZ campaigns have not yet been archived, so only summaries of the NO and NO_y measurements are used here.

As mentioned above, the location of measurements at each of the four altitude ranges are shown in Figs 8, 12, 16, 20, and the NO, NO_2 and NO_y data are shown in Figs 9–11, 13–15, 17–19 and 21–23. Each data region is identified in Tables 2–5.

STRATOZ-3. The STRATOZ-3 campaign started from Europe and continued to Labrador, the Caribbean, along the west and east coasts of South America, across the tropical Atlantic to the west coast of Africa and then returned to Europe. The STRATOZ measurements were made 4–26 June 1984 from a Caravelle 116 aircraft, during which NO, PAN, O_3, CO, CH_4 and light hydrocarbons were measured (Drummond *et al.*, 1988). Most of the flight time was at 12 km, with profiles measured on the takeoff and approach at airports.

ABLE-2. The Amazon Boundary Layer Expedition (ABLE-2) consisted of two phases of ground and airborne measurements made near Manaus, Brazil, designed to help begin understanding the role of the tropics in global atmospheric chemistry. Measurements during the relatively undisturbed dry season

provided a contrast for data perhaps affected by precipitation during the wet season.

The first campaign, 2A, was during the dry season, 11 July to 13 August 1985 (Harriss *et al.*, 1988 in the special issue of *J. geophys. Res.* 20 February 1988). During ABLE-2A NO, O_3, CO, CO_2, CH_4, NMHC, N_2O, dimethylsulfide, aerosols, and ozone and aerosol profiles were measured from the NASA Electra. The wet season phase (2B) took place from 1 April to 13 May 1987 (Harriss *et al.*, 1990 in the special issue of *J. geophys. Res.* 20 September 1990). Aircraft measurements during ABLE-2B were also made from the Electra and included NO, PAN, O_3, CO, sulfur compounds, aerosol and ozone profiles, CO_2, isoprene and radon.

Chemiluminescence measurements of NO were made up to 6 km during both phases (Torres and Buchan, 1988; e.g. Singh *et al.*, 1990). Mixing ratios of NO were somewhat lower during the wet season (2B) than the dry. During 2A most of the measurements were less than 50 pptv, whereas during the wet season values were less than 20 pptv for all altitudes (most of the data were obtained below 4.5 km during 2B). NO values decreased slightly with altitude (up to 6 km) during phase 2A.

CITE-2. The second Chemical Instrumentation Test and Evaluation campaign included ferry flights from Wallops to California with several flights from Ames over the Pacific and the continent from 11 August to 5 September 1986 (Hoell *et al.*, 1990 in special issue of *J. geophys. Res.* 20 June 1990). This intercomparison focused on NO and NO_2 measurements (as well as HNO_3 and PAN), so included several instruments measuring these species; the NOCAR (NOAA and NCAR) results are presented here (Carroll *et al.*, 1990a), along with NO_y measurements by NOAA (Hübler *et al.*, 1992). Other species and parameters sampled from the NASA Electra include O_3, CO, hydrocarbons, CFC-11, aerosols and UV flux.

The data shown here are sorted only by geographical location and not by airmass origin, as was done in Carroll *et al.* (1990a). As expected, distinctly higher values of NO, NO_x and NO_y are seen over the continent than the ocean below 3 km, but the difference is much less in the 3–6 km bin.

ABLE-3A. The airborne measurements of ABLE-3A were made from the NASA Wallops Electra from 7 July to 17 August 1988. Most of the flights were clustered near Bethel and Barrow, but ferry flights were also made over northern and eastern Canada (overview by Harris *et al.*, 1992 in the special issue of *J. geophys. Res.*, 30 October 1992). NO, NO_2, NO_y, O_3, PAN, NMHC, CO, CH_4, HNO_3, aerosols, organic acids, radon and profiles of O_3 and aerosols were measured below 6 km.

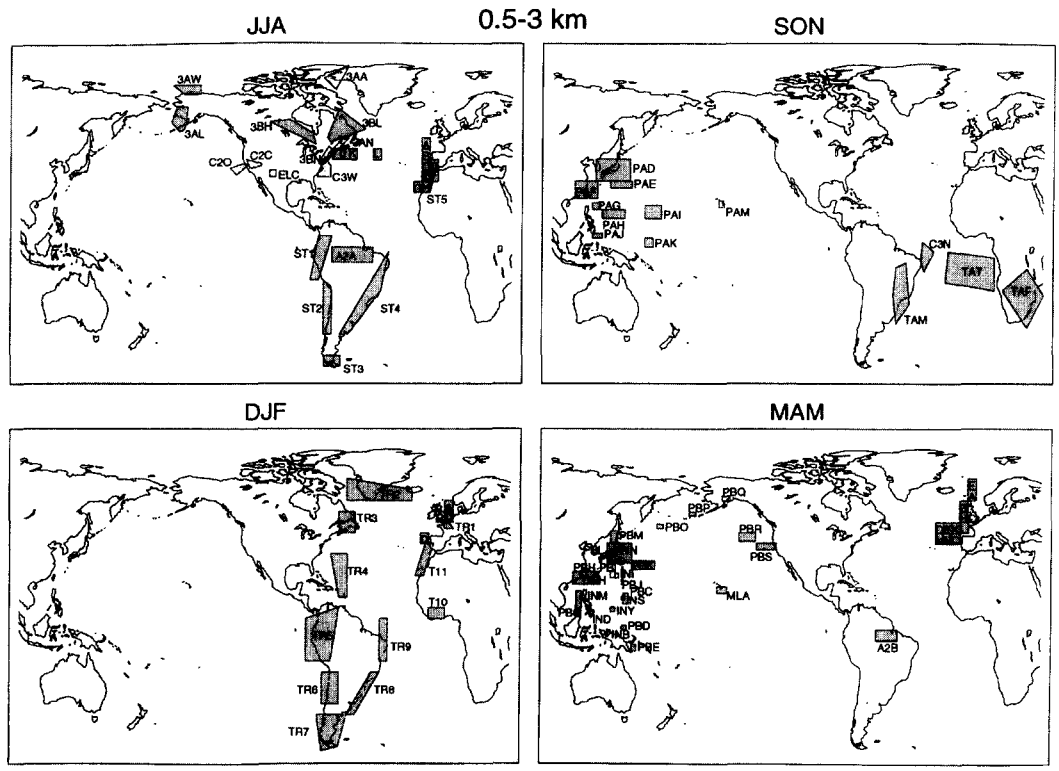

Fig. 8. Location of 0.5–3 km data. Three-character codes are identified in Table 2. Single letters in small boxes are OCTA data, which are prefixed with OC in the data plots and legend.

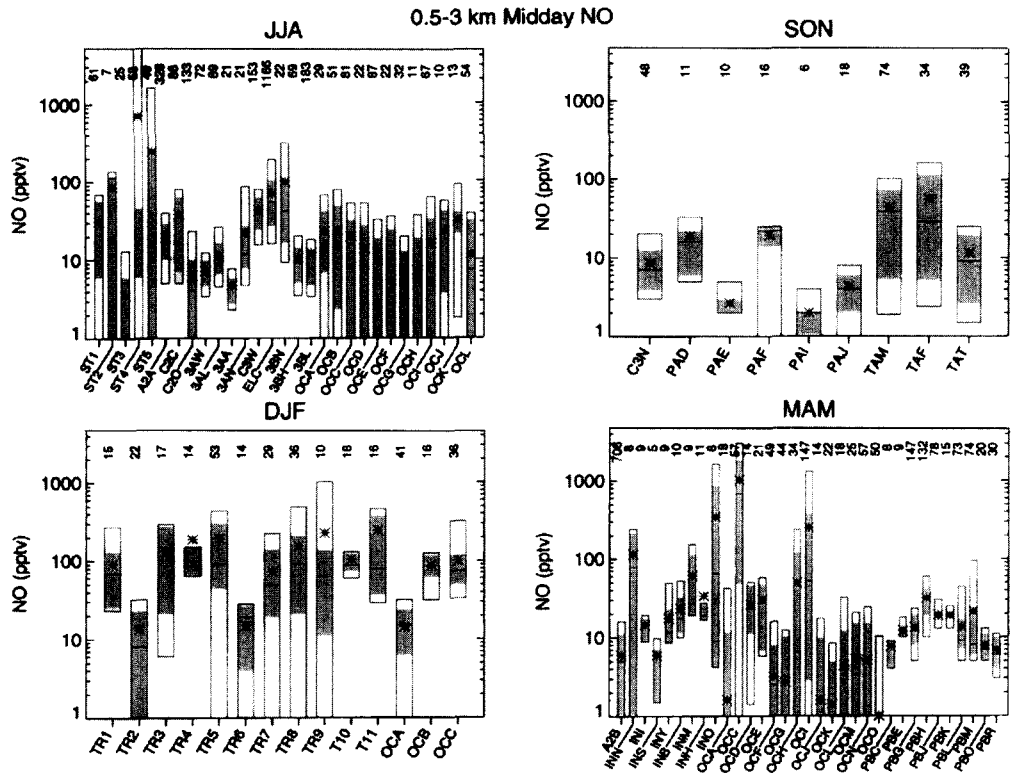

Fig. 9. Midday NO distributions for four seasons for 0.5–3 km. Three-character codes match those on Fig. 8, and are identified in Table 2.

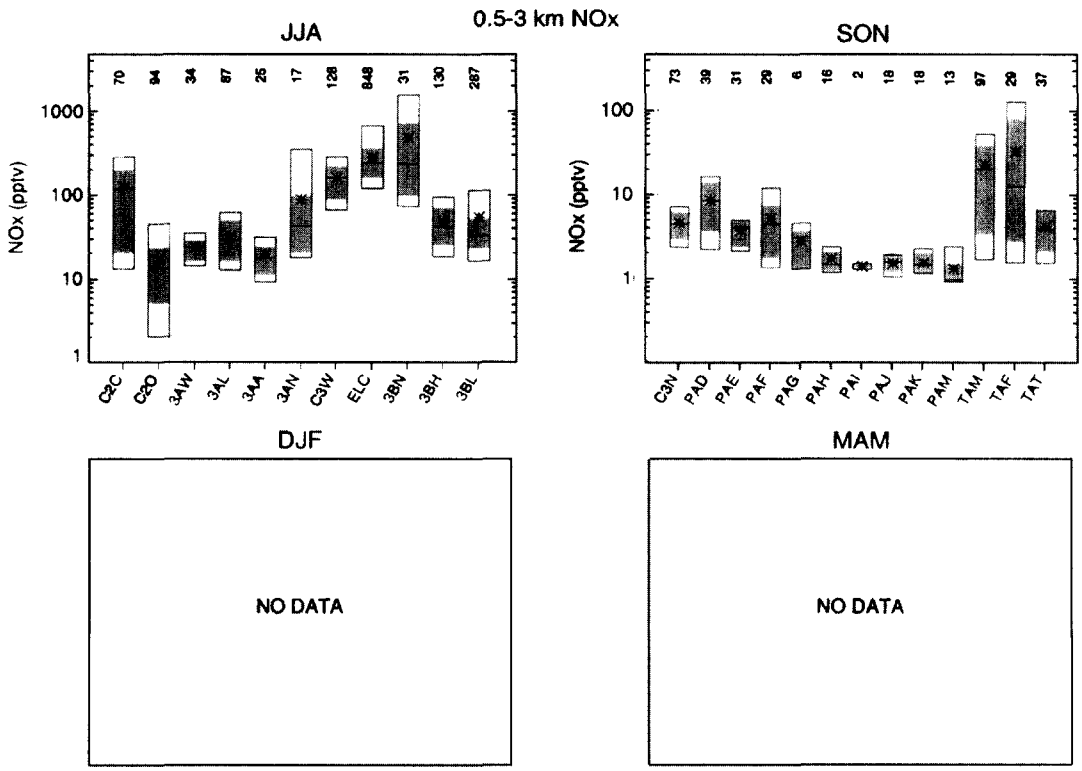

Fig. 10. NO_x distributions for 0.5–3 km.

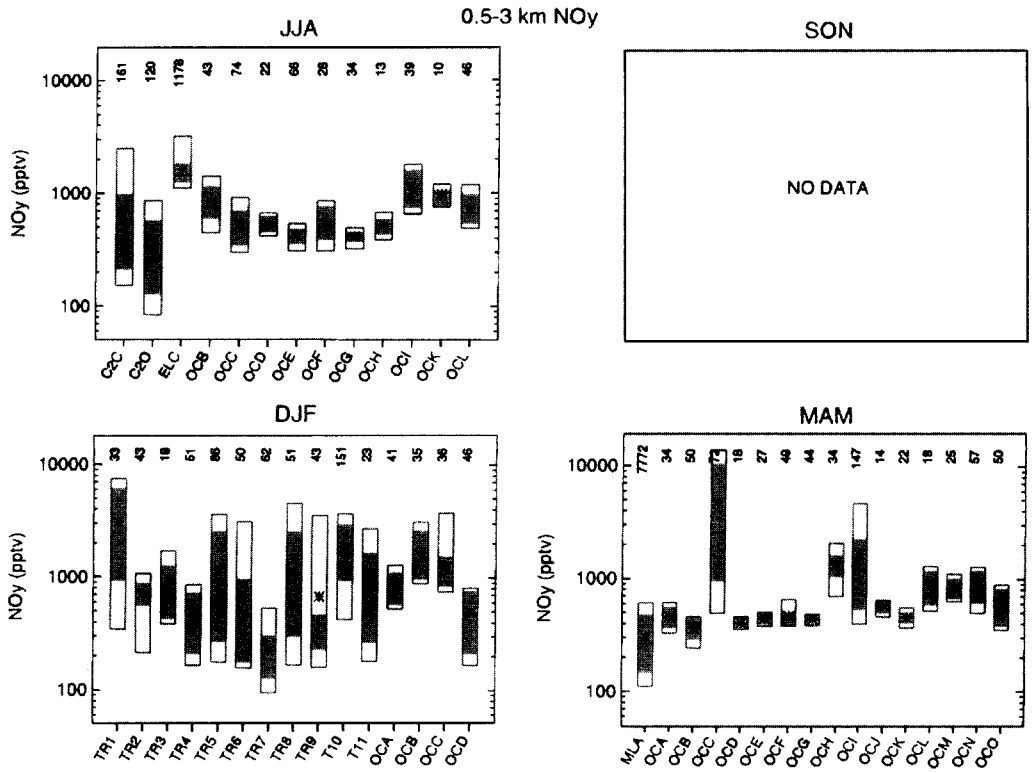

Fig. 11. NO_y distributions for 0.5–3 km.

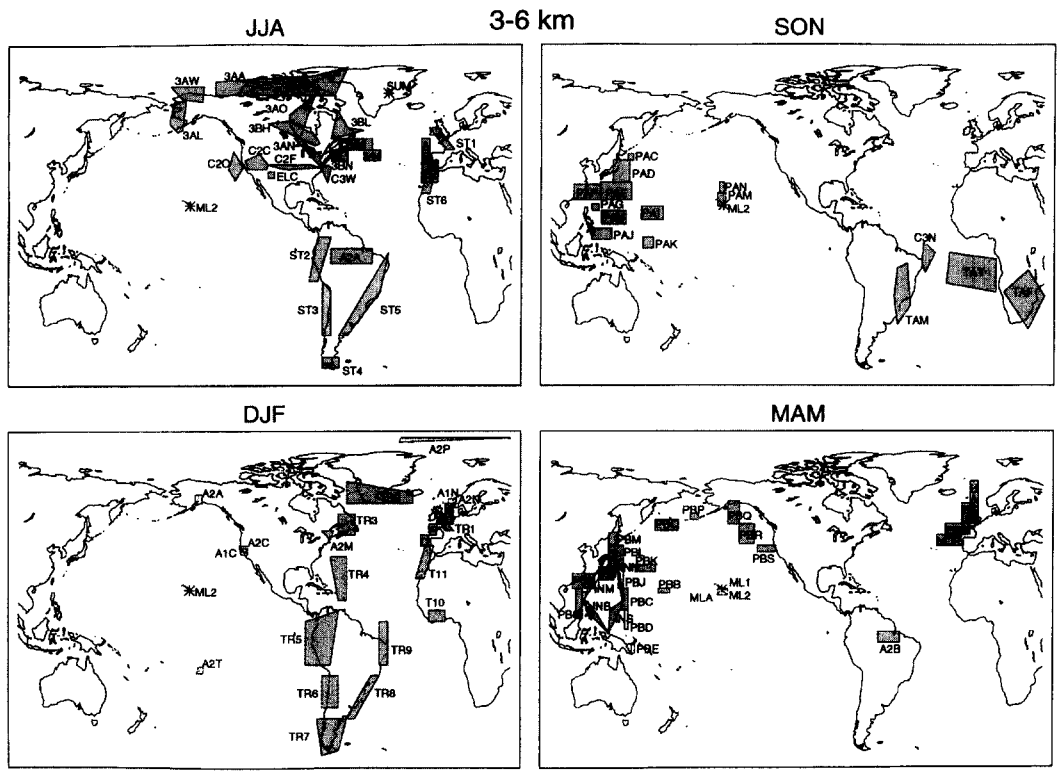

Fig. 12. Location of 3–6 km data. OCTA data are identified by single letters. Three-character codes are identified in Table 3.

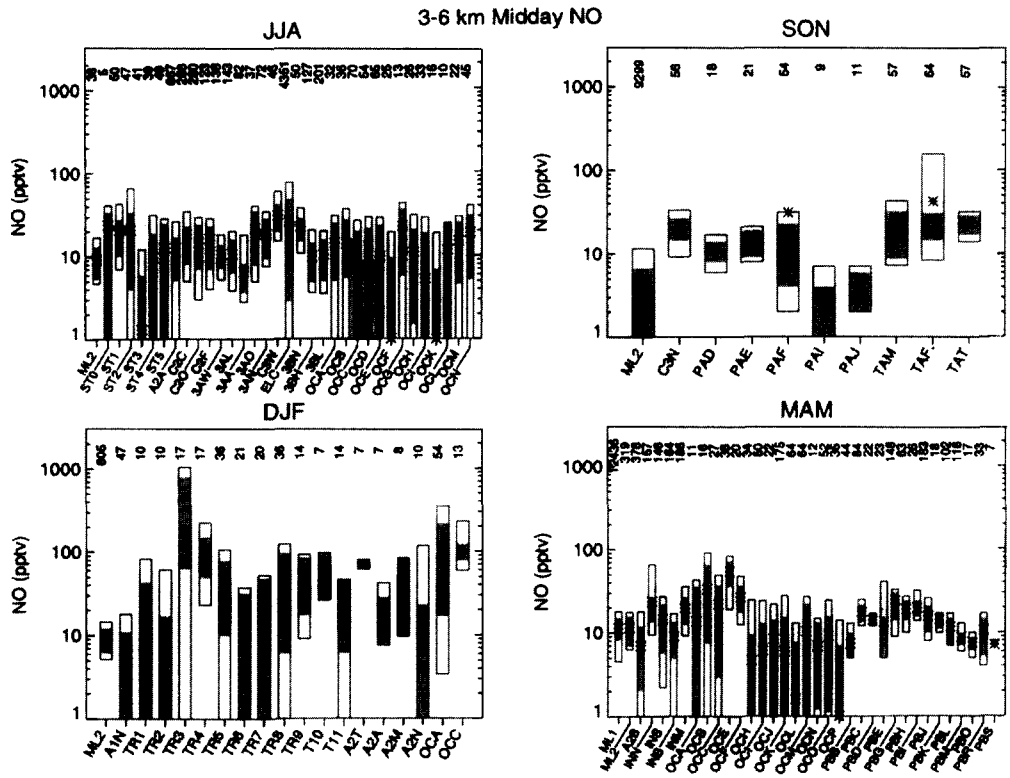

Fig. 13. Midday NO distributions for four seasons for 3–6 km. Three-character codes match those on Fig. 12, and are identified in Table 3.

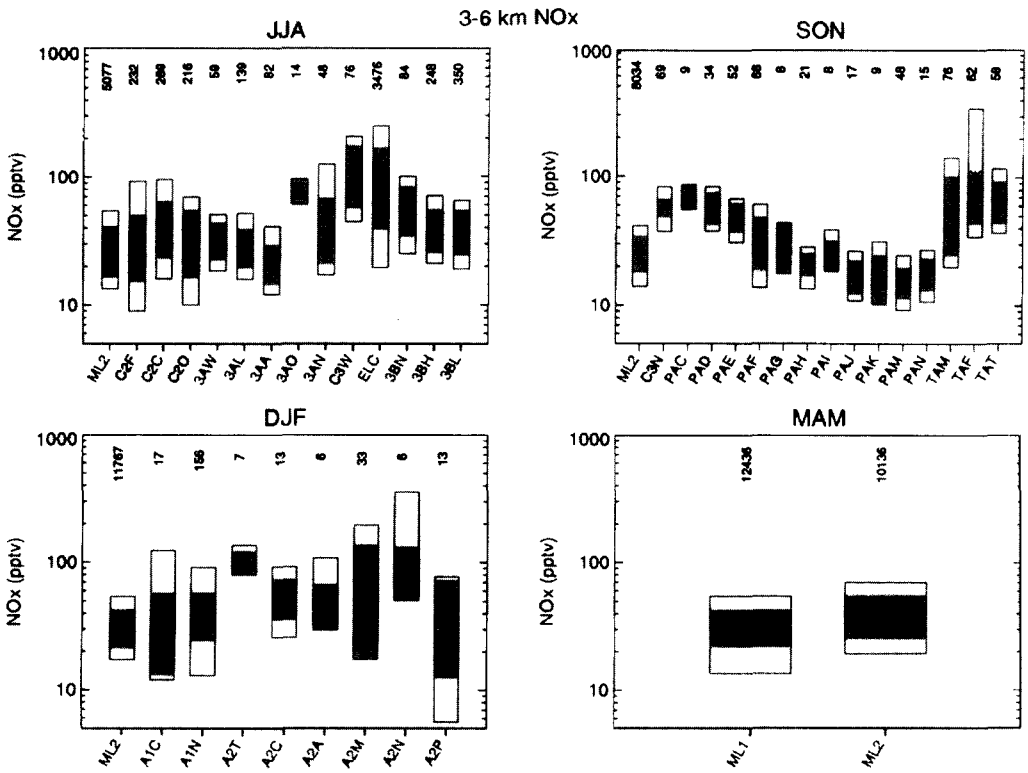

Fig. 14. NO_x distributions for 3–6 km.

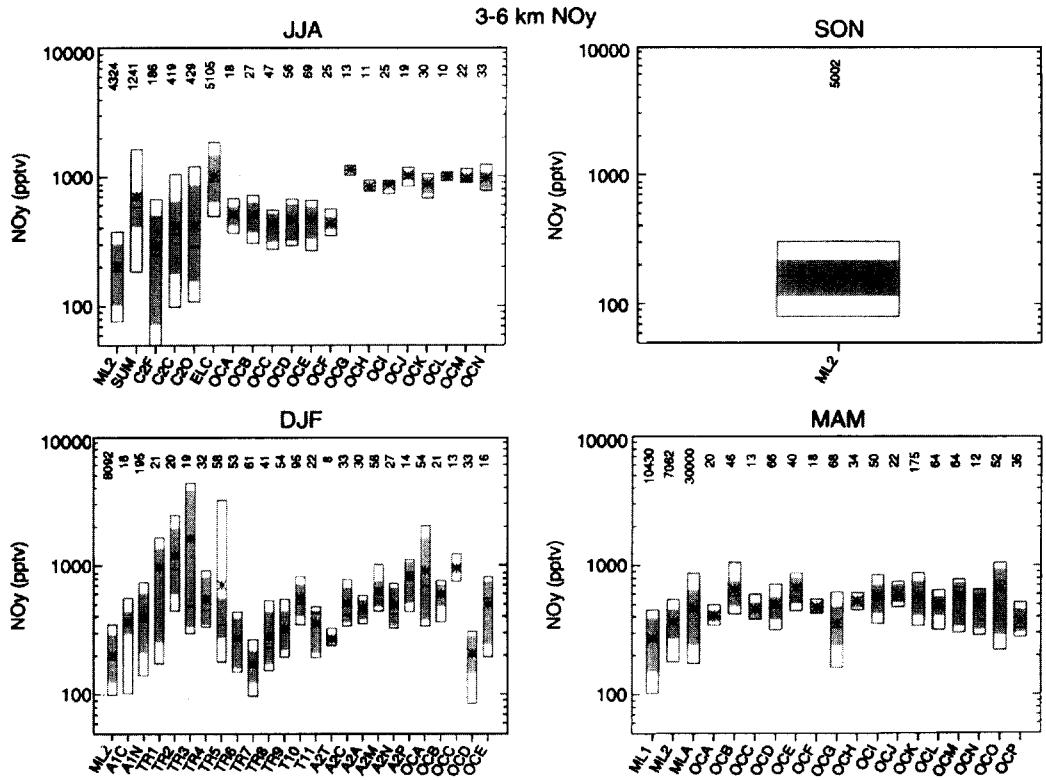

Fig. 15. NO_y distributions for 3–6 km.

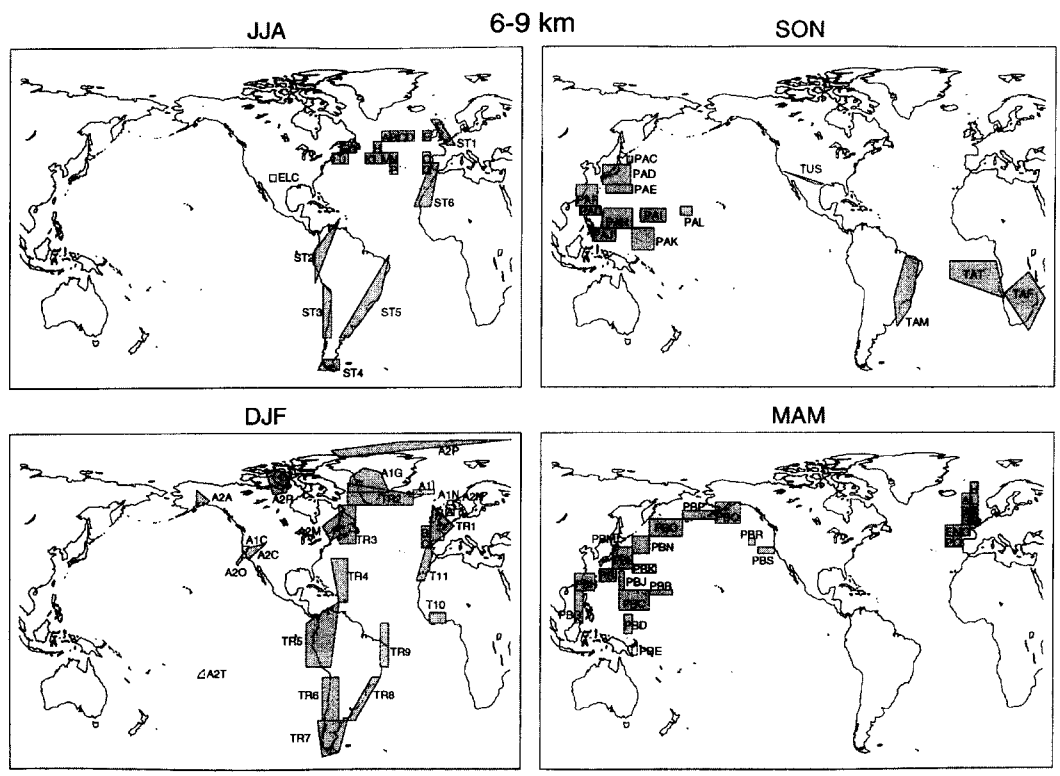

Fig. 16. Location of 6–9 km data. Three-character codes are identified in Table 4. OCTA data are identified by single letter

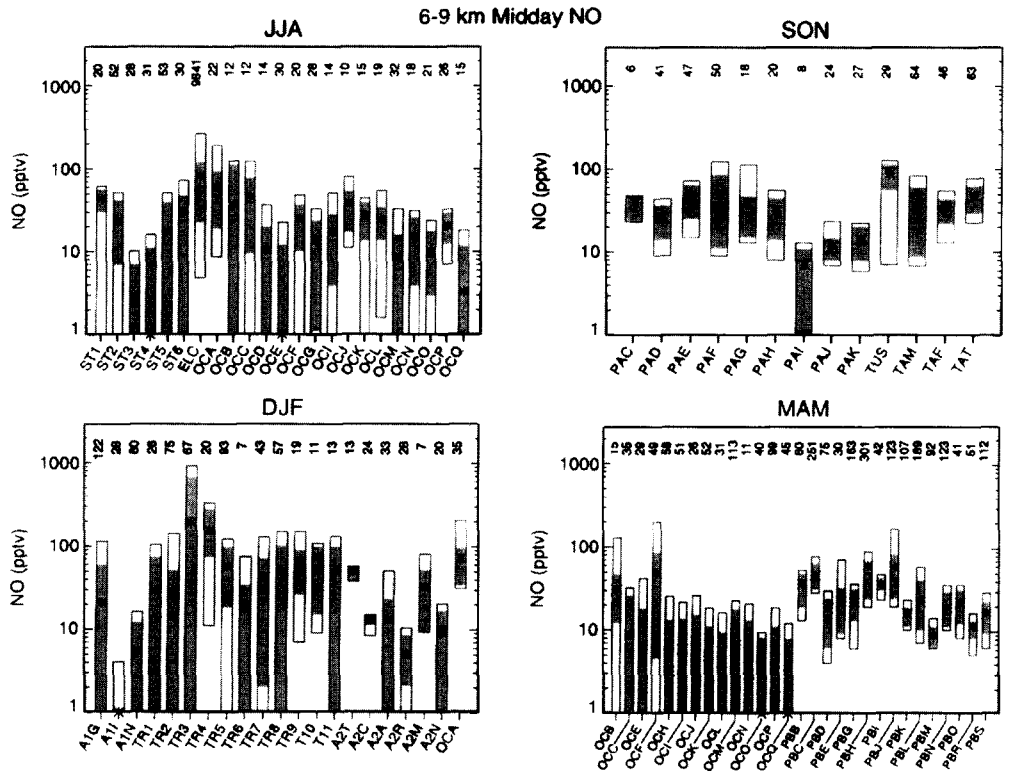

Fig. 17. Midday NO distributions for four seasons for 6–9 km. Three-character codes match those on Fig. 16, and are identified in Table 5.

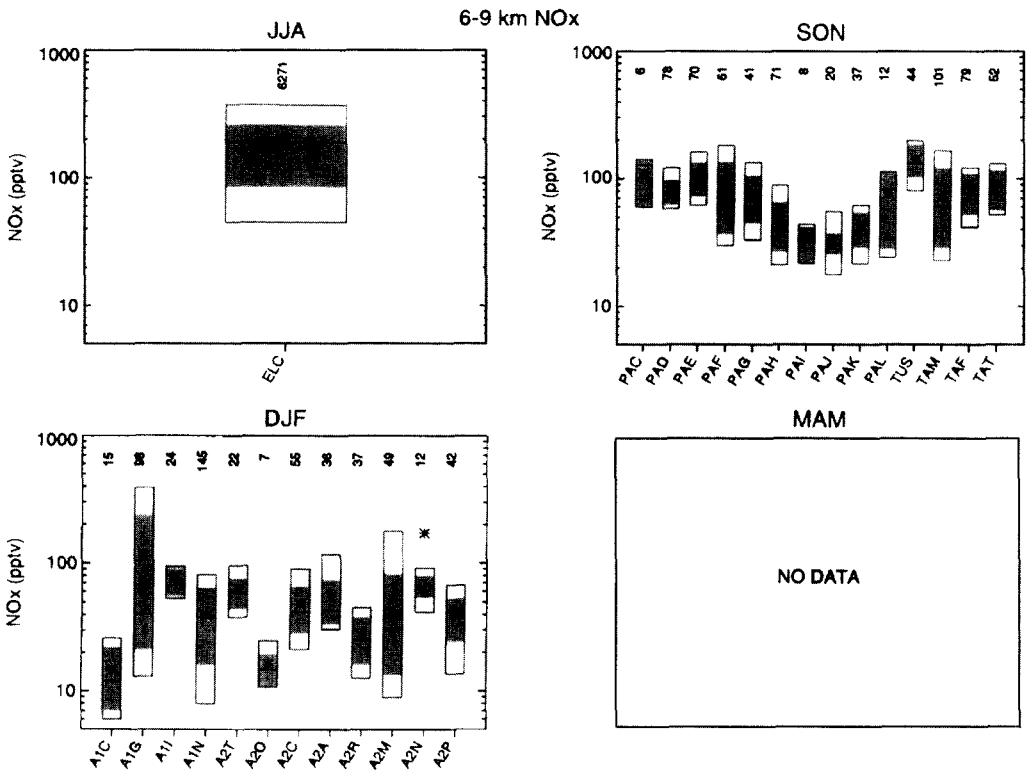

Fig. 18. NO_x distributions for 6–9 km.

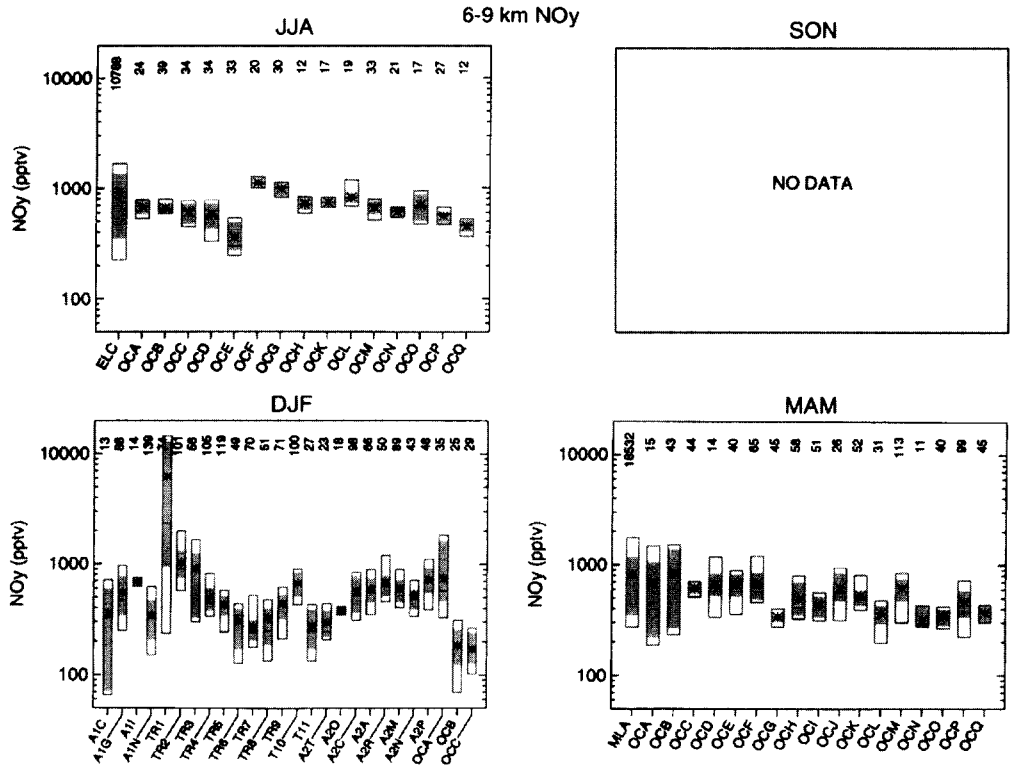

Fig. 19. NO_y distributions for 6–9 km.

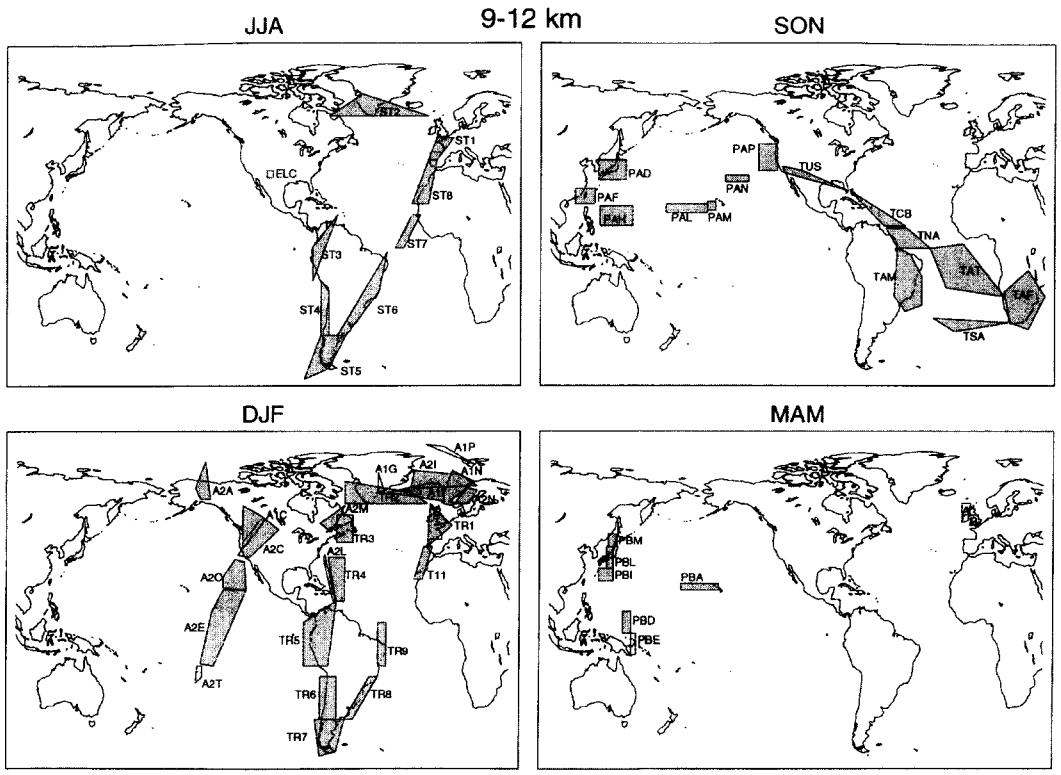

Fig. 20. Location of 9–12 km data. Three-character codes are identified in Table 5. OCTA data are identified by single letters.

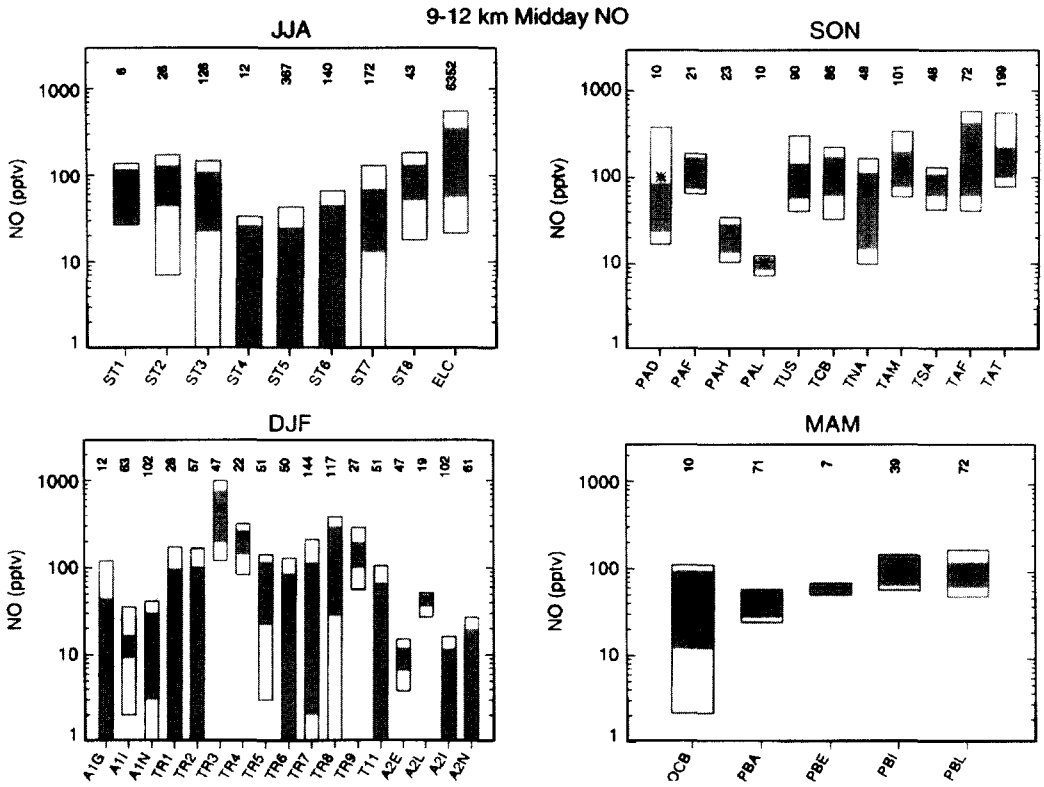

Fig. 21. Midday NO distributions for four seasons for 9–12 km. Three-character codes match those on Fig. 20, and are identified in Table 5.

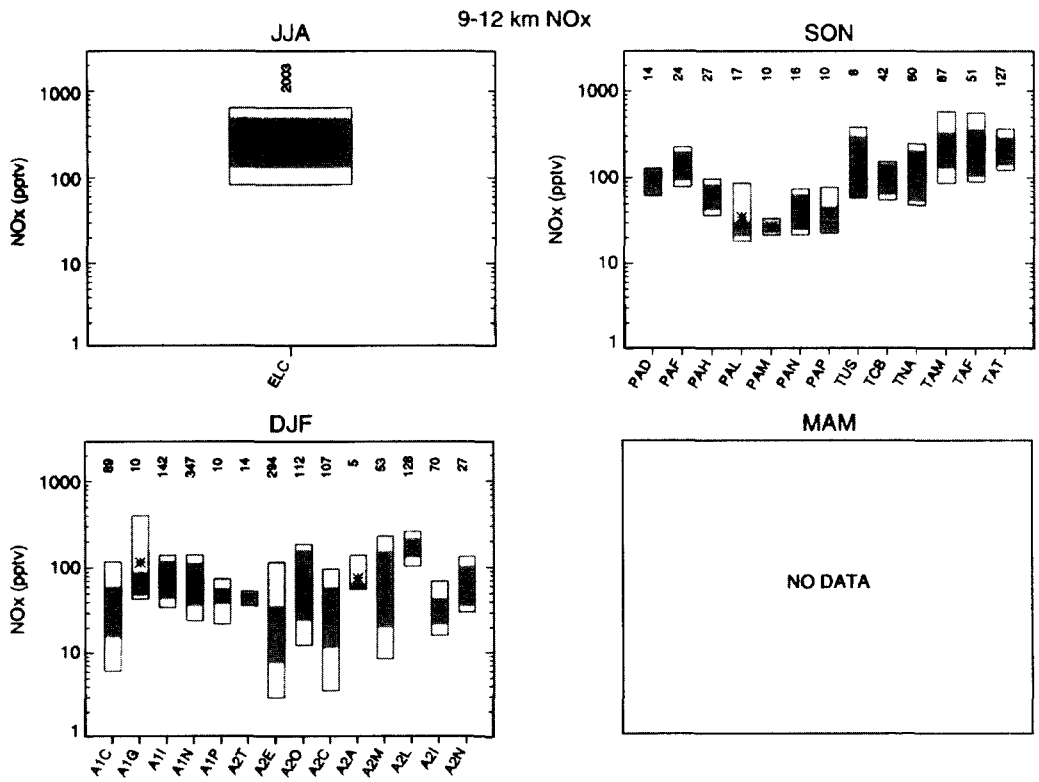

Fig. 22. NO_x distributions for 9–12 km.

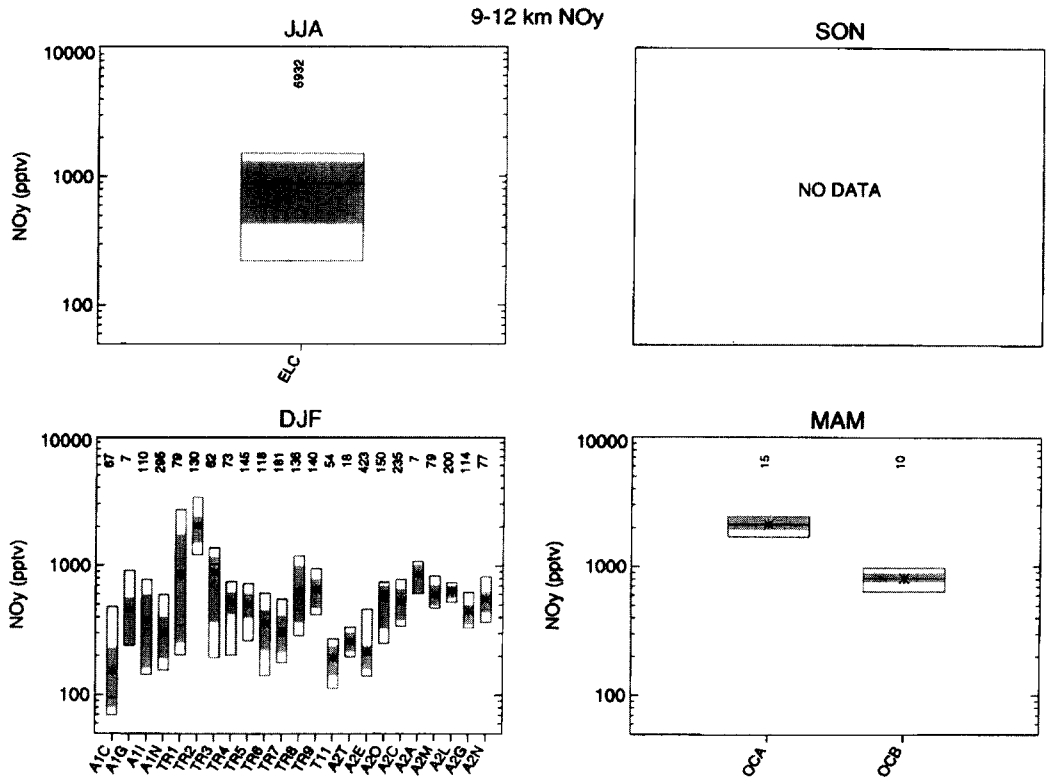

Fig. 23. NO_y distributions for 9–12 km.

One of the principal motivations of this campaign was to understand the changes in ozone concentrations observed over the past 20 years. Distinct layers were observed, which clearly indicated different origins, including haze (pollution), stratosphere, and background air. Mixing ratios of NO and NO_2 were nearly independent of altitude, but NO_y, O_3, CO and hydrocarbons increased with altitude (up to 6 km). Comparison with chemical tracers (e.g. CO) and meteorology indicate that biomass burning in Siberia, as well as stratospheric intrusions were important sources to the NO_y budget. At the higher altitudes 50% of measured NO_y consisted of PAN (Sandholm *et al.*, 1992). The pollution layers, however, were not high in ozone; high ozone amounts were mainly associated with stratospheric intrusions. The important features of the ozone budget appear to be a stratospheric source balanced by photochemical loss (which can be inhibited by increased NO_x) and deposition (Jacob *et al.*, 1992).

CITE-3. The CITE-3 campaign focused on an intercomparison of sulfur species measurements, and NO, NO_2 and NO_y were also measured (Hoell *et al.*, 1993 in a special issue of *J. geophys. Res.*, 20 December, 1993). Flights by the NASA Electra up to 6 km were made over the Atlantic between Florida and New York in August, 1989, followed by a second set over the western South Atlantic from Natal, Brazil during September. Measurements of each SO_2, H_2S, COS, CS_2, DMS were made with several different instruments, as well as single observations of O_3, CO, aerosols, total sulfur, and radon.

High concentrations of ozone and photochemical precursors were observed in outflow from both rural and urban regions of the eastern U.S., in the marine boundary layer and the lower free troposphere. These results also show conditions were favorable for ozone production, in agreement with previous conclusions that emissions from the U.S. are a significant contribution to the enhanced ozone levels over the North Atlantic (Anderson *et al.*, 1993a). The measurements made from Brazil were during the South American dry season, with higher concentrations of ozone observed than in previous wet seasons. Haze layers from burning in South America and Africa, and subsidence from stratospheric or upper tropospheric intrusions to the middle troposphere, were the main sources of ozone to the region (Anderson *et al.*, 1993b) (agreeing well with observations during TRACE-A, discussed below). A photostationary state analysis of NO and NO_2 found significant differences between calculated and measured NO_2 concentrations, which were concluded to be due to interferences in the measurements and/or the presence of hydrocarbons which were not measured (Davis *et al.*, 1993).

AASE 1. Measurements were made between 2 January and 15 February 1989 from the NASA DC-8, based in Stavanger, Norway, as part of the first Airborne Arctic Stratospheric Expedition (overview by Turco *et al.*, 1990 in *Geophys. Res. Lett.* special

issue, March Supplement, 1990). The focus of this campaign was to study polar meteorology, heterogeneous chemistry, and other processes affecting stratospheric ozone in the Arctic. The flights were made between Norway, the North Pole and Greenland, mainly at 10–12 km. There are also data from the ferry flights to and from NASA Ames over the western US. Measurements made on the DC-8 included NO, NO_2, NO_y, O_3, CO, H_2O, CH_4, N_2O, CO_2, aerosols, O_3 profiles, and column amounts of a number of species.

For the measurements above 9 km, the data have been filtered to represent tropospheric air only, using H_2O mixing ratios greater than 10 ppmv and O_3 less than 100 ppbv (following Carroll *et al.*, 1990b) to represent the troposphere. Higher mixing ratios of NO_x were found in the Arctic troposphere than stratosphere, and it was found that in the air masses encountered, the ratio NO_x/NO_y is a good indicator of stratospheric or tropospheric air (Carroll *et al.*, 1990b; Hübler *et al.*, 1990).

INSTAC-1. The International Stratospheric Air Chemistry mission consisted of flights over the western Pacific between Japan and Indonesia, from 7 to10 March 1989. NO was measured by chemiluminescence and O_3 with a modified electrochemical concentration cell (ECC) ozonesonde. Most of the flight time was between 4 and 5 km altitude, with the southbound flight farther from the Asian continent than the northbound. A latitudinal gradient was observed in the NO mixing ratios, with lower values seen near the equator, and slightly higher values near the continent (Kondo *et al.*, 1993).

ELCHEM. One of the goals of the Electrified Cloud Chemistry (ELCHEM) campaign was to study the production of NO_x in thunderstorms. The flights were made over New Mexico in a variety of atmospheric conditions, from 27 July to 22 August 1989. NO, NO_2, NO_y and O_3 were measured simultaneously throughout the troposphere, up to 12 km, during 12 flights (Ridley *et al.*, 1994). Higher values of NO and NO_x were seen above 7 km than between 3 and 6 km. However, a wide range of NO_y mixing ratios were seen throughout the middle and upper troposphere, with the average between 600 and 1000 pptv.

ABLE-3B. During ABLE-3B flights were concentrated over central Canada southwest of Hudson Bay and in northeastern Quebec and Newfoundland, with the goal of studying the importance of long-range transport of pollutants and the production and destruction of ozone in this region (Harriss *et al.*, 1994 in a special issue of *J. geophys. Res.*, 20 January 1994). The flights of the NASA Electra research aircraft were made near Hudson Bay between 6 and 30 July 1990, and in Labrador, from 30 July to 14 August with a maximum altitude of 6 km. Measurements were made of NO, NO_2, NO_y, O_3 (*in situ* and profiles), aerosols CO, CH_4, NMHC, eddy correlation flux of CO, CH_4, O_3 and H_2O, PAN, PPN, C_2Cl_4, aldehydes, ketones, nitric and organic acids.

The air trajectories over eastern Canada in summer are generally variable, and include southerly flow from industrialized region of the central U.S., westerlies, which often carry flow from wildfires, and north and northwesterly flow from the remote Arctic. As in ABLE-3A, stratospheric intrusions and biomass burning were sources of ozone, but the most important source was photochemical production driven by the dispersed regional NO_x background (Mauzerall *et al.*, 1996). Observed NO_x levels (10–50 pptv) are sufficient to slow down O_3 photochemical loss, but the relatively low temperatures of this region cause rapid conversion of NO_x to PAN, thus reducing the impact of NO_x emissions (Harriss *et al.*, 1994). The observations near Hudson Bay occurred in air originating from Alaska and the Northwest Territories, with indications of upper tropospheric or lower stratospheric air and biomass burning. During measurements in Labrador, the air flow had components from biomass burning, tropical origins (brought by Hurricane Bertha), and stratospheric air, but not much evidence of anthropogenic input. NO and NO_x levels were similar, and roughly constant with altitude, for the two regions (approximately 10 and 30–40, respectively).

TROPOZ-2. The TROPOZ-2 campaign had a very similar flight track to STRATOZ-3 (discussed above). Measurements of NO and NO_y were made during TROPOZ, 9 January–1 February 1991 (Rohrer *et al.*, 1997a, b). High values of NO were observed at 3–6 and 9–12 km above eastern Canada and the western Atlantic. The TROPOZ data were not filtered for stratospheric versus tropospheric air, because coincident data were not available, so it is quite likely that some of the measurements near 12 km were in the stratosphere. The data at 3–6 km over Newfoundland ("TR3") are a rather small sample with a wide distribution, indicating a local pollution plume was encountered.

PEM West-A & B. The Pacific Exploratory Missions West were designed to study the outflow of the Asian continent to the western Pacific. PEM West-A took place 16 September–21 October 1991, during the period of minimum outflow (*J. geophys. Res.* special issue, 20 January 1996). The NO and NO_2 measurements made by Georgia Institute of Technology (GIT) during PEM West-A are presented here and NO_y was also sampled (Singh *et al.*, 1996). Measurements of NO and NO_y were also made by Nagoya University (NU) (Kondo *et al.*, 1996; Koike *et al.*, 1996). Also measured from the DC-8 aircraft were O_3, CO, CH_4, N_2O, hydrocarbons, CO_2, SO_2, DMS, CS_2, OCS, PAN, PPN, CFCs, HNO_3, peroxides, and aerosols. Data in the 9–12 km range have been filtered to represent only tropospheric air by using data when $O_3 < 100$ ppbv and $N_2O > 309$ ppbv. Phase B was conducted 7 February–14 March 1994, the season when typically the outflow is at a maximum (*J. geophys. Res.* special issue, in press). Again, measurements of NO, NO_2 and NO_y were

made by GIT and of NO and NO_y by NU (Kondo *et al.*, 1997b, c). Caution should be used in use of the NO_2 measurements during PEM West-A, as these data show significant disagreement with model calculations (J. Bradshaw, private communication). Significant differences were seen between the NO_y measurements made by NU and GIT during both campaigns (neither are shown here). The disagreements during PEM West-A are discussed by Crosley (1996).

AASE 2. The primary goal of the second Airborne Arctic Stratospheric Expedition, as in AASE 1, was to study stratospheric ozone depletion in the northern hemisphere winter, however these flights covered a larger geographical region (overviews by Rodriguez, 1993 in *Science* special section, 27 August 1993; Anderson and Toon, 1993 in *Geophys. Res. Lett.* special section, 19 November 1993; Wofsy *et al.*, 1994 in *Geophys. Res. Lett.* special section, 15 November 1994). Measurements from the DC-8 during AASE 2 were made 11 January–20 March 1992, and included flights between California, Alaska, Maine and Norway, along with a flight to Tahiti and back, and one between Maine and Puerto Rico. Measurements made on the DC-8 included NO, NO_2, NO_y, O_3, CO, CH_4, N_2O, CO_2, aerosols, O_3 profiles, and column amounts of a number of species.

As was done with the AASE 1 and PEM West-A, the 9–12 km data have been filtered using $O_3 < 100$ ppbv and $N_2O > 309$ ppbv to identify tropospheric air.

Zonally averaged distributions of NO_x show significantly lower values at high latitudes, which agree well with the observations of AASE 1 (e.g. Weinheimer *et al.*, 1994). On the flights to and from Tahiti, sharp changes in NO_y and ozone were observed between mid-latitudes and the tropics near and parallel to the subtropical jet, an apparent "chemical front" (Folkins *et al.*, 1995).

MLOPEX-2. Aircraft measurements were made during the spring intensive of MLOPEX-2 from the University of Wyoming's King Air, covering up to 9 km altitude in the vicinity of Mauna Loa. NO_y and O_3 were determined with the NCAR chemiluminescence instruments (Ridley *et al.*, 1996). Other species measured included nitrates and halocarbons, hydrocarbons, CO, H_2O_2 and CH_3OOH.

The measurements of NO_y covered a wide range (200–1000 pptv) at all altitudes, and at 3–6 km were somewhat higher than the mountaintop measurements at Mauna Loa ('ML1', 'ML2', 'MLA' in Fig. 15). Model results for the time of the measurements were also consistently lower than the aircraft observations (Brasseur *et al.*, 1996).

TRACE-A. The goal of the Transport and Atmospheric Chemistry near the Equator–Atlantic campaign was to study ozone and related trace gases in Brazil, and biomass burning in southern Africa and the adjacent Atlantic ocean. Flights were made up to 12 km over eastern South America, southern Africa and the South Atlantic, from 21 September to 26 October 1992 (Fishman *et al.*, 1996 in *J. geophys. Res.* special issue, in press). NO, NO_2 and NO_y measurements made by Bradshaw and coworkers. Measurements were also made of O_3, CO, CH_4, N_2O, hydrocarbons, CO_2, SO_2, DMS, CS_2, OCS, PAN, PPN, CFCs, HNO_3, peroxides, and aerosols. Data in the 9–12 km range have been filtered with $O_3 < 100$ ppbv and $N_2O > 309$ ppbv to obtain tropospheric air only.

High NO_x levels were seen at high altitudes throughout the observation region, as a result of convection over the continents (Walker circulation) carrying biomass burning products. Production of NO by lightning was also an important source to the upper troposphere, but it was found stratospheric input was not (e.g. Smyth *et al.*, 1996).

Measurements made over South America agree very well with those from the CITE-3 flights from Natal, Brazil, which were also made during September. At 3–6 km the NO and NO_x data from the two campaigns are very close, but below 3 km the CITE-3 NO and NO_x results are slightly lower than the TRACE-A data.

OCTA. Data were collected during the European research project Oxidizing Capacity of the Tropospheric Atmosphere (OCTA) aboard the Hercules C-130 of the U.K. Meteorological Office. NO_y and NO were measured with a two channel chemiluminescence instrument (Gerbig *et al.*, 1996), using a gold converter (cf. Fahey *et al.*, 1985) to convert the different NO_y species to NO. The instrument is described in Lerner *et al.* (1994). O_3, CO, H_2O_2, hydrocarbons (grab samples), J_{NO_2} and aerosols were also measured during these flights. Summaries of the data were made for 5° longitude by 5° latitude regions, where there was more than 10 min of data.

The winter and spring 1993 and 1994 flights were located either north or south of the polar front. The meteorological conditions during the summer campaign in 1993 over the west side of the Atlantic have been outlined by Merrill and Moody (1996). A ridge of high pressure was maintained throughout the campaign, which forced airmasses moving eastwards from the North American coast further northwards, lifting them over cooler Arctic air masses. The measurements made during the last three flights of the summer campaign in the eastern Atlantic Ocean in the lowest 3 km ("OCA"–"OCH" in Figs 8–11) were influenced by airmasses coming from the European continent, which is supported by trajectory calculations (Wild *et al.*, 1996).

2.4. *Discussion of data*

It is quite apparent in Figs 5–7 that a wide range of mixing ratios of NO, NO_x and NO_y can be found in the non-urban boundary layer. The NO and NO_y data, in particular, can be separated into "clean" versus "dirty" regimes with little overlap of the two groups. The lowest values of all species are found in

Alaska (3AT, BAR, 3AL, 3AW), the Arctic (3AA), northern Canada (3BH, 3BL) and the eastern Pacific (C2O). In all of these cases the median value of NO is below 10 pptv, NO_x 50 pptv and NO_y 300 pptv during summer. In all seasons the lowest values of NO and NO_y are found at Barrow, Alaska, although the winter NO_y measurements were significantly higher than the other seasons. The higher values in Figs 5–7 are found in industrialized regions of the world, such as eastern North America and Europe. An exception to these high and low regimes appears in the SON data from ground measurements at Oki Island, Japan during PEM West-A. Both the NO and NO_y data lie in the middle of the other values, indicating that a variety of source regions affected the site. Although these measurements were made very close to the large pollution sources of eastern Asia, the predominant flow is not from the continent during fall.

Much less variability is found among the measurements above the surface layer, which are generally some distance from NO_x sources. The 0.5–3 km range in Figs 9–11, however, shows a similar, but less extreme, pattern as the boundary layer data. The measurements in North America (e.g. C3W, ELC, 3BN) are among the higher values of NO, NO_x and NO_y measured, and the observations in Alaska, Canada, the Arctic and the eastern Pacific are lowest. At 3–6 km most of the measurements of NO are close to 10 pptv in the NH summer, whereas there is significantly greater variability in the DJF measurements. The NO mixing ratios during all seasons increase with altitude to roughly 100 pptv at 9–12 km, as the upper tropospheric sources (lightning, convection of surface emissions and the stratosphere) become important (e.g. ELCHEM, TRACE-A). There are fewer measurements of NO_x at 6–9 and 9–12 km than of NO, but the same trend of increasing concentrations with altitude is evident, consistent with the longer lifetime of NO_x at higher altitudes. There is little evidence of an altitude gradient in the NO_y measurements, with mixing ratios between 100 and 1000 pptv for 3–12 km.

An interesting region for comparison is in the western Pacific. Measurements made during PEM West-A in the fall (SON) are in the same location as those during INSTAC-1 in the spring (Figs 8 and 12). Although there are typically very different air flow patterns in these two seasons, the measurements of NO are quite similar, with all of the data falling below 50 pptv. In both data sets, the data are lower near the equator than at mid-latitudes (Figs 1–3). Although during the fall season minimum outflow is expected, the PEM West-A data show decreasing mixing ratios for all species and altitudes with distance from the Asian continent (e.g. Fig. 14).

The large gaps that remain in the mapping of the global distributions of NO, NO_x and NO_y are evident in the free troposphere data shown in Figs 1–3 and the boundary layer data in Fig. 4. Although most of the campaigns plotted here originated from the U.S., the amount of data over North America is quite sparse spatially and temporally (most of the data were obtained during the summer). No measurements have been archived for most of Europe, Africa, Asia and Australia at all altitudes and seasons. Although South America appears well covered in data (in Fig. 1), only NO was measured during several of the campaigns and the temporal coverage is quite limited. Emissions from Antarctica are unlikely to provide a significant source to the global atmosphere, however measurements there will provide information about the lifetime of NO_y species and improve our understanding of the global O_3 distributions.

3. MODEL DESCRIPTIONS

This section briefly describes each of the global chemical transport models (CTMs) that will be used for comparison with the data below. The models of the National Center for Atmospheric Research (NCAR), Lawrence Livermore National Lab (LLNL), NOAA Geophysical Fluid Dynamics Lab (GFDL), Harvard University with the Goddard Institute for Space Studies (GISS), KFA Jülich, and the Royal Netherlands Meteorological Institute (KNMI) are described. Table 7 summarizes a few of the details of each model, including resolution and total nitrogen emissions used. These models are a somewhat arbitrary sample of CTMs currently being developed. Others include IMAGES (Müller and Brasseur, 1995), MOGUNTIA (Zimmerman, 1988) and the Oslo CTM (Isaksen), and ECHAM (Roelofs and Lelieveld, 1995) is an example of a general circulation model with chemistry.

3.1. *NCAR: MOZART*

MOZART (Model of OZone And Related species in the Troposphere) is a three-dimensional (3-D) Chemical Transport Model driven by global wind, temperature, humidity, and cloud fields provided by the NCAR Community Climate Model (CCM, version 2) (Hack *et al.*, 1993). MOZART is described in detail by Brasseur *et al.* (1997). The model has been recently used to investigate the time evolution and distribution of species in the Pacific troposphere in conjunction with the measurements collected during the MLOPEX campaigns (Brasseur *et al.*, 1996). The version of the model used in the present study computes the time history of 45 chemical species on the global scale from the surface to the upper stratosphere. In its present configuration, the model is run with a spatial resolution which is identical to that of "standard" CCM2 (triangular truncation at 42 waves or T42) with a corresponding numerical grid of 64 g latitudes and 128 equidistant longitudes (corresponding to a 2.8° horizontal resolution). In the vertical, the model uses an hybrid σ–p coordinate with 18 levels extending from the surface to the level of 5 mbar. The numerical time-step for both transport and chemistry

Table 7. Summary of the chemical transport models

Feature	MOZART	GRANTOUR	GCTM-1	Harvard	KFA-GISS	CTMK
Resolution:						
Horizontal	2.8° × 2.8°	330 km	265 km	4° × 5°	8° × 10°	4° × 5°
Vertical	18 levels	100 mb	11 levels	9 levels	9 levels	15 levels
Max. altitude	5 mb		10 mb	10 mb	10 mb	5 mb
Months averaged	DJF, JJA	DJF, JJA	DJF, JJA	DJF, JJA	DJF, JJA	Jan, Jul
Emissions (Tg N yr^{-1}):						
Fossil fuel comb.	22	22.4	21.2	21	21.9	22
Biomass burning	4.3	6.5	8.3	11.6	4.4	5.3
Soil	6.7	5	5.5	6.6	4	3.9
Lightning	5	12.9	3.0	4	5	5
Aircraft	0.44	0.95	0.45	0.46	0.45	0.85
Stratosphere		1	0.65	0.5		0.64

is 20 min. MOZART is run "off line" from CCM2, with dynamical variables (e.g., wind components, pressure, temperature, water vapor, convective mass fluxes, diffusion parameters, cloudiness) provided every 6 h from pre-established history tapes.

The model accounts for surface emissions of chemical compounds based on the emission inventories of Müller (1992), advective transport using the semi-Lagrangian Transport scheme of Williamson and Rash (1994), convective transport using the formulation of Hack (1994) adopted in CCM2, diffusive exchanges in the boundary layer based on the parameterization of Holtstag and Boville (1993), wet deposition using the formulation of Giorgi and Chameides (1986), and dry surface deposition (Müller, 1992). The chemical scheme includes approximately 130 chemical and photochemical reactions (including CH_4, C_2H_6, C_2H_4, C_3H_6, C_4H_{10}, isoprene, and terpenes degradation schemes) (Müller and Brasseur, 1995), as well as wash-out for approximately 10 soluble species. The heterogeneous conversions of NO_3 and N_2O_5 into HNO_3 on the surface of sulfate aerosols are parameterized as in Müller and Brasseur (1995), with the sulfate concentrations calculated by Pham *et al.* (1995). The NO_x sources represented in this model include the contributions of fossil fuel combustion (22 Tg N yr^{-1}), biomass burning (4.3 Tg N yr^{-1}), soil emissions (6.7 Tg N yr^{-1}), lightning (fixed to 5 Tg N yr^{-1} and geographically distributed according to the parameterization of Price and Rind (1992)), and aircraft emissions (0.44 Tg N yr^{-1} distributed according to Albritton (1993)).

3.2. *LLNL: GRANTOUR model*

This global, three-dimensional, tropospheric chemical transport model is a Lagrangian parcel model, typically run with 50,000 parcels and a 6 h operator-splitting time step. The chemical solver (Sillman, 1991) treats a suite of non-methane hydrocarbons (Lurmann *et al.*, 1986) and also includes the isoprene mechanism of Paulson and Seinfeld (1992) and several additional $RO_2 + HO_2$ reactions appropriate for the remote atmosphere (Jacob and Wofsy, 1988). The CTM is supplied meteorological fields every 12 h from NCAR's CCM1. For the scenario shown here, the concentration of CH_4 is based on work by Steele *et al.* (1987). Sources include industrial sources of CO, ethane, propane, C_{4-5} alkanes, and C_{6-8} alkanes, (Atherton *et al.*, 1996; Piccot *et al.*, 1992) biomass burning sources of CO, ethane, propane, C_{4-5} alkanes, ethene, propene, butene, and NO_x (Atherton, 1995; Liousse *et al.*, 1996) and NO_x sources due to fossil fuel combustion, aircraft, lightning, soil emissions, and transport from the stratosphere (Atherton *et al.*, 1996). Because the model does not include the full chemical mechanism to describe stratospheric ozone chemistry, for pressures less than $\sigma = 0.2$, concentrations of ozone were specified based on ozonesonde measurements (Komhyr *et al.*, 1994). Stratospheric concentrations of other long-lived species were specified based on results of the LLNL 2D model (Wuebbles *et al.*, 1987).

3.3. *GFDL: GCTM-1*

Phase 1 Global Chemical Transport Model (denoted GCTM-1 here) has a horizontal grid size of ≈265 km and 11 vertical levels at standard pressures of 990, 940, 835, 685, 500, 315, 190, 110, 65, 38, and 10 mb. It is driven by 12 months of 6 h time-averaged wind, temperature, and precipitation fields from a GFDL general circulation model (GCM) (Manabe *et al.*, 1974; Manabe and Holloway, 1975). The model's resolved transport is second order in the horizontal and fourth order in the vertical (see Mahlman and Moxim, 1978) and parameterizations of horizontal sub-grid scale transport, as well as vertical mixing by mechanical turbulence and dry and moist convection, are included (for details see Appendix A in Levy *et al.* (1982), Section 2.1 in Levy and Moxim (1989), and Section 2 in Kasibhatla *et al.* (1993)). The convective transport scheme uses enhanced vertical diffusion when moist or dry instability is diagnosed in the parent GCM. The boundary layer is determined by a shear-dependent tapering l(2) vertical diffusion in the model's bottom three levels. Dry deposition rates are calculated using a drag-coefficient formulation for

surface exchange (Levy and Moxim, 1989) and spatially varying dry deposition velocities, which are calculated using a standard resistance-in-series model (Wesely and Hicks, 1977; Wesely, 1989) and a $1^\circ \times 1^\circ$ vegetation map (Mathews, 1983). The removal of soluble tracers by precipitation is based on the local precipitation rate, and the wet removal tendency is proportional to the local tracer mixing ratio (see Section 2 in Kasibhatla *et al.* (1991) for details).

The off-line reactive nitrogen chemistry is described in Kasibhatla *et al.* (1993) and Moxim *et al.* (1996), and the ozone chemistry is described in Kasibhatla *et al.* (1996). Present NO_x sources are described in Kasibhatla *et al.* (1991), Levy *et al.* (1991), Kasibhatla (1993), Kasibhatla *et al.* (1993), Levy *et al.* (1996), and Yienger and Levy (1995). The isoprene source is from Guenther *et al.* (1995) and the CO and stratospheric O_3 sources are discussed in Kasibhatla *et al.* (1996). Reactions on sulfate aerosol are included and discussed, along with the full reactive nitrogen chemistry, in Levy *et al.* (1997).

3.4. *Harvard: Harvard/GISS CTM*

The Harvard/GISS CTM has a spatial resolution of $4^\circ \times 5^\circ$, with 9 vertical layers in the σ-coordinates, extending from the surface to 10 mb. Meteorological fields are from GISS GCM II (Hansen *et al.*, 1983), and are updated every 4 h. A mass-conserving second-order moment scheme (Prather, 1986) is used in tracer advection. Dry and wet convection fluxes in the model are consistent with the GCM (Prather *et al.*, 1987). Dry deposition is computed with a resistance-in-series scheme similar to that of Gao and Wesely (1995). Wet deposition of soluble tracers is computed with the scheme of Balkanski *et al.* (1993). The CTM has been applied previously to a number of atmospheric chemistry problems (Prather *et al.*, 1987; Jacob *et al.*, 1987; Balkanski *et al.*, 1993; Jacob *et al.*, 1993).

This version of the model transports 15 reactive chemical tracers: odd oxygen ($O_x = O_3 + O + NO_2 + HNO_4 + 2 \times NO_3 + 3 \times N_2O_5$), NO_x($NO + NO_2 + NO_3 + HNO_2$), N_2O_5, HNO_4, PANs (peroxyacetylnitrate and its homologues), alkylnitrates ($\geqslant C_4$ lumped as butylnitrate), HNO_3, CO, ethane, higher alkanes ($\geqslant C_4$ lumped as butane), alkenes ($\geqslant C_3$ lumped as propene), isoprene, acetone, higher ketones ($\geqslant C_4$ lumped as methylethyl ketone), and H_2O_2. The chemical mechanism is based on recent compilations including Paulson and Seinfeld (1992), Atkinson *et al.* (1993), and DeMore *et al.* (1994). The quantum yields of O^1D from ozone photolysis have been updated following Michelsen *et al.* (1994). The termolecular reaction rate constant of $OH + NO_2$ is based on a new recommendation by Donahue *et al.* (1997), 15–20% slower than that by DeMore *et al.* (1994) under tropospheric conditions. Hydrolysis of N_2O_5 to HNO_3 on aerosol surfaces is included with a reaction probability of 0.1 (DeMore *et al.*, 1994). Aerosol surface areas are derived from a CTM simulation of sulfate (Chin *et al.*, 1996). To speed up the chemical computation, the parameterization method introduced by Spivakovsky *et al.* (1990b) is applied.

Global sources of NO_x in the model include: 21 Tg N from fossil fuel combustion (Benkovitz *et al.*, 1996), 0.46 Tg N from the 1992 subsonic aircraft NO_x emissions inventory (Baughcum *et al.*, 1996; Metwally, 1995), 11.6 Tg N from biomass burning based on a preliminary CO emissions inventory by J. Logan, and 6.6 Tg N from soils following the scheme by Yienger and Levy (1995). A lightning source of 4 Tg yr^{-1} is apportioned over convective regions, following Price and Rind (1994). The amount of NO_y transported from the stratosphere is 0.5 Tg N/yr^{-1}. In sum, the total NO_y source in the troposphere is 44 Tg N per year.

3.5. *KFA Jülich: KFA-GISS*

The chemical tracer model (GISS-CTM, adopted from Prather *et al.*, 1987) solves continuity equations for a set of chemically reactive tracers over a global three-dimensional grid. The horizontal extension of a grid box is 8° in latitude and 10° in longitude. In the vertical, the atmosphere between the surface and 10 hPa is divided into 9 σ-layers. The CTM uses a split operator method to compute the separate effects of advection, dry and wet convection, large-scale diffusion, sources, dry and wet deposition and chemistry. The meteorological data which are used as input for the CTM are provided by the GISS general circulation model GCM II (Hansen *et al.*, 1983). The temporal resolution used is 8 h for transport and 1 h for chemistry. The reduced chemistry scheme including the fast interconversion of NO and NO_2, the conversion of NO_2 to HNO_3 via the reaction with OH, and the conversion of NO_2 to nitrate via the reaction with O_3 to NO_3 and N_2O_5 is described by Ehhalt *et al.* (1992). The OH and O_3 concentration fields are prescribed (Spivakovsky *et al.*, 1990a and references therein; Komhyr *et al.*, 1988; London and Liu, 1992; Marenco and Said, 1989; Marenco, personal communication; Pyle *et al.*, 1994; Seiler and Fishman, 1981; Smit *et al.*, 1991; Weller *et al.*, 1996) and so is the photolysis rate of NO_2 (Roth, 1986).

The NO_x sources contributing to the atmospheric burden are (in Tg of N per year): fossil fuel, 21.9 (Dignon, 1982); biomass burning, 4.4 (Müller, 1992); soil emissions, 4 (Williams *et al.*, 1992; Matthews, 1983); aircraft, 0.45 (Wuebbles *et al.*, 1993) lightning, 5; $N_2O + O(^1D)$, 0.64 (Kasibhatla *et al.*, 1991). The emission rate of nitrogen oxides from lightning is extremely uncertain. NO emission by lightning was coupled to the occurrence of deep convection using empirical relations between flash frequency and cloud height (Price and Rind, 1992). The total annual emission rate was then scaled to 5 Tg N yr^{-1}.

3.6. *KNMI: CTMK*

The three-dimensional chemistry transport model of KNMI (CTMK) (Wauben *et al.*, 1997) is adapted

from the global tracer transport model TM2 (Heimann, 1995). CTMK calculates the horizontal and vertical transport of tracers on the basis of 12-hourly output from the ECMWF model (cf. Velders *et al.*, 1994). Analyzed meteorological fields of wind, geopotential height, temperature, and humidity with a horizontal resolution of $2.5° \times 2.5°$ are used for this purpose. These observed meteorological data guarantee a rather realistic description of the actual meteorological situation. The results shown here have been obtained using the meteorological data from 1990.

CTMK was run with a horizontal resolution of 5° in longitude and about 4° in latitude. Vertically, the model has 15 σ-levels extending from the surface up to 5 mb. The meteorological data are integrated/interpolated to this grid and updated every 12 h. Advection can be calculated either with the slopes scheme by Russell and Lerner (1981) or with the second-order moments scheme by Prather (1986) where vertical adjustment is applied in order to conserve mass. The subscale convection fluxes are evaluated according to the scheme by Tiedtke (1989). The parameterization by Louis (1979) is used for the boundary layer. The model time step used for the computations is 1 h. Each model time step involves 4 advection time steps in the East–West, 2 in North–South, and 1 in the vertical direction.

CTMK contains a chemical scheme adopted from the MOGUNTIA model (Zimmermann, 1988; Crutzen and Zimmermann, 1991; Hein, 1994). It evaluates the daytime chemistry of 13 trace gases by using the temperature and relative humidity fields from the ECMWF analyses. Daytime averaged photolysis rates for O_3, NO_2, H_2O_2, HNO_3, CH_3OOH, and HCHO are used, which have been computed with the method described in Brühl and Crutzen (1989). A total of 25 chemical reactions are considered together with dry deposition for O_3, NO_x, H_2O_2, HNO_3, CH_3OOH and NO, and wet deposition for H_2O_2, HNO_3, and CH_3OOH. Climatological precipitation data are used for the parameterization of the wet deposition. The nighttime chemistry includes, besides the deposition, an off-line parameterized heterogeneous reaction. This parameterization, which is based on the work of Dentener and Crutzen (1993), converts NO_2 and O_3 into HNO_3. The chemical scheme uses prescribed surface concentrations for CH_4 and CO according to Fung *et al.* (1991), and Dianov–Klokov and Yurganov (1981), respectively. In addition, the ozone concentrations from the stratosphere above 50 hPa are prescribed according to climatological values (Fortuin and Langematz, 1995). The gases with relatively long lifetimes, i.e., O_3, NO_x, H_2O_2, CH_4, CO, HNO_3, and CH_3OOH, are transported in CTMK, whereas HCHO, NO, HO_2, CH_3O_2, $O(^1D)$, and OH are calculated assuming a quasi-steady state. The simulations are performed using the NO_x emissions prepared for the AERONOX project (Lee *et al.*, 1997). The effect of aircraft NO_x emissions on atmospheric ozone has been studied with CTMK (Wauben *et al.*, 1996).

4. COMPARISON OF MODELS AND DATA

This comparison focuses on summer and winter distributions of NO_x (NO + NO_2 for data and models) and NO_y in the boundary layer and the middle troposphere. The boundary layer measurements are compared with the lowest model layer and data in the 3–6 km range with model results at approximately 500 mbar. For the following discussion, comparison of data and model results qualify as "agreement" if the range of the model output in the region of the observations overlaps a majority of the central 67% of the data. Discussion will be limited to the lower and middle troposphere here; comparison of data and models in the upper troposphere and lower stratosphere will be saved for a later paper.

4.1. *Boundary layer*

Ground measurements are compared with the lowest model layer results. Although there are overall problems with this sort of simple, coarsely averaged comparison of CTMs and small amounts of data, it is especially difficult for the boundary layer. Surface data are particularly susceptible to influences from local sources, which are typically on a scale too small to be resolved or reflected in global models. For most of the data sets used here, only measurements not influenced by nearby urban sources have been used (e.g., in the Harvard Forest and Schauinsland data), and in general have been filtered for local pollution from generators, cars, etc. For many cases it seems to be reasonable to compare these measurements during airflow from rural regions with the coarser distributions of the models. However, the models differ in how sources and sinks of NO_x are handled and, consequently, there are a variety of reasons why model results and observations differ. At some locations it is possible that the data do not represent the average airflow, and consequently the average chemical distributions, of the region, or of the model grid box. In addition, the models do not reproduce the diurnally varying boundary layer heights observed at most continental sites. Differing numerical schemes for convection and transport out of the boundary layer can cause significant differences between models even when emissions (such as from fossil fuels) are similar.

The surface model results for NO_x and NO_y are shown in Figs 24–29. The model outputs have been averaged over 3 months, June–August and December–February, except for the CTMK results which are single month averages of July and January. The comparisons of model results with boundary layer observations are summarized in Tables 8 and 9.

NO_x, *June–August*. Panel (a) in Figs 24–29 shows the model results for June–August of NO_x in the lowest model layer. The shape of the distributions are quite similar for all of the models, with the highest

NO_x levels over North America and Europe, and moderately high values extending from the eastern edges of the continents. The distributions from MOZART (NCAR), the Harvard/GISS and the KFA-GISS models show quite similar values: both the eastern half of the U.S. and a large portion of Europe show ambient levels over 1 ppbv. GRANTOUR (LLNL) yields the lowest maxima, with less than 1 ppbv throughout North America, and above 1 ppbv in just a small region over Europe. GRANTOUR, however, has the highest values over the Atlantic, 20–50 pptv in most regions, whereas all of the other models produce less than 10 or 20 pptv. These differences are most likely due to differing dynamics and chemistry schemes in the models, as all of the models use similar emission rates for fossil fuel combustion ($\sim 22\,Tg\,N\,yr^{-1}$), which is the largest source in the models (see Table 7), and the most significant for the continental boundary layer. However, greater differences between models are seen in the biomass burning (4.3–11.6) and soil (3.9–6.7) emissions, which will be more important in rural and non-industrialized regions of the world.

One explanation for the low-mixing ratios in the boundary layer for CTMK may be that although a boundary layer diffusion parametrization is included, the description of the boundary layer is only very coarse since the transport is based on ECMWF analyses with a coarse vertical resolution on pressure levels (1000, 850, 700, ... hPa). The consequence is too much exchange between the boundary layer and free troposphere, and hence lower concentrations of pollutants in the boundary layer. In a newer version of the CTMK model this has been improved upon by using the analysis at ECMWF model levels.

The median of measured NO_x values in the eastern half of North America range from 800 to 2000 pptv (HAR, SOS, SCO, BND, EGB, KNT in Fig. 6 and Table 8) in general agreement with all of the models. GRANTOUR, however, does not show any values in this region greater than 1 ppbv, where the other models are all greater than 1 ppbv. All of the models except GRANTOUR indicate mixing ratios between 1 and 5 ppbv at Schauinsland, Germany (TOR). The data from southwesterly flow periods, shown here, have a median of 800 pptv, with a significant fraction of the data above 1000 pptv. Data during southeasterly flow are roughly twice as large as the southwesterly flow, and when all data are used there is good agreement with the higher values produced during the models. However, Schauinsland is often above the inversion layer (at night 50% of the time and some during the day in winter), therefore additional filters of the data will be needed to completely characterize the differences between data and model results.

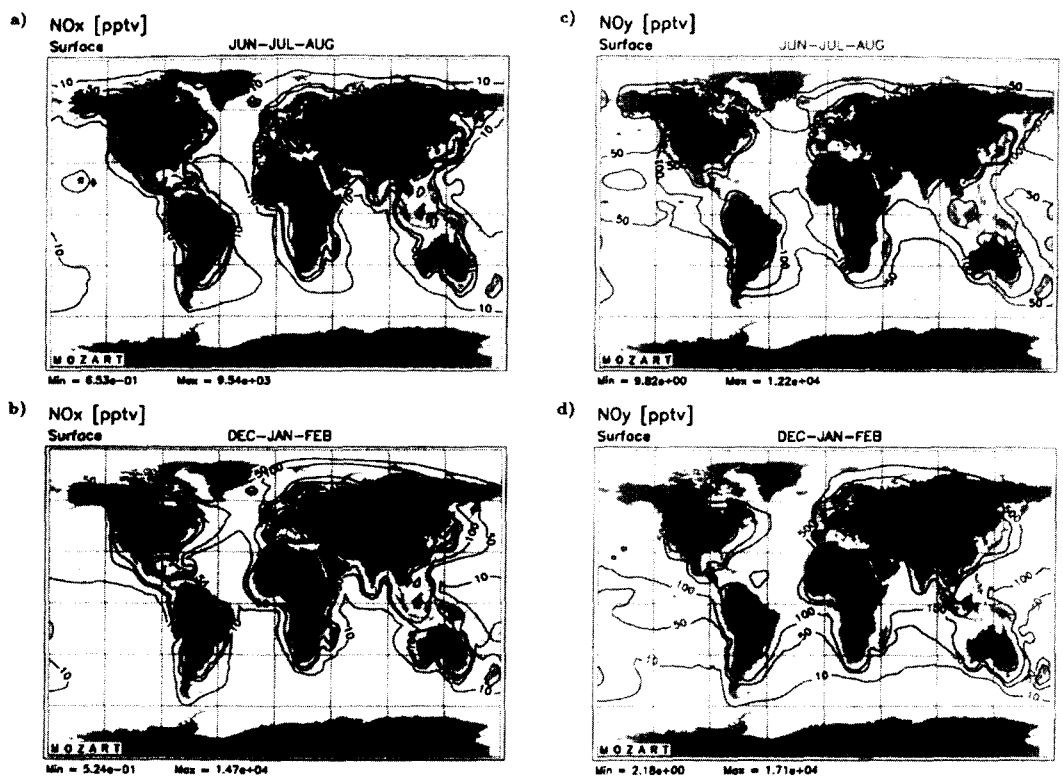

Fig. 24. Model results from MOZART for NO_x and NO_y at the surface: (a) NO_x, June–August; (b) NO_x, December–February; (c) NO_y, June–August; (d) NO_y, December–February. Contour levels are 10, 50, 100, 500, 1000, 5000, 10,000 pptv.

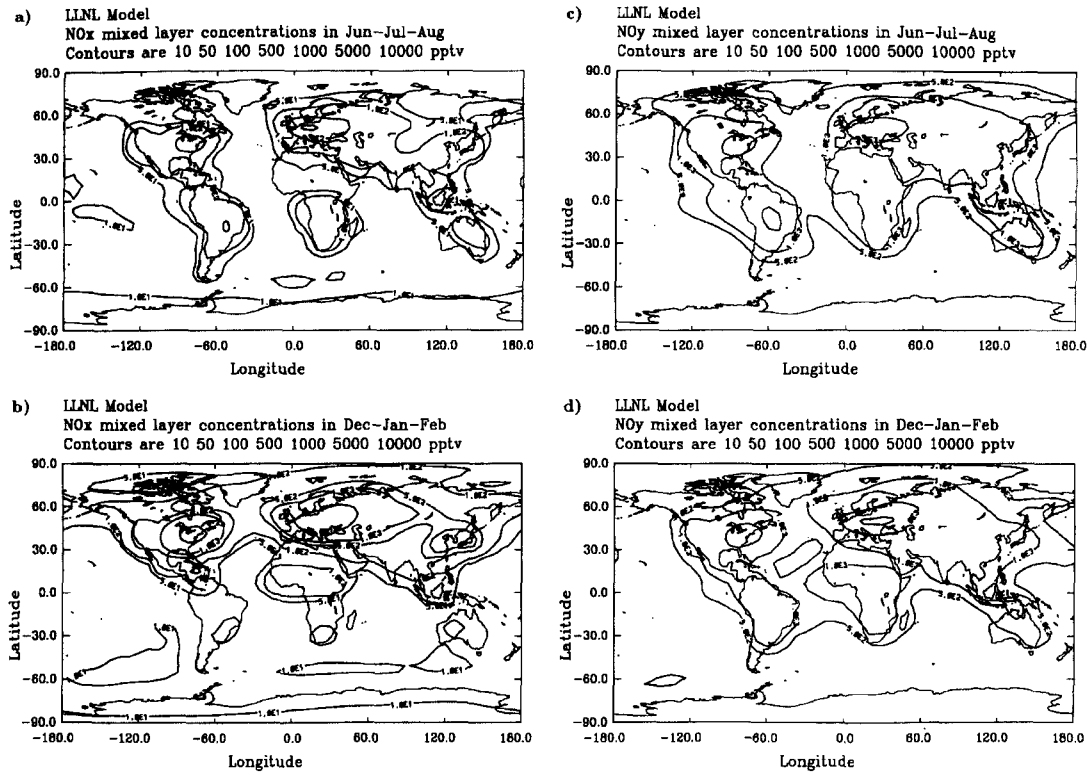

Fig. 25. Model results from GRANTOUR for NO_x and NO_y in the mixed layer: (a) NO_x, June–August (b) NO_x, December–February (c) NO_y, June–August (d) NO_y, December–February.

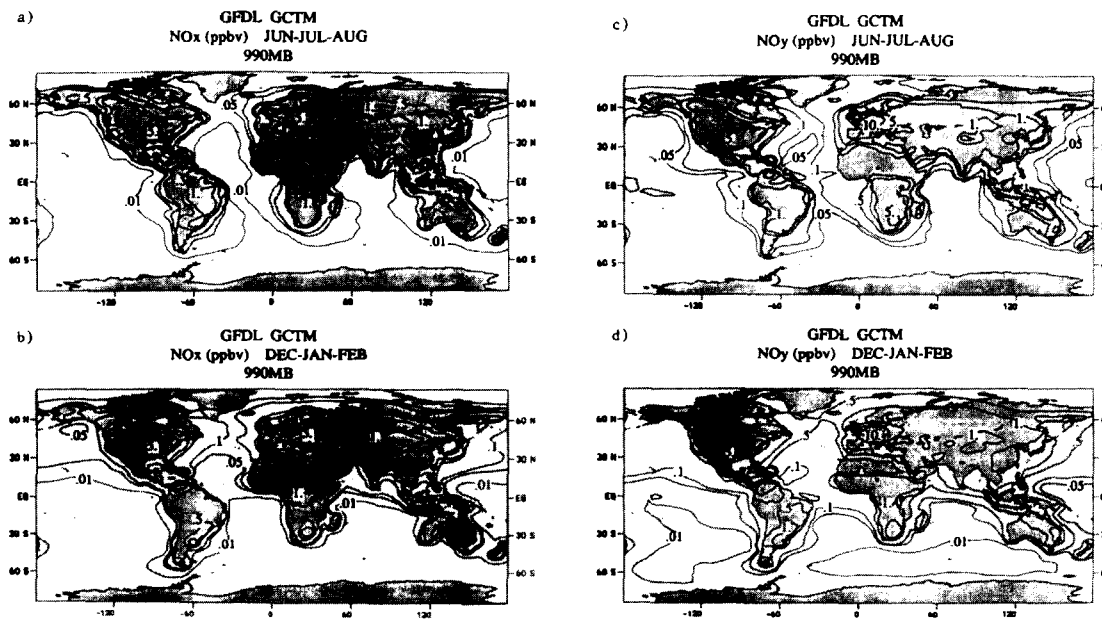

Fig. 26. Model results from GCTM-1 for NO_x and NO_y at 990 mbar: (a) NO_x, June–August; (b) NO_x, December–February; (c) NO_y, June–August; (d) NO_y, December–February. Contour levels are 10, 50, 100, 500, 1000, 5000, 10,000 pptv.

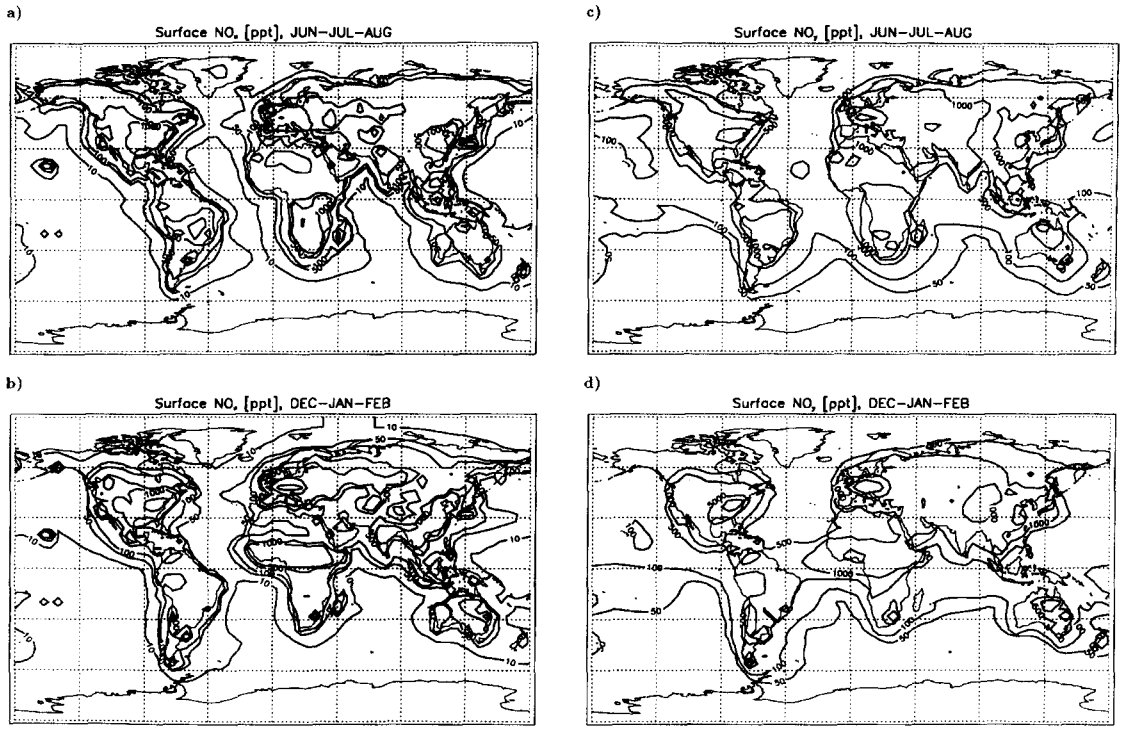

Fig. 27. Model results from Harvard/GISS for NO_x and NO_y at the surface: (a) NO_x, June–August (b) NO_x, December–February (c) NO_y, June–August (d) NO_y, December–February. Contour levels are 10, 50, 100, 500, 1000, 5000, 10,000 pptv.

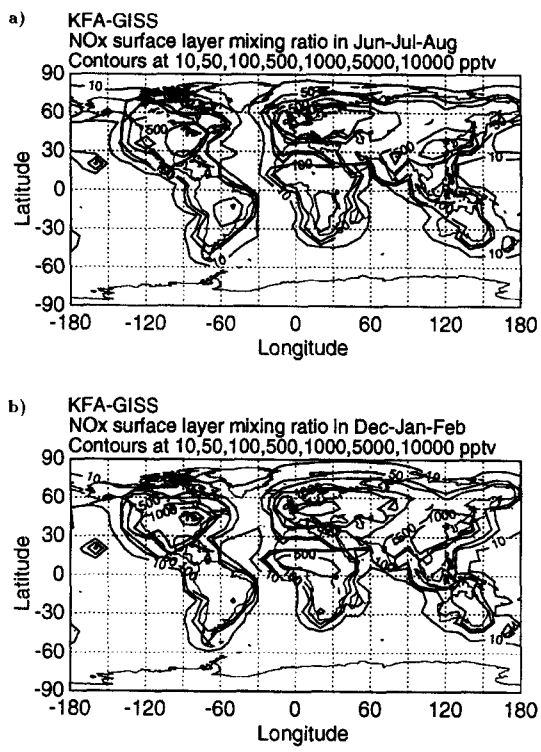

Fig. 28. Model results from KFA-GISS for NO_x in the surface layer: (a) NO_x, June–August; (b) NO_x, December–February.

GRANTOUR, GCTM-1, Harvard and CTMK results agree with all of the observations in the remote regions of Alaska, Hudson Bay and Labrador, whereas MOZART and KFA-GISS show values greater than 100 pptv in Canada (3BT, 3BH, 3BL) where the observed medians were less than 50 pptv. Although the biomass emissions used by the models vary by a factor of >2.5, these differences do not correlate with the model results. Tests of the model IMAGES (which uses the same emissions as MOZART) show that biomass burning contributes at most 10–20% of the total NO_y over northern Canada during summer (Lamarque *et al.*, 1996). As mentioned above (in the description of ABLE-3B), the dispersed NO_x was found to be the most significant source of ozone (Mauzerall *et al.*, 1996), therefore it is likely that convection and transport out of the boundary layer will have a significant effect on the calculated and actual NO_x distributions in these regions. The differences in model outputs are evidence that the models have significantly different convection schemes. The GFDL and CTMK models' results (10–1000 and 20–200 pptv, respectively) are the only ones to approach the observed values over the ocean near California, where the CITE-2 observations were less than 20 pptv (C2O). The other models yield more than 10 times greater.

NO_x, *December–February.* The NH winter boundary layer NO_x model results are shown in panel (b) of Figs 24–29. All of the models show higher levels of

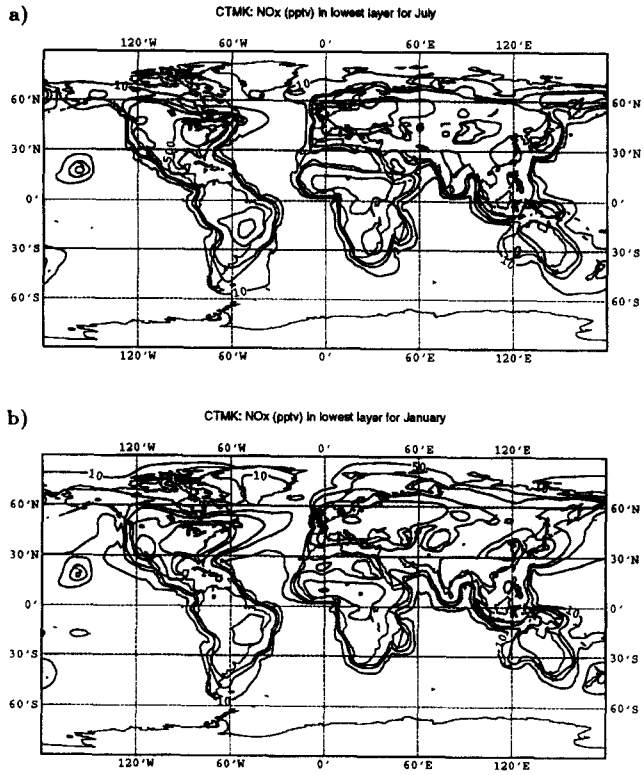

Fig. 29. Model results from CTMK for NO_x at the surface: (a) NO_x, July (b) NO_x, January. Contour levels are 10, 50, 100, 500, 1000, 5000, 10,000 pptv.

NO_x than summer in North America, Europe and eastern Asia, and lower values in South America and southern Africa. The austral summer maximum over central Africa appears in all of the models except CTMK. As in the JJA results, the GRANTOUR values are significantly lower than the other models, particularly over Africa.

The winter NO_x measurements from 2 yr-round sites were shown in Fig. 6. The GRANTOUR, MOZART and GCTM-1 models yield values roughly twice as large as the observed median of 2200 pptv at Harvard Forest, while the Harvard/GISS, KFA-GISS and CTMK model results are within about 20%. However, all of the model outputs lie within the central 67% of the data 1–15 ppbv (see Table 8). All of the models are 2–5 times higher than the observations at Schauinsland. As in the summer data, this disparity may be attributable to the inclusion of only clean sector air (southwesterly), when the winds are frequently from the southeast in winter (see previous section and Section 2.2).

NO_y, *June–August*. Figs 24–27 show the model results for NO_y in the boundary layer, which are only available for four models, MOZART, GRANTOUR, GCTM-1 and Harvard/GISS. The MOZART results for both summer and winter are somewhat lower than the other three models, with smaller regions of NO_y above 1 ppbv in South America, Europe, Asia and Africa. In June–August, GRANTOUR, GCTM-1 and Harvard/GISS have larger regions of NO_y values above 5 ppbv than MOZART in North America and Europe. Another significant difference between the models is in the transport of NO_y across the Pacific Ocean. Between the equator and 30°N, GCTM-1 produces less than 50 pptv, MOZART 50–200 pptv, Harvard and GRANTOUR 100–500 pptv. The high NO_y in GRANTOUR is due in part to organic nitrates associated with the model isoprene chemistry. Organic nitrates other than PAN account for approximately 30% of total NO_y in remote locations in GRANTOUR.

The measurements made in Alaska during summer, at Barrow (BAR in Fig. 7 and Table 9) and the ABLE-3A Bethel tower site (3AT) (medians 70–150 pptv), agree within a factor of two with all four models. Most of the measurements at Barrow, however, fall below the range observed during ABLE-3A (Fig. 7). Both local and regional pollution events, including emissions from the Prudhoe Bay oil refineries, were screened from the Barrow data set used here. The refinery emissions ($\sim$12,000 Tg as NO_2, due to the flaring of gas) are comparable to a medium-sized city and are the largest source in Alaska, and therefore ought to have a significant impact on the region (Jaffe *et al.*, 1995). Many emission inventories do not include this source, however, so it is reasonable to use these filtered data for comparison to model results. In Labrador, the MOZART, GCTM-1 and Harvard results

Table 8. Summary of data–model comparisons for NO_x in the boundary layer. The median and central 67% of the observed data are given. The three-character codes are identified in Table 1, and are used in Figs 4–7. All quantites are in pptv

		Data		Model results					
Location	Codes	Med	67%	MOZART	GRANTOUR	GCTM-1	Harvard	KFA-GISS	CTMK
JJA									
Alaska	3AT, 3AL, 3AW	25	9–96	10–70	20–50	10–500	10–100	10–50	10–50
N. Greenland	3AA	12	9–12	< 10	20–50	10–50	10–50	< 10	< 10
E. Pacific	C2O	17	9–25	50–2000	100–200	10–1000	100–1000	500–1000	10–500
Hudson Bay	3BH	36	23–78	100–400	20–100	50–500	~100	100–500	50–500
Labrador	3BT, 3BL	30	18–76	100–400	20–50	50–500	50–100	100–500	10–100
Nova Scotia	SBL	98	44–266	400–700	100–200	100–500	100–500	~100	100–500
Mass.	HAR	603	422–1159	1000–4000	500–1000	~5000	500–100	~1000	> 2000
N. Carolina	SOS	981	610–2101	1000–4000	~500	1000–5000	1000–5000	~1000	1000–5000
W. Atlantic	C3W	242	134–534	100–1000	200–500	50–1000	100–1000	100–1000	100–1000
NE U.S.	3BO	381	42–1232	1000–4000	500–1000	1000–5000	500–1000	1000–2500	1000–5000
Colorado	NRG	315	125–970	~700	~200	500–5000	500–1000	500–1000	100–500
Penn.	SCO	1970	910–5100	1000–4000	500–1000	> 5000	1000–5000	~2500	1000–5000
Illinois	BND	1620	840–4400	1000–4000	500–1000	> 5000	1000–5000	2500–5000	1000–5000
Ontario	EGB	2300	680–6200	1000–4000	500–1000	~5000	500–1000	2500–5000	1000–5000
Alabama	KNT	1200	590–2670	1000–4000	200–500	1000–5000	1000–5000	1000–2500	500–1000
Germany	TOR	812	550–1462	1000–4000	500–1000	1000–5000	1000–5000	~2500	1000–5000
DJF									
Mass.	HAR	2249.0	1053.0–14,981.0	4000–7000	> 5000	> 5000	1000–5000	~2500	1000–5000
Germany	TOR	960.0	495.0–1953.0	4000–7000	> 5000	~5000	5000–10,000	2500–5000	1000–5000

For more than one data set per location, the full range of the central 67% of the data and the average of the medians is given. Some model values are taken from figures with finer contours than those shown here.

Table 9. Summary of data–model comparisons for NO_y in the boundary layer. The median and central 67% of the data are given. The three-character codes are identified in Table 1, and are used in Figs 4–7. All quantites are in pptv

		Data		Model results			
Location	Codes	Median	Central 67%	MOZART	GRANTOUR	GCTM-1	Harvard
JJA							
Barrow	BAR	69	61–84	77–100	200–500	100–500	100–500
Alaska	3AT	150	116–208	30–100	200–500	100–500	100–500
E. Pacific	C2O	109	81–182	100–3000	~2000	100–1000	500–1000
Labrador	3BT	241	138–443	100–300	500–1000	100–500	100–500
Nova Scotia	SBL	267	118–589	~1000	1000–2000	500–5000	500–1000
Mass.	HAR	2684	1334–6826	3000–5000	~5000	> 5000	1000–5000
Virginia	SNP	3480	2270–5660	~3200	> 5000	~5000	> 5000
N. Carolina	SOS	4666	3131–7045	~3200	> 5000	~5000	~5000
Germany	TOR	3010	1994–4592	3200–5500	> 5000	> 5000	5000–10,000
DJF							
Alaska	BAR	558	488–657	100–400	200–500	100–500	100–500
Mass.	HAR	4386	1728–19,510	7000–10,000	5000–10,000	> 5000	1000–5000
Virginia	SNP	5000	2710–8640	4000–7000	5000–10,000	> 5000	5000–10,000
Germany	TOR	2296	1266–4107	4000–7000	5000–10,000	> 5000	> 10, 000

For more than one data set per location, the full range of the central 67% of the data and the average of the medians is given. Some model values are taken from figures with finer contours than those shown here.

agree with the measurements during ABLE-3B, but the GRANTOUR output is 2–5 times larger.

At Sable Island, off Nova Scotia, a median of 250 pptv was observed, but all of the models produced more than 500 pptv there. The air flow was mostly from the north and northwest during these measurements, whereas flow is typically much more frequently from the southwest (over much more polluted regions) during this season (Merrill and Moody, 1996). The GRANTOUR, GCTM-1 and Harvard/GISS results have greater than 5 ppbv in the locations of the Harvard Forest, Shenandoah and North Carolina measurements (HAR, SNP, SOS), as well as Schauinsland (TOR), which all had medians between 2 and 5 ppbv. The MOZART results agree well with all four sites, with 3–5 ppbv. All three model results have a steep gradient in the region of the flights off the coast of California (C2O), where mixing ratios between 80 and 200 pptv were observed. The MOZART and GCTM-1 results yield from 100 to 3000 pptv and Harvard/GISS produces 500–1000 pptv over the extent of the measurements, whereas the lowest value in the GRANTOUR results is 1000 pptv.

NO_y, *December–February*. The NO_y model results for the northern hemisphere winter are higher than for summer in all four models (panel (d) of Figs 24–27). The four models all show regions above 5 ppbv in eastern North America, and Europe. Conversely, the mixing ratios are somewhat lower in the southern hemisphere, which is most obvious by the smaller regions above 1 ppbv in South America and Africa.

The NO_y measurements at Barrow during winter (500–700 pptv) are slightly higher than the model results (100–500 pptv), in contrast to the summer comparison (Table 9), however the results from GCTM-1 show a small region above 500 pptv to the east of Barrow, near Prudhoe Bay. At Harvard Forest, Shenandoah and Schauinsland, the GRANTOUR and GCTM-1 results are greater than 5 ppbv, where the observed medians are between 2 and 5 ppbv. All four models' output ranges lie within the central 67% of the observations at Harvard Forest. MOZART agrees well with the Shenandoah data, and the GCTM-1, GRANTOUR and Harvard/GISS results lie in the upper half of the data. As in the previous cases, all of the models produce higher results than observed in Germany, with MOZART and GCTM-1 showing a few ppbv greater, and Harvard/GISS resulting in at least 7 ppbv greater than the 2.3 ppbv median.

4.2. *Middle troposphere*

The model results for the middle troposphere are shown in Figs 30–35. The results produced by MOZART have been averaged over 3–6 km, but the other model results are shown for one pressure level near 500 mb. The same temporal averages have been used for these model runs as those discussed in Section 4.1. Tables 10 and 11 summarize the comparison of the model results with measurements of NO_x and NO_y.

NO_x, *June–August*. The results of the five model runs for NO_x in summer and winter at 500 mbar are shown in Figs 30–35. The results from both seasons differ significantly in the locations of NO_x maxima and minima. In the summer results (panel (a) of Figs 30–35) MOZART and GCTM-1 show large regions with mixing ratios above 100 pptv, whereas GRANTOUR predicts only a small region above the Himalayas greater than 100 pptv, and Harvard/GISS produces more than 100 pptv only over southeast Asia. KFA-GISS calculates values above 100 pptv

only in northern Europe and CTMK small regions in eastern Europe, southeastern Asia and east of Mexico. Most of the models show local maxima over South America and Africa, but in differing amounts and locations. GRANTOUR is the only model to show a slight maximum between Africa and Antarctica. The CTMK and KFA-GISS models have coarser resolution than the other models, which may result in weaker convection than the others, and consequently lower mixing ratios in the middle troposphere.

Results from GCTM-1 and Harvard/GISS span the 20–40 pptv NO_x observed in Alaska during ABLE 3A (3AL, 3AW in Fig. 14 and Table 10), whereas GRANTOUR produces 40–60 pptv, and the other three models lie below the data. At Mauna Loa, 20–40 pptv were observed, and all of the models except KFA-GISS indicate values in this range; it produces < 10 pptv. All of the models agree with the observations near Hudson Bay during ABLE-3B (3BH), except the GRANTOUR results which are at least 15% higher. Measurements during ABLE-3A over Hudson Bay (3AO) are more than twice as high, but were made during just one flight through the region. In Labrador GCTM-1, which produces 50–100 pptv there, is the only model to not agree with the 20–50 pptv observed. The highest median value observed was during ELCHEM in New Mexico, which was a study of transport in convective cloud systems. However, a wide range of NO_x levels (40–200 pptv) were seen and all of the models produce values in good agreement with these, except KFA-GISS which shows ~25 pptv. The models are all much closer (within 50%) to the observations west of California (C2O) at this altitude than in the boundary layer.

NO_x, *December–February*. Panel (b) of Figs 30–35 shows the model results for northern hemisphere winter. CTMK produces the largest regions with mixing ratios above 100 pptv in North America, Europe and Asia, whereas the Harvard model does not calculate any mixing ratios above 100 pptv. GCTM-1, however, produces slightly higher values than the other models in the southern hemisphere. Lower levels of NO_x are produced over the continents than in summer, due to weaker convection of emissions to the middle troposphere in winter.

The only data sets available for comparison with the winter NO_x data are the MLOPEX-2 and AASE campaigns (see Fig. 14 and Table 10), and since the AASE measurements were mostly at higher altitudes, the geographical coverage is quite limited. Both the models and data at Mauna Loa (ML2) show essentially the same values for winter as for summer, except the results from GRANTOUR and Harvard/GISS are slightly lower. In Alaska, the observations fall within the ranges of the models, except for MOZART,

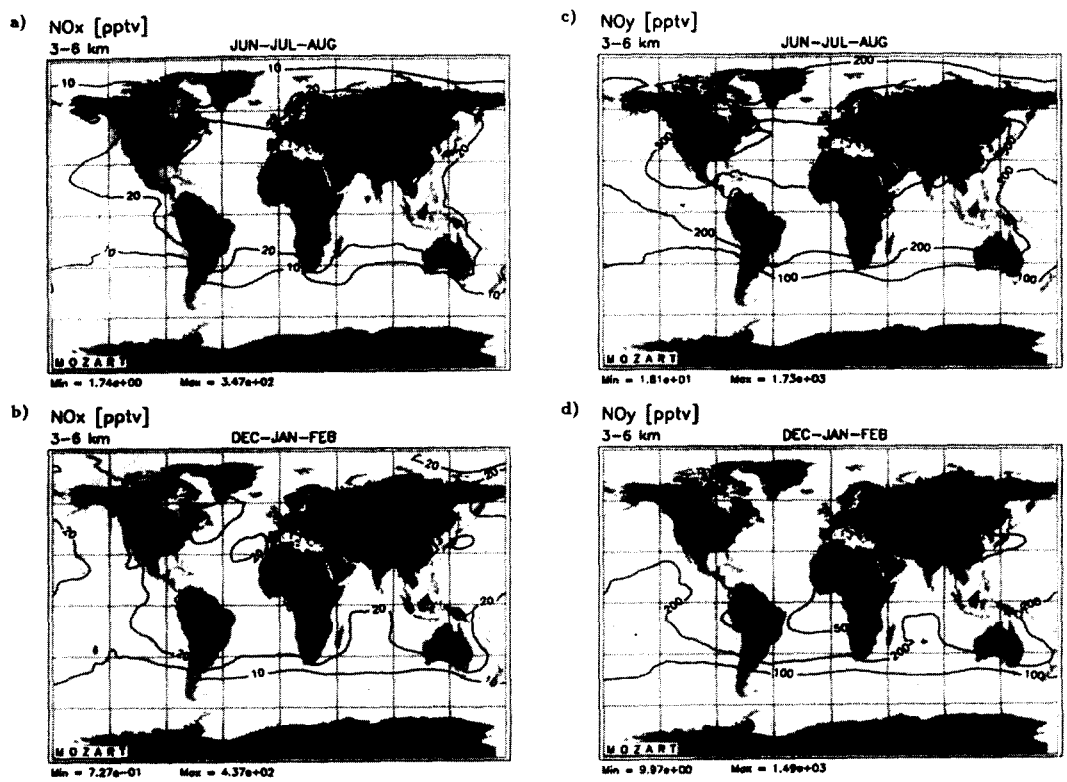

Fig. 30. Model results from MOZART for NO_x and NO_y at 3–6 km: (a) NO_x, June–August; (b) NO_x, December–February; (c) NO_y, June–August; (d) NO_y, December–February. Contour levels are 10, 20, 50, 100, 200, 500, 1000, 1500 pptv.

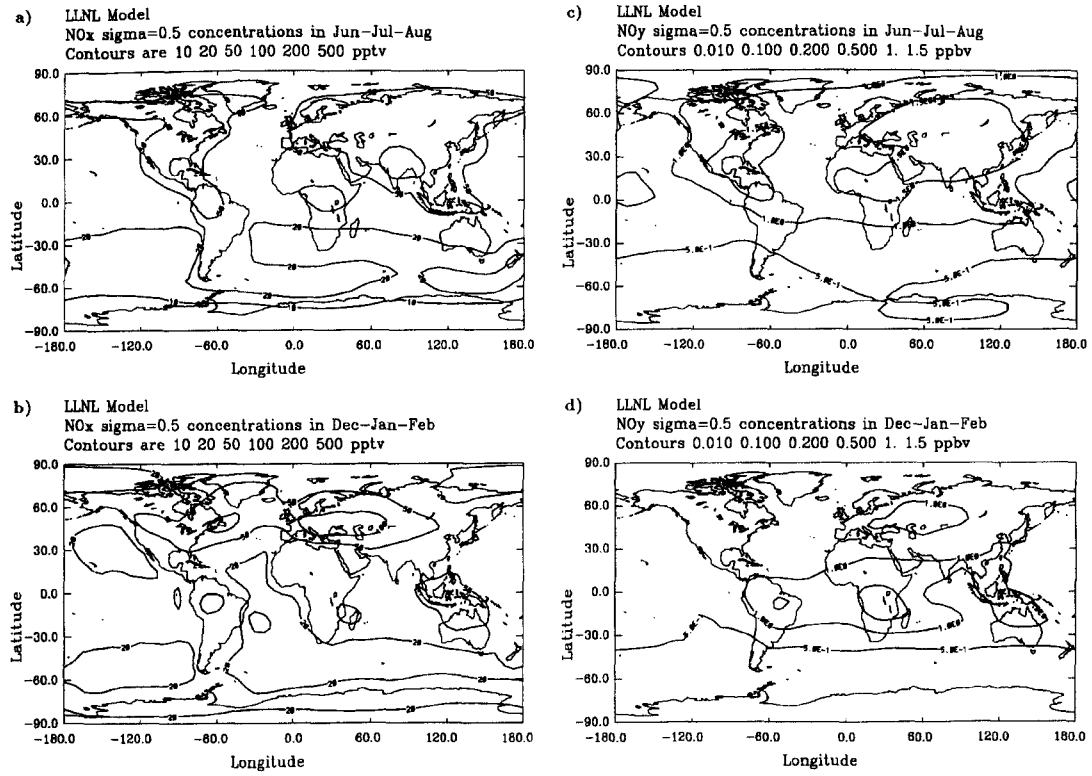

Fig. 31. Model results from GRANTOUR for NO_x and NO_y at 500 mb: (a) NO_x, June–August (b) NO_x, December–February (c) NO_y, June–August (d) NO_y, December– February.

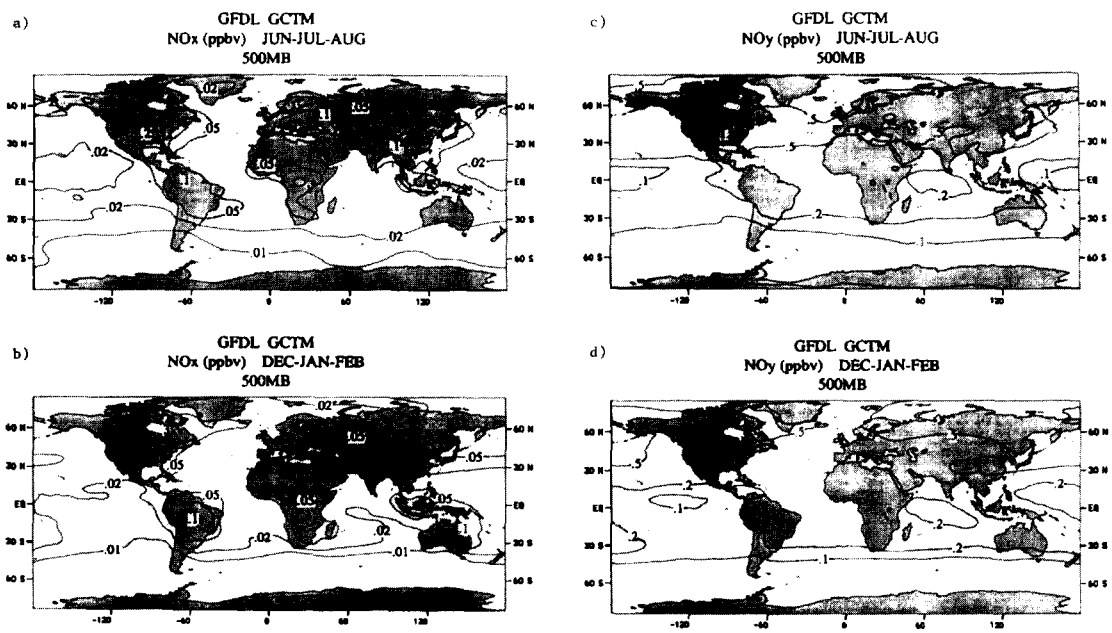

Fig. 32. Model results from GCTM-1 for NO_x and NO_y at 500 mb: (a) NO_x, July–September; (b) NO_x, January–March; (c) NO_y, July–September; (d) NO_y, January–March. Contour levels are 10, 20, 50, 100, 200, 500, 1000, 1500 pptv.

Harvard and KFA-GISS, which are about 50% lower. A much wider range of values were measured near the North Pole (A2P), and these generally agree with all of the models. The NO_x levels observed over Norway in AASE 2 (A2N) were significantly higher than in AASE 1 (A1N). All of the models agree well with the higher values, which are between 50 and 150 pptv, except the Harvard results which match the

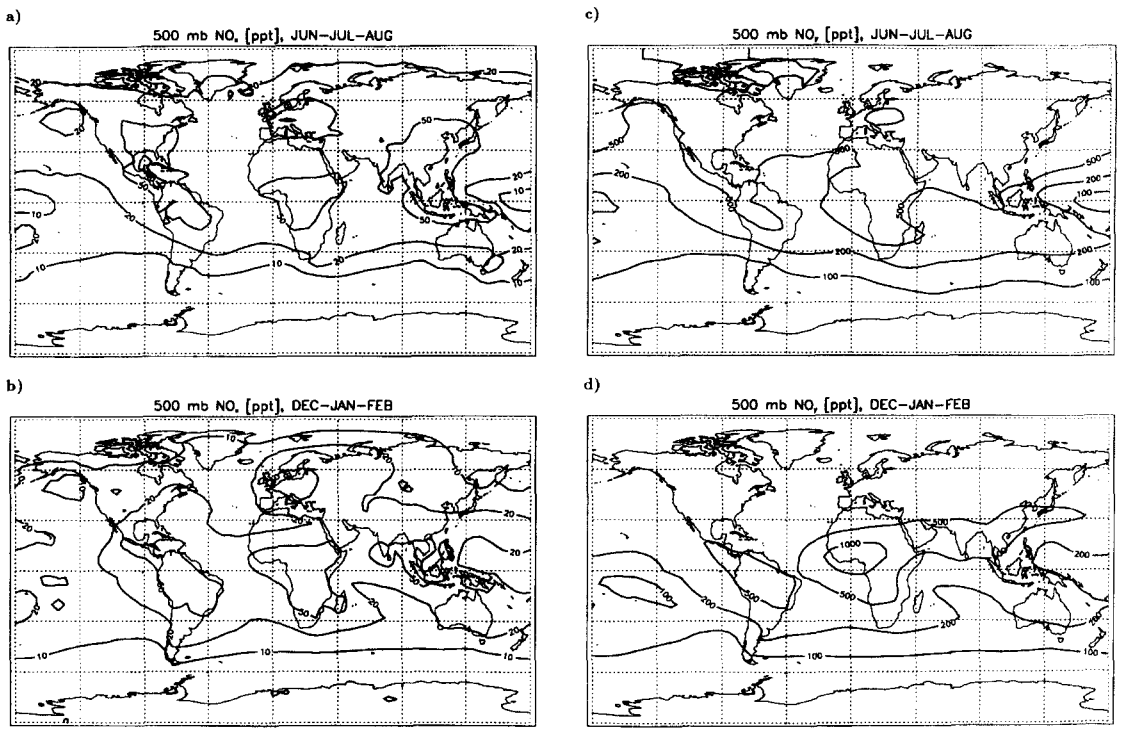

Fig. 33. Model results from Harvard/GISS for NO_x and NO_y at 500 mb: (a) NO_x, June–August; (b) NO_x, December–February; (c) NO_y, June–August; (d) NO_y, December–February. Contour levels are 10, 20, 50, 100, 200, 500, 1000, 1500 pptv.

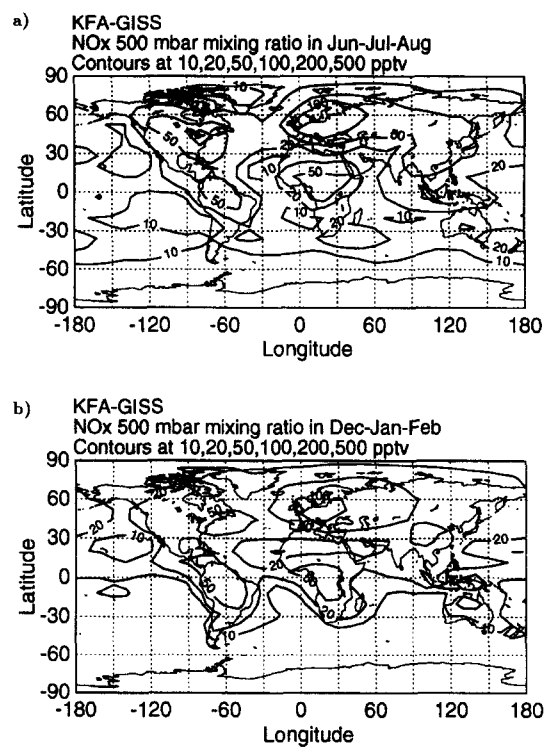

Fig. 34. Model results from KFA-GISS for NO_x at 500 mb: (a) NO_x, June–August; (b) NO_x, December–February.

A1N data. A broad distribution of values was observed over Maine (20–100 pptv) (A2M); the Harvard results agree well with the median and lower values observed, whereas the other five models agree with mixing ratios at the higher end; CTMK produces over 100 pptv, but the others have between 50 and 100 pptv. Over Tahiti (A2T), the observed levels near 100 pptv are up to 10 times larger than all of the model results, most likely due to the influence of local sources.

NO_y, *June–August*. Figures 30–33 show the NO_y model results for 500 mbar, which are compared with the data in Fig. 15 and summarized in Table 11. One of the regions with the most striking differences between the MOZART, GRANTOUR, GCTM-1 and Harvard/GISS boreal summer NO_y results at 3–6 km is at high northern latitudes ((c) panels). MOZART and Harvard/GISS produce less than 500 pptv for much of the region above 60°N, whereas the GRANTOUR results show roughly 1 ppbv in northern Canada and Greenland and approaching 1.6 ppbv above Siberia. By contrast GCTM-1 has high values at the pole (500–1000 pptv), and lower values immediately south, instead of a constant increase to mid-latitudes as in the other three results. There is a significant difference also at the South Pole. In the GCTM-1 results NO_y is 100–500 pptv at the pole with 50–100 pptv at 60°S. GRANTOUR produces 400–600 pptv for almost everywhere below 30°S, and MOZART

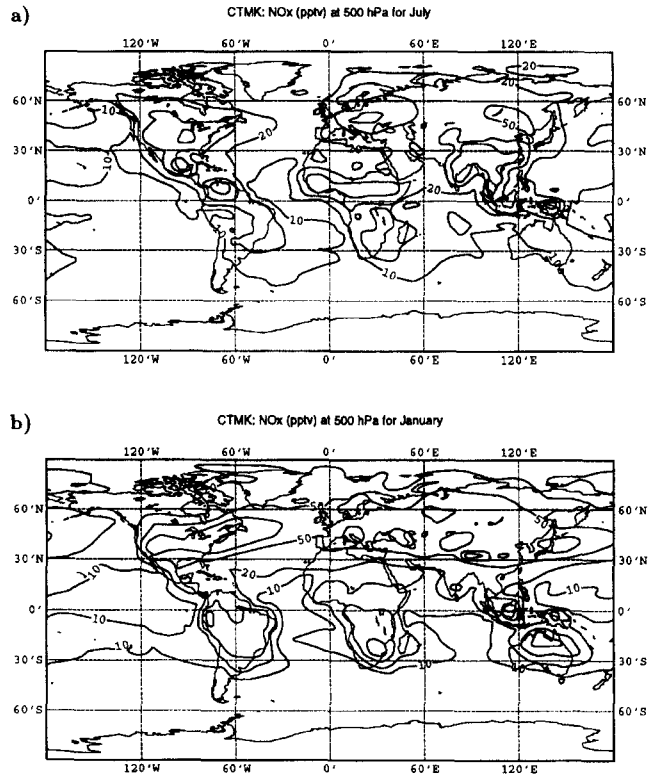

Fig. 35. Model results from CTMK for NO_x at 500 mb: (a) NO_x, July; (b) NO_x, January. Contour levels are 10, 20, 50, 100, 200, 500 pptv.

and Harvard/GISS show less than 100 pptv. These differences are likely due to the differing wind fields and transport schemes between the models and, in the case of GRANTOUR, to the presence of organic nitrates associated with isoprene chemistry.

The measurements along the mid-section of the US (C2F, C2C) agree well with the GCTM-1 and Harvard results in the west, but MOZART and GRANTOUR produce 2–3 times as high values throughout the region of the measurements. The ELCHEM results in New Mexico agree with the GCTM-1 and Harvard outputs, but are a few hundred pptv lower than MOZART and GRANTOUR's results. The range of values observed over the western Pacific (C2O) agree well with the results from MOZART, GCTM-1 and Harvard, however the GRANTOUR output is a few hundred pptv higher than the maximum measured and 3–4 times higher than the median. The comparison at Mauna Loa is similar, with MOZART and GCTM-1 results agreeing with the observed values, The Harvard output overlapping the upper half of the data, and the GRANTOUR results showing about 300 pptv ($< 3\times$) higher than observed.

The models have difficulty reproducing the observations at Summit, Greenland (SUM). The results from MOZART, GCTM-1 and Harvard overlap the lower half of the measurements, but GRANTOUR is a factor of 2 higher.

One of the interesting regions for comparison is over the Atlantic, between North America and Europe, which is mainly influenced by outflow from the United States. The results from MOZART, GCTM-1 and Harvard agree well with the measurements during OCTA in the region 40–50°N, 35–65°W (OCG–OCN). GRANTOUR produces several hundred pptv higher than the observed 700–1200 pptv. In the eastern Atlantic, between northwest Africa and Great Britain, 300–600 pptv were observed. MOZART produces lower NO_y here than to the west, but it is just above the measured values. GRANTOUR also shows slightly lower values in the eastern Atlantic than the west, but they are still several times higher than those observed. The GCTM-1 and Harvard results are in the same range across the North Atlantic.

NO_y, *December–February*. During winter, MOZART (Fig. 30d) produces less than 500 pptv of NO_y through most of the northern hemisphere, and yields mixing ratios above 1 ppbv only in air above eastern Asia. GRANTOUR (Fig. 31d) predicts much higher values than MOZART, with higher than 1 ppbv above central Asia and the southern hemisphere tropics. The GCTM-1 results (Fig. 32d) have

Table 10. Summary of data—model comparisons for NO_x in the middle troposphere. The median and central 67% of the data at 3–6 km are given. The three-character codes are identified in Table 3, and are used in Figures 12–15. All quantites are in pptv

		Data		Model results					
Location	Codes	Median	Central 67%	MOZART	GRANTOUR	GCTM-1	Harvard	KFA-GISS	CTMK
JJA									
Hawaii	ML2	29	16–42	10–25	20–30	10–50	20–50	~10	10–20
Alaska	3AW, 3AL	30	19–44	10–25	40–60	10–50	10–50	10–20	10–20
N. Canada	3AA	21	14–30	8.5–25	40–60	10–50	10–50	10–50	10–20
Hudson Bay	3BH, 3AO	55	25–94	10–40	40–60	10–50	20–50	20–50	20–50
Labrador	3BL	38	24–55	10–40	40–60	50–100	20–50	20–50	20–50
NE U.S.	3AN, 3BN	50	21–84	50–100	60–80	100–500	20–100	50–100	50–100
E. Pacific	C2O	27	16–55	25–40	30–40	10–50	20–50	10–20	10–20
Calif.	C2C	46	23–65	25–100	40–60	10–50	20–50	20–50	~20
VA–CO	C2F	34	15–51	> 100	60–80	50–500	20–100	20–100	50–100
New Mexico	ELC	96	39–170	100–240	60–80	50–100	20–50	20–50	~50
W Atlantic	C3W	76	56–178	40–85	~60	50–500	50–100	50–100	20–100
DJF									
Hawaii	ML2	31	21–44	10–25	10–20	10–50	10–20	2–10	10–20
Tahiti	A2T	101	80–124	10–25	20–30	10–50	10–20	2–10	10–20
Calif.	A1C, A2C	40	13–75	10–50	~30	10–50	10–20	20–50	20–50
Alaska	A2A	38	30–68	10–25	30–40	10–50	10–20	10–20	10–20
Maine	A2M	30	18–140	55–100	80–100	50–100	20–50	50–100	100–200
N. Pole	A2P	46	12–74	25–40	20–30	10–50	< 10	10–20	10–20
Norway	A1N, A2N	50	24–134	40–55	~60	~50	20–50	~100	50–100

For more than one data set per location, the full range of the central 67% of the data and the average of the medians is given. Some model values are taken from figures with finer contours than those shown here.

Table 11. Summary of data–model comparisons for NO_y in the middle troposphere. The median and central 67% of the data at 3–6 km are given. The three-character codes are identified in Table 3, and are used in Figs 12–15. All quantites are in pptv

Location	Codes	Data		Model Results			
		Median	Central 67%	MOZART	GRANTOUR	GCTM-1	Harvard
JJA							
Hawaii	ML2	188	103–305	250–400	600–800	100–500	200–500
Greenland	SUM	583	417–770	100–250	1000–1200	100–500	~500
E. Pacific	C2O	289	155–867	550–850	1000–1200	100–500	200–500
Calif.	C2C	363	177–648	700–1500	1000–1200	100–500	500–1000
VA–CO	C2F	249	73–505	1000–1700	1200–1800	100–5000	500–1000
New Mexico	ELC	926	637–1472	1000–1700	~1400	500–1000	500–1000
NW Atlantic	OCG–OCN	955	735–1196	700–1700	1400–1800	500–1000	500–1000
E. Atlantic	OCA–OCF	468	316–641	550–750	1200–1400	500–1000	500–1000
DJF							
Hawaii	ML2	187	124–290	100–250	600–800	100–500	200–500
Tahiti	A2T	275	242–285	100–250	400–600	100–500	100–200
Calif.	A1C, A2C	390	298–683	100–250	600–800	100–500	200–500
Maine	A2M	599	489–770	250–500	600–800	500–1000	200–500
Alaska	A2A	472	390–544	250–400	~600	500–1000	200–500
Newfoundland	TR3	490	335–3870	250–500	~800	500–1000	200–500
Greenland	TR2	950	612–1960	250–400	600–800	500–1000	200–500
N. Pole	A2P	894	517–1087	250–400	600–800	500–1000	200–500
Norway	A1N, A2N	398	210–679	250–400	~800	~500	200–500
England	TR1, OCA–OCC	820	259–1648	250–400	800–1000	100–500	200–500
E. Atlantic	T11, OCD, OCE	400	147–757	250–400	600–800	100–500	200–500
W Atlantic	TR4	455	350–821	250–500	600–800	100–500	200–500
NW S. America	TR5	349	278–564	400–700	800–1000	100–500	500–1000
W. S. America	TR6	280	163–397	100–400	400–800	100–500	200–500
S. S. America	TR7	171	126–221	10–100	200–400	50–100	~100
E. S. America	TR8	233	176–449	100–550	400–1000	100–500	100–500
NE S. America	TR9	310	226–453	400–550	1200–1400	100–500	200–500
W. Africa	T10	513	410–715	550–700	~1200	100–500	> 1000

For more than one data set per location, the full range of the central 67% of the data and the average of the medians is given. Some model values are taken from figures with finer contours than those shown here.

500–1000 pptv in the northern mid to high latitudes, similar to GRANTOUR, and higher than MOZART, but with only a small region over eastern Asia over 1000 pptv. There is a maximum (over 500 ppbv) in central Africa, but none over South America, unlike the other two models.

NO_y measurements in winter were made during the MLOPEX-2, AASE, OCTA and TROPOZ campaigns. As in the summer comparison, the observed NO_y values at Mauna Loa lie within the model results of MOZART and GCTM-1, the upper half of the data agree with the Harvard model output, but the results from GRANTOUR are 3–4 times higher than data (see Table 11). The model results over Tahiti are much closer to the observed values than are the NO_x results (discussed above). MOZART and Harvard are slightly lower than the data, GCTM-1 agrees well, but GRANTOUR produces about twice as much as observed. MOZART produces about 200 pptv lower than the median 400 pptv observed over California (A1C, A2C), whereas GRANTOUR shows twice as much as observed, and the GCTM-1 and Harvard values agree with the data. All four model results are close to the observations in Alaska (A2A), with Harvard agreeing with the data, MOZART about 100 pptv lower, GCTM-1 and GRANTOUR within 150 pptv of the observed median. Agreement is also good over Maine, where the mixing ratios observed are about 100 pptv above the MOZART results, and within the ranges of the other two models. Rather high mixing ratios were observed at the North Pole (median of 900 pptv), which agree well with the GCTM-1 results. A significant portion of the observed values are consistent with the 600–800 pptv produced by GRANTOUR, but most of the observations are above the 250–400 pptv shown in the MOZART results.

In Norway, the results from MOZART, GCTM-1 and Harvard agree with observations during both AASE campaigns, however GRANTOUR produces about several hundred pptv greater values. The model results are in general agreement with observations during OCTA and TROPOZ over England and the eastern Atlantic. Over England, the results from MOZART, GCTM-1 and Harvard overlap only the lower half of the measurements (TR1, OCA–OCC), and the output from GRANTOUR agrees with the higher portion of the data. Between northwest Africa and over the Atlantic west of France, the observations were 150–750 pptv. Again, MOZART, GCTM-1 and

Harvard produce results that agree with the lower end of the data (100–500 pptv) and GRANTOUR outputs 600–800 pptv.

The measurements during TROPOZ in South America (TR5–TR9) agree well with the results from MOZART, GCTM-1 and Harvard, but are generally a factor of 2 lower than the GRANTOUR results. All three model results have values decreasing to the south, but at the southern tip of South America, MOZART, GCTM-1 and Harvard show less than or about 100 pptv, whereas GRANTOUR has 200–400 pptv and the observed values, 100–200 pptv, lie in between.

5. CONCLUSIONS

The model results differ from each other in each of the comparisons above, however no one model's results are systematically different than the other models or the observations for all of the seasons and altitudes discussed here. It is interesting to note that although the KFA-GISS model has coarser horizontal resolution ($8° \times 10°$) than the other models and a simplified chemistry scheme, the distributions that they produce are not greatly (nor systematically) different from the others or the observations.

In the boundary layer the results from GCTM-1 generally show the greatest extremes, with the highest values over the continents and lowest values of all the models over the oceans. In the summer NO_x boundary layer results, the results from GRANTOUR and CTMK are not as high as the other models in the heavily polluted regions (with highest fossil fuel emissions) of eastern North America, Europe and eastern Asia, and GCTM-1 produces the highest levels of NO_x. In winter, the GCTM-1 and Harvard results are very similar with the highest values over Africa, but all of the models are similar over North America and Europe. The NO_y results from GRANTOUR, GCTM-1 and, in some cases, Harvard are higher than MOZART and the observations in both the northern hemisphere summer and winter. In regions of generally low values, such as over the oceans, GRANTOUR produces higher mixing ratios than MOZART, GCTM-1 and Harvard.

In the middle troposphere, MOZART and GCTM-1 have larger regions of high NO_x (>100 pptv) than GRANTOUR, Harvard, KFA-GISS and CTMK during June–August. During winter, however, CTMK has the largest regions above 100 pptv in North America, Europe and Asia and Harvard has no values >100 pptv. In the southern hemisphere (summer) GCTM-1 has slightly higher values than the others. The NO_y model results differ the most at both north and south high latitudes. GRANTOUR produces the highest values near both poles, as well as over all of the northern hemisphere, during summer. The GRANTOUR results are the highest of the four models during December–February in the southern hemisphere, and GRANTOUR and GCTM-1 produce more than Harvard and MOZART in the northern hemisphere.

In the comparison of models as well as data and model results, the regions of discrepancy are likely due to a variety of reasons. For instance, in the boundary layer of the industrial regions of North America and Europe, the data have been filtered in several cases so as to represent the background levels of the region, as opposed to the average concentration at the site. By contrast, the numerical diffusion and arbitrary grid geometry of the models make it difficult to accurately represent an isolated surface site, or regions of sharp concentration gradients. At all altitudes differences may lie largely in the differing emission rates used by the models (see Table 7), as well as different convection and washout schemes. The different lightning production rates of NO used by the models is probably the most significant difference in sources at 3–6 km, as aircraft emissions contribute less than 10% at this altitude (Lamarque *et al.*, 1996). The large uncertainty remaining in the effect of lightning on NO concentrations can be a significant cause of differences between observed and modeled distributions (e.g., Goldenbaum and Dickerson, 1993; Lawrence *et al.*, 1994). In cases, both at the surface and in the free troposphere, where the measurements spanned a much shorter period than the three month averages of the model results, the actual meteorological conditions may differ significantly from the modeled winds and temperatures. More detailed comparisons for specific campaigns can help determine how well the models reflect the NO_x and NO_y distributions of the troposphere.

Several campaigns, which were made during spring or fall or in which only NO was measured, were not directly compared here to the model results, but have provided valuable information about the reactive nitrogen distributions in the troposphere. The recent aircraft campaigns of TRACE-A and PEM West-A and B, with measurements of a full complement of chemical species, have improved our understanding of photochemistry and ozone production over South America, Africa and the South Atlantic, strongly influenced by convection and biomass burning, and the western Pacific in the region of continental outflow. The PEM-Tropics campaign, planned for August–September 1996, will cover the central and eastern tropical Pacific, where the only measurements in this climatology are from two flights between California and Tahiti during AASE 2 and the STRATOZ and TROPOZ flights along the west coast of South America (see Figs 1–3).

5.1. *Outstanding questions*

In addition to beginning to understand the distributions of reactive nitrogen species, this compilation of data helps test our understanding of the sources of NO_x and NO_y. This start to a climatology also makes obvious where measurements are lacking which could

answer outstanding questions of photochemistry and tropospheric NO_x production and transport, and consequently ozone production. It is clear from Figs 1–3, which do not show the entire globe, that the current set of measurements of NO_x and NO_y are still far from providing a global view of their distributions. Some of the most obvious gaps in this climatology are over Europe, Asia, Australia and the polar regions. Many of the significant differences between the model results were over these regions, so cannot be understood with the aid of observations.

It is quite evident from Figs 4–7, especially in seasons other than summer, that it is very difficult to test our understanding of the boundary layer distributions with the present set of measurements. Since a significant proportion of NO_x sources are from the boundary layer (fossil fuel and biomass burning, soil emissions), further measurements at the surface can improve our understanding of their contribution to regions away from these sources. However, the interpretation of boundary layer measurements must be made with careful consideration of meteorological conditions in order to understand the source of airmasses sampled. This is particularly difficult at remote sites some distance from high source regions, such as Sable Island, Nova Scotia (Carroll *et al.*, 1996). In remote regions, however, boundary layer and flux measurements will continue to help us quantify and monitor biogenic emissions as land use changes in regions such as the Amazon rain forests.

The ABLE-3A and 3B campaigns provided valuable information about NO_x in the arctic and subarctic regions of North America in the lower half of the troposphere. The measurements there, though, also left questions about the distributions above 6 km. It was evident from measurements and back trajectory calculations that the stratosphere can be a significant source of ozone to the region, and further measurements (of chemical species and dynamics) and at higher altitudes are needed for a better quantification of stratosphere/troposphere exchange in the Arctic. Similar studies were made of measurements at Chebogue Point and Sable Island and the stratosphere was again found to be an important source (Moody *et al.*, 1996). Measurements in other seasons throughout the troposphere will help improve our understanding of the chemical distributions in the Arctic, and quantify the contribution of sources from Siberia and Russia and clean air from the North Pacific, to the region (Sandholm *et al.*, 1992; Harriss *et al.*, 1994). Comparisons of results from GCTM-1 with the ABLE-3A and 3B data, have shown a shortfall of predicted NO_y in some regions, but good agreement between the sum of NO_x, HNO_3 and PAN from the model with observations (Levy *et al.*, 1997). Further individual comparisons of data and models for HNO_3, PAN and organic nitrates will help isolate the differences between models and between observations and models for many regions. Differences in model HNO_3 are due primarily to dynamics and rainout, while PAN and organic nitrates are more dependent on chemistry. The high concentration of organic nitrates in GRANTOUR has caused attention to be focused on the chemistry of isoprene and associated nitrates, peroxy radicals and organic peroxides. The GRANTOUR chemistry is currently being modified with updated reaction rates for peroxy radicals (Kirchner and Stockwell, 1996) and with more detailed chemistry of organic peroxides. Both of these changes may reduce model concentration of organic nitrates. As some concern has recently arisen about the accuracy and specificity of NO_y measurements (e.g. Crosley, 1996, and discussed above), data–model comparisons of individual species may provide a simpler means for determining the causes of differences in model results.

Although the model results of summer NO_y from MOZART and GCTM-1 agree with the MLOPEX 2 measurements, there are indications that the processes governing the NO_x and NO_y budgets in the remote troposphere are not completely understood. GCTM-1 model results of NO_x in summer are one-half to one-third of observed values during MLOPEX 1 and 2 (although not evident in these figures, due to the coarseness of the contours), but agree well in all other seasons. In contrast, MOZART overestimated HNO_3 and H_2O_2, implying that the model does not provide sufficient washout of soluble species. However, an additional source of NO_y will be needed, if modeled HNO_3 is reduced, to maintain good agreement with observations of NO_x, PAN and NO_y (Brasseur *et al.*, 1997).

Data from the NARE and OCTA campaigns, parts of which were shown here, will provide valuable information about the concentrations across the North Atlantic and help determine, among other things, the contribution of pollutants from North America to this region and their lifetime.

More can be learned about the ability of three-dimensional chemical tracer models to predict observed concentrations by looking at the statistics of the model results over the region and time of individual campaigns, and comparing those with the observations. Looking at the midday NO values of the model results will also be valuable, since the community has the highest confidence in the measurement of this species (of NO, NO_x and NO_y). Comparisons of observed HNO_3/NO_x, PAN and NO_x deposition rates with model results will also help to improve our understanding of the accuracy of the models. The modeling of the O_3 budget can also be improved by comparing observational climatologies of O_3 and CO with the models. However, in order to produce truly meaningful climatologies, further work is needed on understanding the limitations of the existing set of measurements and to improve the observations. New and better methods of detecting NO_2 and total NO_y, or its components, and a continuation of measurement techniques intercomparisons are greatly needed to improve our understanding of tropospheric and

stratospheric photochemistry (cf, Albritton *et al.*, 1990).

5.2. *Summary*

Climatologies developed from observations of NO, NO_x and NO_y have been presented for the surface and the free troposphere in 3 km altitude bins for four seasons. Although the spatial coverage of data is limited, this summary shows our present knowledge of the global distributions of these species, and is a beginning for improving our understanding of tropospheric transport and chemistry. The statistics, including mean, median, central 67% and 90%, of the data in small regions have been shown for each season at 5 altitude layers. Comparisons with six chemical transport models have been made for summer and winter data in the boundary layer and the middle troposphere. In many places agreement between the models and data is good, however the wide ranges of values observed at any given site, and the coarse averaging and plotting of model results, may mask additional discrepancies. Further work must be done to understand the cause of both differences in the results of the several models and between the models and the data. It is likely that in many (if not all) of the data–model comparisons made here real differences exist between modeled and actual meteorology, emissions, washout, convection and transport out of the boundary layer which result in disagreement, as well as fortuitous agreement. Studying other species (e.g., O_3 and OH) which affect the NO_x budget can help identify differences between the models and the true atmosphere. Improving our understanding of the NO_x distributions will consequently improve our ability to accurately model ozone and ozone production.

Acknowledgements—We would like to thank B. Ridley for his helpful comments. The data for the ABLE-3A, and -3B campaigns were obtained from the Langley EOSDIS Distributed Active Archive Center. All other GTE data (ABLE-2A, -2B, CITE-2, -3, PEM West-A, TRACE-A) were available from the GTE Archives. The AASE data have been released on CD-ROM (available from NASA). Thanks to J. Hoell and D. Owen for making available GTE data from the GTE Archive, and to B. Ridley and J. Walega for providing NCAR's archives of the MLOPEX data sets (now available on CD). Use was also made of merged data files compiled by S. Sandholm. This work, in particular the archiving of published measurements of NO_x and NO_y, was funded by NASA Atmospheric Effects of Aviation Program, Subsonic Assessment (AEAP/SASS). D.H. is supported by a postdoctoral fellowship from the Advanced Study Program (ASP) at the National Center for Atmospheric Research (NCAR). NCAR is sponsored by the National Science Foundation.

REFERENCES

Albritton D. L. (1993) The atmospheric effects of stratospheric aircraft: Interim Assessment Report of the NASA High-Speed Research Program. NASA Reference Publication 1333.

Albritton D. L., Fehsenfeld F. C. and Tuck A. F. (1990) Instrumental requirements for global atmospheric chemistry. *Science* **250,** 75–81.

Anderson J. G. and Toon O. B. (1993) Airbone Arctic Stratospheric Expedition II: An overview. *Geophys. Res. Lett.* **20,** 2499–2502.

Anderson B. E., Gregory G. L., Barrick J. D. W., Collins J. E. Jr., Sachse G. W., Bagwell D., Shipham M. C., Bradshaw J. D. and Sandholm S. T. (1993a) The impact of U.S. continental outflow on ozone and aerosol distributions over the western Atlantic. *J. geophys. Res.* **98,** 23,477–23490.

Anderson B. E., Gregory G. L., Barrick J. D. W., Collins J. E. Jr., Sachse G. W., Hudgins C. H., Bradshaw J. D. and Sandholm S. T. (1993b) Factors influencing dry season ozone distributions over the tropical south Atlantic. *J. geophys. Res.* **98,** 23,491–23,500.

Atherton C. S. (1995) Biomass burning sources of nitrogen oxides, carbon monoxide, and non-methane hydrocarbons. LLNL Report UCRL-10-122583, Livermore, California.

Atherton C. S., Grotch S., Parrish D. D., Penner J. E. and Walton J. J. (1996) The role of anthropogenic emissions of NO_x on tropospheric ozone over the North Atlantic Ocean: A three dimensional, global model study. *Atmospheric Environment* **30,** 1739–1749.

Atkinson R. A., Baulch D. L., Cox R. A., Hampson R. F. Jr., Kerr J. A. and Troe J. (1993) Evaluated kinetic and photochemical data for atmospheric chemistry, supplement IV. IUPAC subcommittee on gas kinetic data evaluation for atmospheric chemistry. *J. Phys. Chem. Ref. Data* **21,** 1125–1568.

Atlas E. L. and Ridley B. A. (1996) The Mauna Loa Observatory Photochemistry Experiment: Introduction. *J. geophys. Res.* **101,** 14,531–14,541.

Atlas E. L., Ridley B. A., Hubler G., Walega J. G., Carroll M. A., Montzka D. D., Huebert B. J., Norton R. B., Grahek F. E. and Schauffler S. (1992) Partitioning and budget of NO_y species during the Mauna Loa Observatory Photochemistry Experiment. *J. geophys. Res.* **97,** 10,449–10,462.

Bakwin P. S., Wofsy S. C., Fan S.-M., Keller M., Trumbore S. E. and da Costa J. M. (1990a) Emission of nitric oxide (NO) from tropical forest soils and exchange of NO between the forest canopy and atmospheric boundary layers. *J. geophys. Res.* **95,** 16,755–16,764.

Bakwin P. S., Wofsy S. C. and Fan S.-M. (1990b) Measurements of reactive nitrogen oxides (NO_y) within and above a tropical forest canopy in the wet season. *J. geophys. Res.* **95,** 16,765–16,772.

Bakwin P. S., Wofsy S. C. and Fan S.-M. (1992) Measurements of NO_x and NO_y concentrations and fluxes over Arctic tundra. *J. geophys. Res.* **97,** 16,545–16,557.

Bakwin P. S., Jacob D. J., Wofsy S. C., Munger J. W., Daube B. C., Bradshaw J. D., Sandholm S. T., Talbot R. W., Singh H. B., Gregory G. L. and Blake D. R. (1994) Reactive nitrogen oxides and ozone above a taiga woodland. *J. geophys. Res.* **99,** 1927–1936.

Balkanski Y. J., Jacob D. J., Gardner G. M., Graustein W. M. and Turekian K. K. (1993) Transport and residence times of continental aerosols inferred from a global 3-dimensional simulation of ^{210}Pb. *J. geophys. Res.* **98,** 20,573–20,586.

Baughcum S. L., Tritz T. G., Henderson S. C. and Pickett D. C. (1996) Scheduled civil aircraft emission inventories for 1992: database development and analysis. NASA CR-4700.

Benkovitz C. M., Dignon J., Pacyna J., Scholtz T., Tarrassón L., Voldner E. and Graedel T. E. (1996) Global gridded inventories of anthropogenic emissions of SO_2 and NO_x. *J. geophys. Res.*, **101,** 29,239–29,254.

Bollinger M. J., Sievers R. E., Fahey D. W. and Fehsenfeld F. C. (1983) Conversion of nitrogen dioxide, nitric acid and *n*-propyl nitrate to nitric oxide by gold-catalyzed reduction with carbon monoxide. *Anal. Chem.* **55,** 1980–1986.

Bradshaw J. D., Rodgers M. O., Sandholm S. T., Kesheng S., and Davis D. D. (1985) A two-photon laser-induced fluorescence field instrument for ground based and airborne measurements of atmospheric NO. *J. geophys. Res.* **90,** 12,861–12,873.

Brasseur G. P., Hauglustaine D. A. and Walters S. (1996) Chemical compounds in the remote Pacific troposphere: Comparison between MLOPEX measurements and chemical-transport-model calculations. *J. geophys. Res.* **10,** 14,795–14,813.

Brasseur G. P., Hauglustaine D. A., Granier C., Müller J.-F., Rasch P., Tie X.-X. and Walters S. (1997) MOZART: A global three-dimensional chemical-transport-model of the atmosphere. *J. geophys. Res.* (to be submitted).

Brühl C. and Crutzen P. J. (1989) On the disproportionate role of tropospheric ozone as a filter against solar UV–B radiation. *Geophys. Res. Lett.* **16,** 703–706.

Carroll M. A., Hastie D. R., Ridley B. A., Rodgers M. O., Torres A. L., Davis D. D., Bradshaw J. D., Sandholm S. T., Schiff H. I., Karecki D. R., Harris G. W., Mackay G. I., Gregory G. L., Condon E. P., Trainer M., Hübler G., Montzka D. D., Madronich S., Albritton D. L., Singh H. B., Beck S. M., Shipman M. C. and Bachmeier A. S. (1990a) Aircraft measurements of NO_x over the eastern Pacific and continental United States and implications for ozone production. *J. geophys. Res.* **95,** 10,205–10,234.

Carroll M. A. and Thompson A. M. (1995) NO_x in the non-urban troposphere. In *Progress and Problems in Atmospheric Chemistry* (edited by Barker J. R.) World Scientific, Singapore.

Carroll M. A., Montzka D. D., Hübler G., Kelly K. K., Gregory G. L. (1990b) In situ measurements of NO_x in the Airborne Arctic Stratospheric Expedition. *J. geophys. Res. Lett.* **17,** 493–396.

Carroll M. A., Ridley B. A., Montzka D. D., Hubler G., Walega J. G., Norton R. B., Huebert B. J. and Grahek F. E. (1992) Measurements of nitric oxide and nitrogen dioxide during the Mauna Loa Observatory Photochemistry Experiment. *J. geophys. Res.* **97,** 10,361–10,374.

Chin M., Jacob D. J., Gardner G. M., Foreman-Fowler M. S., Spiro P. A. and Savoie D. L. (1996) A global three-dimensional model of tropospheric sulfate. *J. geophys. Res.* **101,** 18,667–18,690.

Crawford J., Davis D., Chen G., Bradshaw J., Sandholm S., Gregory G., Sachse G., Anderson B., Collins J., Blake D., Singh H., Heikes B., Talbot R. and Rodriguez J. (1996) Photostationary state analysis of the NO_2–NO system based on airborne observations from the western and central North Pacific. *J. geophys. Res.* **101,** 2053–2072.

Crosley D. R. (1994) Issues in the measurement of reactive nitrogen compounds in the atmosphere. SRI Int. Report MP 94-035, Menlo Park, California.

Crosley D. R. (1996) NO_y blue ribbon panel. *J. geophys. Res.* **101,** 2049–2052.

Crutzen P. J. and Zimmermann P. H. (1991) The changing photochemistry of the troposphere. *Tellus* **43AB,** 136–151.

Davis D. D., Chen G., Chameides W., Bradshaw J., Sandholm S., Rodgers M., Schendal J., Madronich S., Sachse G., Gregory G., Anderson B., Barrick J., Shipham M., Collins J., Wade L. and Blake D. (1993) A photostationary state analysis of the NO_2–NO system based on airborne observations from the subtropical/tropical North and South Atlantic. *J. geophys. Res.* **98,** 23,501–23,523.

DeMore W. B., Samder S. P., Golden D. M., Molina M. J., Hampson R. F., Kurylo M. J., Howard C. J. and Ravishankara A. R. (1994) Chemical kinetics and photochemical data for use in stratospheric modeling. JPL publication 94-26, Pasadena, California.

Dentener F. and Crutzen P. J. (1993) Reaction of N_2O_5 on tropospheric aerosols: Impact on the global distributions of NO_x, O_3 and OH. *J. geophys. Res.* **98,** 7149–7163.

Dianov–Klokov V. I. and Yurganov L. N. (1981) A spectroscopic study of the global space–time distribution of atmospheric CO. *Tellus* **33,** 262–273.

Dignon J. (1992) NO_x and SO_x emissions from fossil fuels: A global distribution. *Atmospheric Environment* **26A,** 1157–1163.

Doddridge B. G., Dickerson R. R., Holland J. Z., Cooper J. N., Wardell R. G., Poulida O. and Watkins J. G. (1991) Observations of tropospheric trace gases and meteorology in rural Virginia using an unattended monitoring system: Hurricane Hugo, a case study. *J. geophys. Res.* **96,** 9341–9360.

Doddridge B. G., Dickerson R. R., Wardell R. G., Civerolo K. L. and Nunnermacker L. J. (1992) Trace gas concentrations and meteorology in rural Virginia 2: Reactive nitrogen compounds. *J. geophys. Res.* **97,** 20,631–20,646.

Donahue N. M., Dubey M. K., Mohrschlatdt R., Demerjian K. L. and Anderson J. G. (1997) A high pressure flow study of the reaction $NO_2 + OH \rightarrow HONO_2$ in nitrogen. *J. geophys. Res.* (submitted).

Drummond J. W., Ehhalt D. H. and Volz A. (1988) Measurements of nitric oxide between 0–12 km altitude and 67°N–60°S latitude obtained during STRATOZ III. *J. geophys. Res.* **93,** 15,831–15,849.

Ehhalt D. H., Rohrer F. and Wahner A. (1992) Sources and distribution of NO_x in the upper troposphere at northern mid-latitudes. *J. geophys. Res.* **97,** 3725–3738.

Emmons L. K. and Carroll M. A. (1996) Access NO_x and NO_y measurements on-line. *Eos* **77,** 34.

Fahey D. W., Eubank C. S., Huebler G. and Fehsenfeld F. C. (1985) Evaluation of a catalytic reduction technique for the measurement of total reactive odd-nitrogen NO_y in the atmosphere. *J. Atmos. Chem.* **3,** 435–468.

Fehsenfeld F. C., Dickerson R. R., Hübler G., Luke W. T., Nunnermacker L. J., Williams E. J., Roberts J. M., Calvert J. G., Curran C. M., Delany A. C., Eubank C. S., Fahey D. W., Fried A., Gandrud B. W., Langford A. O., Murphy P. C., Norton R. B., Pickering K. E. and Ridley B. A. (1987) A ground-based intercomparison of NO, NO_x and NO_y measurement techniques. *J. geophys. Res.* **92,** 14,710–14,722.

Fehsenfeld F. C., Parrish D. D. and Fahey D. W. (1988) The measurement of NO_x in the non-urban troposphere. In *Tropospheric Ozone* (edited by Isaksen I. S. A.), pp. 183–215. D. Reidel, Dordrecht.

Fishman J., Hoell J. M. Jr., Bendura R. D., Kirchoff V. W. J. H. and McNeal R. J. Jr. (1996) The NASA GTE TRACE-A experiment (September–October, 1992) Overview. *J. geophys. Res.* **101,** 23,865–23,880.

Folkins I. A., Weinheimer A. J., Ridley B. A., Walega J. G., Anderson B., Collins J. E., Sachse G., Pueschel R. F. and Blake D. R. (1995) O_3, NO_y and NO_x/NO_y in the upper troposphere of the equatorial Pacific. *J. geophys. Res.* **100,** 20,913–20,926.

Fortuin J. P. F. and Langematz U. (1995) An update on the global ozone climatology and on concurrent ozone and temperature trends. *Proc. SPIE Atmospheric Sensing and Modeling,* Vol. 2311, pp. 207–216.

Fung I., John J., Lerner J., Matthews E., Prather M., Steele L. P. and Fraser P. J. (1991) Three–dimensional model synthesis of the global methane cycle. *J. geophys. Res.* **96,** 13,003–13,065.

Gao W. and Wesely M. L. (1995) Modeling gaseous dry deposition over regional scales with satellite observations: I. Model development. *Atmospheric Environment* **29,** 727–737.

Gerbig C., Kley D., Volz-Thomas A., Kent J., Dewey K. and McKenna D. S. (1996) Fast-response resonance fluorescence CO measurements aboard the C-130: Instrument characterization and measurements made during North Atlantic Regional Experiment 1993. *J. geophys. Res.* **101,** 29,229–29,238.

Giorgi F. and Chameides W. L. (1986) Rainout lifetimes of highly soluble aerosols and gases as inferred from simulations with a general circulation model. *J. geophys. Res.* **91,** 14,367–14,376.

Goldenbaum G. C. and Dickerson R. R. (1993) Nitric oxide production by lightning discharges, *J. geophys. Res.* **98,** 18,333–18,337.

Guenther A., Hewitt C. N., Erickson D., Fall R., Geron C., Graedel T., Harley P., Klinger L., Lerdau M., McKay W. A., Pierce T., Scholes B., Steinbrecher R., Tallamraju R., Taylor J. and Zimmerman P. (1995) A global model of natural volatile organic compound emissions. *J. geophys. Res.* **100,** 8873–8892.

Hack J. J. (1994) Parameterization of moist convection in the NCAR community climate model (CCM2). *J. geophys. Res.* **99,** 5551–5568.

Hack J. J., Boville B. A., Briegleb B. P., Kiehl J. T., Rash P. J., and Williamson D. L. (1993) *Description of the NCAR Community Climate Model (CCM2)*, NCAR Technical Note NCAR/TN-382 + STR, National Center for Atmospheric Research, Boulder, Colorado.

Hansen J., Russell G., Rind D., Stone P., Lacis A., Lebedeff S., Ruedy R. and Travis L. (1983) Efficient three-dimensional global models for climate studies: Models I and II. *Mon. Weather Rev.* **111,** 609–662.

Harriss R. C., Wofsy S. C., Garstang M., Browell E. V., Molion L. C. B., McNeal R. J., Hoell Jr. J. M., Bendura R. J., Beck S. M., Navarro R. L., Riley J. T. and Snell R. L. (1988) The Amazon Boundary Layer Experiment (ABLE 2A): dry season 1985. *J. geophys. Res.* **93,** 1351–1360.

Harriss R. C., Garstang M., Wofsy S. C., Beck S. M., Bendura R. J., Coelho J. R. B., Drewry J. W., Hoell J. M. Jr., Matson P. A., McNeal R. J., Molion L. C. B., Navarro R. L., Rabine V. and Snell R. L. (1990) The Amazon Boundary Layer Experiment: wet season 1987. *J. geophys. Res.* **95,** 16,721–16,736.

Harriss R. C., Wofsy S. C., Bartlett D. S., Shipham M. C., Jacob D. J., Hoell J. M. Jr., Bendura R. J., Drewry J. W., McNeal R. J., Navarro R. L., Gidge R. N. and Rabine V. E. (1992) The Arctic Boundary Layer Expedition (ABLE 3A): July–August 1988. *J. geophys. Res.* **97,** 16,383–16,394.

Harriss R. C., Wofsy S. C., Hoell J. M. Jr., Bendura R. J., Drewry J. W., McNeal R. J., Pierce D., Rabine V. and Snell R. L. (1994) The Arctic Boundary Layer Expedition (ABLE 3B): July–August 1990. *J. geophys. Res.* **99,** 1635–1644.

Hauglustaine D. A., Madronich S., Ridley B. A., Walega J. G., Cantrell C. A., Shetter R. E. and Hübler G. (1996) Observed and model-calculated photostationary state at Mauna Loa Observatory during MLOPEX II. *J. geophys. Res.* 14,681–14,696.

Heimann M. (1995) The global atmospheric tracer model TM2: DKRZ TM2 model documentation. Max–Planck– Institut für Meteorologie. Technical Report No. 10, Hamburg.

Hein R. (1994) Inverse Modellierung des atmosphärischen Methan–Kreislaufs unter Verwendung eines drei–dimensionalen Modells des Transports und der Chemie der Troposphäre. Max–Planck–Institut für Meteorologie, Examensarbeit No. 25, Hamburg, ISSN 0938–5177, 125pp.

Hoell J. M. Jr., Albritton D. L., Gregory G. L., McNeal R. J., Beck S. M., Bendura R. J. and Drewry J. W. (1990) Operational overview of NASA GTE/CITE-2 airborne instrument intercomparisons: Nitrogen dioxide, nitric acid and peroxyacetyl nitrate. *J. geophys. Res.* **95,** 10,047–10,054.

Hoell Jr J. M., Davis D. D, Gregory G. L., McNeal R. J., Bendura R. J., Drewry J. W., Barrick J. D., Kirchhoff V. W. J. H., Motta A. G., Navarro R. L., Dorko W. E. and Owen D. W. (1993) Operational overview of NASA GTE/CITE-3 airborne instrument intercomparisons for sulfur dioxide, hydrogen sulfide, carbonyl sulfide, dimethyl sulfide, and carbon disulfide. *J. geophys. Res.* **98,** 23,291–23,304.

Holstag A. and Boville B. (1993) Local versus nonlocal boundary-layer diffusion in a global climate model. *J. Clim.* **6,** 1825–1842.

Honrath R. E. and Jaffe D. A. (1992) The seasonal cycle of nitrogen oxides in the Arctic troposphere at Barrow, Alaska. *J. geophys. Res.* **97,** 20,615–20,630.

Hübler G., Fahey D. W., Kelly K. K., Montzka D. D., Carroll M. A., Tuck A. F., Heidt L. E., Pollock W. H., Gregory G. L. and Vedder J. F. (1990) Redistribution of reactive odd nitrogen in the lower Arctic stratosphere. *Geophys. Res. Lett.* **17,** 453–456.

Hübler G., Fahey D. W., Ridley B. A., Gregory G. L. and Fehsenfeld F. C. (1992) Airborne measurements of total reactive odd nitrogen (NO_y). *J. geophys. Res.* **97,** 9833–9850.

Hübler G., Montzka D. D., Norton R. B., Murphy P. C., Fehsenfeld F. C., Liu S. C., Ridley B. A., Walega J. G., Atlas E., Grahek F. E., Heidt L. E., Merrill J., Huebert B. J. and Bodhaine B. A. (1992) Total reactive oxidized nitrogen (NO_y) in the remote Pacific troposphere and its correlation with O_3 and CO: Mauna Loa Observatory Photochemistry Experiment 1988. *J. geophys. Res.* **97,** 10,427–10,448.

Jacob D. J. and Wofsy S. C. (1988) Photochemistry of biogenic emissions over the Amazon Forest. *J. geophys. Res.* **93,** 1477–1486.

Jacob D. J., Prather M. J., Wofsy S. C. and McElroy M. B. (1987) Atmospheric distribution of ^{85}Kr simulated with a general circulation model. *J. geophys. Res.* **92,** 6614–6626.

Jacob D. J., Wofsy S. C., Bakwin P. S., Fan S.-M., Harriss R. C., Talbot R. W., Bradshaw J. D., Sandholm S. T., Singh H. B., Browell E. V., Gregory G. L., Sachse G. W., Shipham M. C., Blake D. R. and Fitzjarrald D. R. (1992) Summertime photochemistry of the troposphere at high northern latitudes. *J. geophys. Res.* **97,** 16,421–16,432.

Jacob D. J., Logan J. A., Yevich R. M., Gardner G. M., Spivakovsky C. M., Wofsy S. C., Munger J. W., Sillman S., Prather M. J., Rodgers M. O., Westberg H. and Zimmerman P. R. (1993) Simulation of summertime ozone over North America. *J. geophys. Res.* **98,** 14,797–14,816.

Jaffe D. A., Honrath R. E., Zhang L., Akimoto H., Schimizu A., Mukai H., Murano K., Hatakeyama S. and Merril J. (1996) Measurements of NO, NO_y, CO and O_3 and estimation of the ozone production rate at Oki Island, Japan, during PEM-West. *J. geophys. Res.* **101,** 2037–2048.

Jaffe D. A., Honrath R. E., Furness D., Conway T. J., Dlugokencky E. and Steele L. P. (1995) A determination of the CH_4, NO_x, and CO_2 emissions from the Prudhoe Bay, Alaska Oil Development. *J. atmos Chem.* **20,** 213–227.

Johnson J. E., Koropalov V. M., Pickering K. E., Thompson A. M., Bond N. and Elkins J. W. (1993) Third Soviet-American gases and aerosols (SAGA 3) experiment: Overview and meteorological and oceanographic conditions. *J. geophys. Res.* **98,** 16,893–16,908.

Kasibhatla P. S. (1993) NO_y from sub-sonic aircraft emissions: A global three-dimensional model study. *Geophys. Res. Lett.* **20,** 1707–1710.

Kasibhatla P. S., Levy II H., Moxim W.J. and Chameides W. L. (1991) The relative impact of stratospheric photochemical production on tropospheric NO_y levels: A model study. *J. geophys. Res.* **96,** 18,631–18,646.

Kasibhatla P. S., Levy II H. and Moxim W. J. (1993) Global NO_x, HNO_3, PAN and NO distributions from fossil-fuel combustion emissions: A model study. *J. geophys. Res.* **98,** 7165–7180.

Kasibhatla P. S., Levy II H., Klonecki A. and Chameides W. L. (1996) A three-dimensional view of the large-scale tropospheric ozone distribution over the North Atlantic Ocean during summer. *J. geophys. Res.* **101,** 29,305–29,316.

Kirchner F. and Stockwell W. R. (1996) Effect of peroxy radical reactions on predicted concentrations of ozone, nitrogenous compounds and radicals. *J. geophys. Res.* **101**.

Kley D. and McFarland M. (1980) Chemiluminescence detector for NO and NO_2. *Atmos. Tech.* **12**, 63–69.

Kliner D. A. V., Daube B. C., Burley J. D. and Wofsy S. C. (1997) Laboratory investigation of the catalytic reduction technique for measurement of atmospheric NO_y. *J. geophys. Res.* (submitted).

Koike M., Kondo Y., Kawakami S., Singh H. B., Ziereis H. and Merrill J. T. (1996) Ratios of reactive nitrogen over the Pacific during PEM-West A. *J. geophys. Res.* **101**, 1829–1851.

Komhyr W. D., Oltmans S. J., Franchois P. R., Evans W. F. J. and Matthews W. A. (1988) *Ozone in the Atmosphere, Proc. Quadrennial Ozone Symp. 1988 and Tropospheric Ozone Workshop* (edited by Bojkov R. D. and Fabian P.).

Komhyr W. D., Oltmans S. J., Lathrop J. A., Kerr J. B. and Matthews W. A. (1994) The latitudinal distribution of ozone to 35 km altitude from ECC ozonesonde observations, 1982–1990. *Proc. Quadrennial Ozone Symp. of 1992* (edited by Hudson R.), NASA Pub. CP-3266.

Kondo Y., Kitada T., Koike M., Kawakami S. and Makino Y. (1993) Nitric oxide and ozone in the free troposphere over the western Pacific Ocean. *J. geophys. Res.* **98**, 20,527–20,535.

Kondo Y., Ziereis H., Koike M., Kawakami S., Gregory G. L., Sachse G. W., Singh H. B., Davis D. D. and Merrill J. T. (1996) Reactive nitrogen over the Pacific ocean during PEM-West A. *J. geophys. Res.* **101**, 1809–1828.

Kondo Y., Koike M., Kawakami S., Singh H. B., Nakajima H., Gregory G. L., Blake D. R., Davis D. D., Sachse G. W. and Merrill J. T. (1997a) Profiles and partitioning of reactive nitrogen over the Pacific Ocean in winter and early spring. *J. geophys. Res.* (submitted).

Kondo Y., Kawakami S., Koike M., Fahey D. W., Nakajima H., Zhao Y., Toriyama N., Kanada M., Sachse G. W. and Gregory G. L. (1997b) The performance of an aircraft instrument for the measurement of NO_y. *J. geophys. Res.* (submitted).

Lawrence, M. G., Chameides W. L., Kasibhatla P. S., Levy II H. and Moxim W. (1994) Lightning and atmospheric chemistry: The rate of atmospheric NO production. In *Handbook of Atmospheric Electrodynamics*, Vol. 1. CRC Press, Boca Raton, Florida.

Lerner A., Kley D., Volz-Thomas A. and McKenna D. S., (1994) Ozon-Stickoxid-Korrelationen in der Troposphere. Berichte des Forschungszentrums Juelich, Juel-3008, ISSN 0944-2952.

Levy II H., Mahlman J. D. and Moxim W. J. (1982) Tropospheric N_2O variability. *J. geophys. Res.* **87**, 3061–3080.

Levy II H. and Moxim W. J. (1989) Simulated global distribution and deposition of reactive nitrogen emitted by fossil fuel combustion. *Tellus* **41**, 256–271.

Levy II H., Moxim W. J., Kasibhatla P. S. and Logan J. A. (1991) The global impact of biomass burning on tropospheric reactive nitrogen. In *Global Biomass Burning: Atmospheric, Climatic, and Biospheric Implications.* (edited by Levine J. S.), pp. 363–369. MIT Press, Cambridge, Massachusetts.

Levy II H., Moxim W. J. and Kasibhatla P. S. (1996) A global 3-dimensional time-dependent lightning source of tropospheric NO_x. *J. geophys. Res.* **101**, 22,911–22,922.

Levy II H., Moxim W. J. and Kasibhatla P. S. (1997) Tropospheric NO_x: Its sources and distribution (in preparation).

Liousse C., Penner J. E., Chuang C., Walton J. J., Eddleman H. and Cachier H. (1996) A global three-dimensional model study of carbonaceous aerosols. *J. geophys. Res.* **101**, 19,411–19,432.

London J. and Liu S. C. (1992) Long-term tropospheric and lower stratospheric ozone variations from ozonesonde observations. *J. Atmos. Terrest. Phys.* **54**, 599–625.

Louis J. F. (1979) A parametric model of vertical eddy fluxes in the atmosphere. *Boundary-Layer Met.* **17**, 187–202.

Luke W. T. and Dickerson R. R. (1987) The flux of reactive nitrogen compounds from eastern North America to the western Atlantic Ocean. *Global Biogeochem. Cycles* **1**, 329–343.

Lurmann F. S., Lloyd A. C. and Atkinson R. (1986) A chemical mechanism for use in long-range transport/acid deposition computer modeling. *J. geophys. Res.* **91**, 10,095–10,936.

Mahlman J. D. and Moxim W. J. (1978) Tracer simulation using a global general circulation model: Results from a midlatitude instantaneous source experiment. *J. Atmos. Sci.* **35**, 1340–1374.

Manabe S., Hahn D. G. and Holloway J. L. Jr. (1974) The seasonal variation of the tropical circulation as simulated by a global model of the atmosphere. *J. Atmos. Sci.* **31**, 43–83.

Manabe S. and J. L. Holloway Jr. (1975) The seasonal variation of the hydrologic cycle as simulated by a global model of the atmosphere. *J. geophys. Res.* **80**, 1617–1649.

Marenco A. and Said F. (1989) Meridional and vertical ozone distribution in the background troposphere (70°N-60°S; 0–12 km altitude) from scientific aircraft measurements during the STRATOZ III experiment (June 1984). *Atmospheric Environment* **23**, 201–214.

Matthews E. (1983) Global vegetation and land use: New high-resolution data bases for climate studies. *J. Clim. Appl. Meteor.* **22**, 474–487.

Mauzerall D. L., Jacob D. J., Fan S.-M., Bradshaw J. D., Gregory G. L., Sachse G. W. and Blake D. R. (1996) Origin of tropospheric ozone at remote high northern latitudes in summer. *J. geophys. Res.* **101**, 4175–4188.

Merrill J. T. and Moody J. L. (1996) Synoptic meteorology and transport during the North Atlantic Regional Experiment (NARE) intensive. *J. geophys. Res.* (in press).

Metwally M. (1995) *Jet Aircraft Engine Emissions Database Development—1992 Military, Charter, and Nonscheduled Traffic.* NASA CR-4684.

Michelsen H. A., Salawitch R. J., Wennberg P. O. and Anderson J. G. (1994) Production of O^1D from photolysis of O_3. *Geophys. Res. Lett.* **21**, 2227–2230.

Moody J. L., Davenport J. C., Merrill J. T., Oltmans S. J., Parrish D. D., Holloway J. S., Levy II H., Forbes G. L., Trainer M. and Buhr M. (1996) Meteorological mechanisms for transporting O_3 over the Western North Atlantic Ocean: a case study for August 24–30th, 1993. *J. geophys. Res.* **101**, 29,213–29,228.

Moxim W. J., Levy II H. and Kasibhatla P. S. (1996) Simulated global tropospheric PAN: Its transport and impact on NO_x. *J. geophys. Res.* **101**, 12,621–12,638.

Müller J.-F. (1992) Geographical distribution and seasonal variation of surface emissions and deposition velocities of atmospheric trace gases. *J. geophys. Res.* **97**, 3787–3804.

Müller J.-F. and Brasseur G. (1995) IMAGES: a three-dimensional chemical transport model of the global troposphere. *J. geophys. Res.* **100**, 16,445–16,490.

Munger J. W., Wofsy S. C., Bakwin P. S., Fan S.-M., Goulden M. L., Daube B. C. and Goldstein A. H. (1996) Atmospheric deposition of reactive nitrogen oxides and ozone in a temperate deciduous forest and a sub-Arctic taiga woodland. 1. Measurements and mechanisms. *J. geophys. Res.* **101**, 12,639–12,657.

Nunnermacker L. J. (1990) Calibration and detection techniques for trace nitrogen compounds in the atmosphere. Ph.D. Dissertation, Department of Chemistry, University of Maryland, College Park, MD.

Parrish D. D., Hahn C. H., Fahey D. W., Williams E. J., Bollinger M. J., Hübler G., Buhr M. P., Murphy P. C., Trainer M., Hsie E. Y., Liu S. C. and Fehsenfeld F. C. (1990) Systematic variations in the concentration of NO_x (NO plus NO_2) at Niwot Ridge, Colorado. *J. geophys. Res.* **95**, 1817–1836.

Parrish D. D., Buhr M. P., Trainer M., Norton R. B., Shimshock J. P., Fehsenfeld F. C., Anlauf K. G., Bottenheim J. W.,Tang Y. Z., Wiebe H. A., Roberts J. M., Tanner R. L., Newman L., Bowersox V. C., Olszyna K. J., Bailey E. M., Rodgers M. O., Wang T., Berresheim H., Roychowdhury U. K. and Demerjian K. L. (1993) The total reactive oxidized nitrogen levels and the partitioning between the individual species at six rural sites in eastern North America. *J. geophys. Res.* **98,** 2927–2939.

Paulson S. E. and Seinfeld J. H. (1992) Development and evaluation of a photooxidation mechanism for isoprene, *J. geophys. Res.* **97,** 20,703–20,715.

Pham M., Müller J.-F., Brasseur G. P., Granier C. and Mégie G. (1995) A three-dimensional study of the tropospheric sulfur cycle. *J. geophys. Res.* **100,** 26,061–26,092.

Piccot S. D., Watson J. J. and Jones J. W. (1992) A global inventory of volatile organic compound emissions from anthropogenic sources. *J. geophys. Res.* **97,** 9897–9912.

Poulida O., Dickerson R. R., Doddridge B. G., Holland J. Z., Wardell R. G. and Watkins J.G., (1991) Trace gas concentrations and meteorology in rural Virginia 1: Ozone and carbon monoxide. *J. geophys. Res.* **96,** 22,461–22,475.

Poulida O., Civerolo K. L. and Dickerson R. R. (1994) Observations and tropospheric photochemistry in central North Carolina. *J. geophys. Res.* **99,** 10,553–10,563.

Prather M. (1986) Numerical advection by conservation of second order moments. *J. geophys. Res.* **91,** 6671–6681.

Prather M., McElroy M., Wofsy S., Russell G. and Rind D. (1987) Chemistry of the global troposphere: Fluorocarbons as tracers of air motion. *J. geophys. Res.* **92,** 6579–6613.

Price C. and Rind D. (1992) A simple lightning parameterization for calculating global lightning distributions. *J. geophys. Res.* **97,** 9919–9933.

Price C. and Rind D. (1994) Modeling global lightning distributions in a general circulation model. *Mon. Weath Rev.* **122,** 1930–1939.

Pyle J. A., Harris N. R. P., Farman J. C., Arnold F., Braathen G., Cox R. A., Faucon P., Jones R., Megie G., O'Neill A., Platt U., Pommereau J.-P., Schmidt U. and Stordal F. (1994) An overview of the EASOE campaign. *Geophys. Res. Lett.* **21,** 1191–1194.

Ridley B. A. and Howlett L. C. (1974) An instrument for NO measurements in the stratosphere. *Rev. Sci. Instrum.* **45,** 742–746.

Ridley B. A. and Robinson E. (1992) The Mauna Loa Observatory Photochemistry Experiment. *J. geophys. Res.* **97,** 10,285–10,290.

Ridley B. A., Walega J. G., Dye J. E. and Grahek F. E. (1994) Distributions of NO, NO_x, NO_y, and O_3 to 12 km altitude during the summer monsoon season over New Mexico. *J. geophys. Res.* **99,** 25,519–25,534.

Ridley B. A., Atlas E. L., Walega J. G., Kok G. L., Staffelbach T. A., Greenberg J. P., Hess P. G., Grahek F. E. and Montzka D. D. (1996) Aircraft measurements during the spring intensive of MLOPEX II: Peroxides, CO, O_3, NO_y, condensation nuclei, selected hydrocarbons, and alkyl nitrates between 0.5 and 9 km altitude. *J. geophys. Res.* (submitted).

Rodriguez J. (1993) Probing stratospheric ozone. *Science* **261,** 1128–1129.

Roelofs G.J. and Lelieveld J. (1995) Distribution and budget of O_3 in the troposphere calculated with a chemistry general circulation model. *J. geophys. Res.* **100,** 20,983–20,998.

Rohrer F., Brüning D. and Ehhalt D. H. (1997a) Tropospheric Mixing Ratios of NO obtained during TROPOZ II in the latitude region 67°N–56°S. *J. geophys. Res.* (submitted).

Rohrer F., Brüning D. and Ehhalt D. H. (1997b) Tropospheric Mixing Ratios of NO_y obtained during TROPOZ II in the latitude region 67°N–56°S. (in preparation).

Roth E. P. (1986) Description of a one dimensional model for atmospheric chemistry. Jül Bericht 2098 (Available from KFA Jülich, Library, 52425 Jülich, Germany).

Russell G. L. and Lerner J. A. (1981) A new finite-differencing scheme for the tracer transport equation. *J. Appl. Met.* **20,** 1483–1498.

Sandholm S. T., Bradshaw J. D., Dorris K. S., Rodgers M. O. and Davis D. D. (1990) An airborne compatible photofragmentation two-photon laser-induced fluorescence instrument for measuring background tropospheric NO, NO_x and NO_2. *J. geophys. Res.* **95,** 10,155–10,161.

Sandholm S. T., Bradshaw J. D., Chen G., Singh H. B., Talbot R. W., Gregory G. L., Blake D. R., Sachse G. W., Browell E. V., Barrick J. D. W., Shipham M. A., Bachmeier A. S. and Owen D. (1992) Summertime tropospheric observations related to N_xO_y distributions and partitioning over Alaska: Arctic Boundary Layer Expedition ^{J}3A. *J. geophys. Res.* **97,** 16,481–16,509.

Sandholm S., Olson J., Bradshaw J., Talbot R., Singh H., Gregory G., Blake D., Anderson B., Sachse G., Barrick J., Collins J., Klemm K., Lefer B., Klemm O., Gorzelska K., Herlth D. and O'Hara D. (1994) Summertime partitioning and budget of NO_y compounds in the troposphere over Alaska and Canada: ABLE 3B. *J. geophys. Res.* **99,** 1837–1861.

Seiler W. and Fishman J. (1981) The distribution of carbon monoxide and ozone in the free troposphere. *J. geophys. Res.* **86,** 7255–7265.

Sillman S. S. (1991) A numerical solution for the equations of tropospheric chemistry based on an analysis of sources and sinks of odd hydrogen. *J. geophys. Res.* **96,** 1837–1851.

Singh H. B., Herlth D., O'Hara D., Salas L., Torres A. L., Gregory G. L., Sachse G. W. and Kasting J. F. (1990) Atmospheric peroxyacetyl nitrate measurements over the Brazilian Amazon basin during the wet season: relationships with nitrogen oxides and ozone. *J. geophys. Res.* **95,** 16,945–16,954.

Singh H. B., Herlth D., Kolyer R. Salas L., Bradshaw J. D., Sandholm S. T., Davis D. D., Crawford J., Kondo Y., Koike M., Talbot R., Gregory G. L., Sachse G. W., Browell E., Blake D. R., Rowland F. S., Newell R., Merrill J., Heikes B., Liu S. C., Crutzen P. J. and Kanakidou M. (1996) Reactive nitrogen and ozone over the western Pacific: Distribution, partitioning, and sources. *J. geophys. Res.* **101,** 1793–1808.

Smit H. G. J., Gilde S. and Kley D. (1991) Ozone profiles over the Atlantic Ocean between 36°S and 52°N in March/April 1987 and September/October 1988, Jül Bericht 2567 (available from KFA Jülich Library, 52425 Jülich, Germany).

Smyth S. B., Sandholm S. T., Bradshaw J. D., Talbot R. W., Blake D. R., Blake N. J., Rowland F. S., Singh H. B., Gregory G. L., Anderson B. E., Sachse G. W., Collins J. E. and Bachmeier A. S. (1996) Factors influencing the upper free tropospheric distribution of reactive nitrogen over the South Atlantic during the TRACE-A experiment. *J. geophys. Res.* **101,** 24,165–24,186.

Spivakovsky C. M., Yevich R., Logan J. A., Wofsy S. C., McElroy M. B. and Prather M. J. (1990a) Tropospheric OH in a three-dimensional chemical tracer model: An assessment based on observations of CH_3CCl_3. *J. geophys. Res.* **95,** 18,441–18,471.

Spivakovsky C. M., Wofsy S. C. and Prather M. J. (1990b) A numerical method for parameterization of atmospheric chemistry: Computation of tropospheric OH. *J. geophys. Res.* **95,** 18,433–18,440.

Steele L. P., Fraser P. J., Rasmussen R. A., Khalil M. A. K., Conway T. J., Crawford A. J., Gammon R. H., Masarie K. A. and Thoning K. W. (1987) The global distribution of methane in the troposphere. *J. atmos. Chem.* **5,** 125–171.

Tiedtke M. (1989) A comprehensive mass flux scheme for cumulus parameterization in large scale models. *Mon. Weath. Rev.* **117,** 1779–1800.

Torres A. and Buchan H. (1988) Tropospheric nitric oxide measurements over the Amazon basin. *J. geophys. Res.* **93,** 1396–1406.

Torres A. and Thompson A. M. (1993) Nitric oxide in the equatorial Pacific boundary layer: SAGA 3 Measurements. *J. geophys. Res.*, **98,** 16,949–16,954.

Turco R., Plumb A. and Condon E. (1990) The Airborne Arctic Stratospheric Expedition: Prologue. *Geophys. Res. Lett.* **17,** 313–316.

Velders G. J. M., Heijboer L. C. and Kelder H. (1994) The simulation of the transport of aircraft emissions by a three-dimensional global model. *Ann. Geophys.* **12,** 385–393.

Volz-Thomas A. *et al.* (1990) EUROTRAC Annual Report 1989, Part 9: TOR, 57–62.

Volz-Thomas A. *et al.* (1991) EUROTRAC Annual Report 1990, Part 9: TOR, 83–88.

Volz-Thomas A. *et al.* (1992) EUROTRAC Annual Report 1991, Part 9: TOR, 122–1129.

Volz-Thomas A., Pätz and Geiss H. (1994) Schauinsland, Germany. In *The TOR Network—A Description of TOR Measurement Stations* (edited by Cvitaš T. and Kley D.) pp. 82–94. EUROTRAC ISS, Garmisch-Partenkirchen.

Wang T., Carroll M. A., Alber G. M., Owens K. R., Duderstadt K. A., Markevitch A. N., Parrish D., Holloway J., Fehsenfeld F. C., Forbes G. and Ogren J. (1996) Ground-based measurements of NO_x and total reactive oxidized nitrogen (NO_y) at Sable Island, Nova Scotia during the NARE 1993 summer intensive. *J. geophys. Res.* **101,** 28,991–29,004.

Wauben W. M. F., van Velthoven P. F. J. and Kelder H. (1997) A 3D chemistry transport model study of changes in atmospheric ozone due to aircraft emissions. *Atmospheric Environment* **31,** 1819–1836.

Weinheimer A. J., Walega J. G., Ridley B. A., Gary B. L., Blake D. R., Blake N. J., Rowland F. S., Sachse G. W., Anderson B. E. and Collins J. E. (1994) Meridional distributions of NO_x, NO_y, and other species in the lower stratosphere and upper troposphere during AASE II. *Geophys. Res. Lett.* **21,** 2583–2586.

Weller R., Lilischkis R., Schrems O., Neuber R. and Wessel S. (1996) Vertical ozone distribution in the marine atmosphere over the central Atlantic Ocean (56°S–50°N). *J. geophys. Res.* **101,** 1387–1399.

Wesely M. L. (1989) Parameterizations of surface resistances to gaseous dry deposition in regional-scale numerical models. *Atmospheric Environment* **23,** 1293–1304.

Wesely M. L. and Hicks B. B. (1977) Some factors that affect the deposition rates of sulfur dioxide and similar gases on vegetation. *J. Air Pollut. Control Ass.* **27,** 1110–1116.

Wild O., Law K. S., Pyle J. A., Gerbig C., Volz-Thomas A., Bandy B. J., Penkett S. A. and McKenna D. S. (1996) Photochemical trajectory modeling of the North Atlantic region during August 1993. *J. geophys. Res.* **101,** 29,269–29,288.

Williams E. J., Hutchinson G. L. and Fehsenfeld F. C. (1992) NO_x and N_2O emissions from soil. *Global Biogeochem. Cycles.* **6,** 351–388.

Williamson D. L. and Rasch P. (1994) Water vapor transport in the NCAR CCM2. *Tellus* **46,** 34–51.

Wofsy S. C., Cohen R. C. and Schmeltekopf A. L. (1994) Overview: The Stratospheric Photochemistry Aerosols and Dynamics Expedition (SPADE) and airborne arctic stratospheric expedition II (AASE-II). *Geophys. Res. Lett.* **21,** 2535–2538.

World Meteorological Organisation (1953) World distribution of thunderstorm days, WMO No.21, TP.6 and supplement (1956), Geneva.

Wuebbles D. J., Connell P. S., Grant K. E. Tarp R. and Taylor K. E. (1987) Initial results with the LLNL 2D chemical-radiative-transport model of the troposphere and stratosphere, LLNL Internal Rep. UCID-21178, LLNL, Livermore, California.

Wuebbles D. J., Maiden D., Seals Jr. R. K., Baughcum S. L., Metwally M. and Mortlock A. (1993) Emission scenarios development: Report of the Emissions Scenarios Committee. In *The Atmospheric Effects of Stratospheric Aircraft: A Third Program Report,* (edited by Stolarski R. S. and Wesoky H. L.), NASA Reference Publication 1313.

Yienger J. J. and Levy II H. (1995) Empirical model of global soil-biogenic NO_x emissions. *J. geophys. Res.* **100,** 11,447–11,464.

Zimmermann P. H. (1988) MOGUNTIA: a handy global tracer model. In *Air Pollution Modeling and its Applications VI,* (edited by van Dop H.), NATO/CCMS, pp. 593–608. Plenum, New York.

APPENDIX: ACRONYMS

AASE	Airborne Arctic Stratospheric Expedition
AERONOX	The Impact of NO_x Emissions from Aircraft Upon the Atmosphere at Flight Altitudes 8–15 km
ABLE-2	Amazon Boundary Layer Expedition
ABLE-3	Arctic Boundary Layer Expedition
ASHOE/ MAESA	Airborne Southern Hemisphere Ozone Experiment/ Measurements for Assessing the Effects of Stratospheric Aircraft
CITE	Chemical Instrumentation Test and Evaluation
CMDL	Climate Monitoring and Diagnostics Laboratory
CTMK	Chemistry Transport Model KNMI
ELCHEM	Electrified Cloud Chemistry
EUROTRAC	European Experiment on Transport and Transformation of Environmentally Relevant Trace Constituents in the Troposphere over Europe
GISS	Goddard Institute for Space Studies
GTE	Global Tropospheric Experiment
IMAGES	Intermediate Model of Global Evolution of Species
KNMI	Koninklijk Nederlands Meteorologisch Instituut (Royal Netherlands Meteorological Institute)
MLOPEX	Mauna Loa Observatory Photochemistry Experiment
MOZART	Model of OZone And Related species in the Troposphere
NARE	North Atlantic Regional Experiment
NOAA	National Oceanic and Atmospheric Administration
OCTA	Oxidizing Capacity of Tropospheric Atmosphere
PAM	Portable automated mesonet station
PAN	Peroxyacetylnitrate
PEM	Pacific Exploratory Mission
SASS	Subsonic Assessment (part of NASA's Atmospheric Effects of Aviation Program)
SOS	Southern Oxidants Study
SPADE	Stratospheric Photochemistry, Aerosols and Dynamics Expedition
TOR	Tropospheric Ozone Research
TRACE-A	Transport and Atmospheric Chemistry near the Equator—Atlantic